Searching for black holes and other massive, compact bodies using the gravitational waves from binary inspirals

Thesis by

Fintan D. Ryan

In Partial Fulfillment of the Requirements

for the Degree of

Doctor of Philosophy

California Institute of Technology

Pasadena, California

1997

(Defended May 16, 1997)

ACKNOWLEDGMENTS

I would like to thank Kip S. Thorne for suggesting many of the topics in this thesis, suggesting methods of solving some of them, reviewing my papers, and the countless other ways that he helped me. I am grateful to Alan Wiseman for valuable discussions about radiation reaction applied to the Carter constant. I am grateful to Daniel Kennefick for discussions concerning the proof that circular orbits in the Kerr metric remain circular.

ABSTRACT

We consider several issues involved with searching for and studying different types of compact bodies using the gravitational waves from binary inspirals. In Chapter 2, we use a radiation-reaction force formalism to compute (to leading post-Newtonian order) the inspiral evolution of a circular, nonequatorial orbit around a spinning black hole. We find that an initially circular orbit remains circular under radiation reaction and is driven towards antialignment with the black hole's spin direction. In Chapter 3, we apply this same formalism to orbits which are elliptical as well as nonequatorial. In addition, we prove that circular orbits remain circular exactly. In Chapter 4, we show that all the multipole moments of a massive, compact body (whose gravitational field is stationary, axially symmetric, and reflection symmetric across the equatorial plane) can be determined from the gravitational waves produced by a much less massive, compact object inspiraling in a contracting circle in the equatorial plane. We show that the moments are encoded in the waves' evolution in (at least) four independent functions of the gravitational-wave frequency: the gravitational-wave energy, the precession frequency of the orbit when slightly eccentric, the precession frequency of the orbit when slightly nonequatorial, and the gravitational-wave phase evolution. In Chapter 5, we compute the structure and the multipole moments of a spinning boson star with large self-interaction. We find that only three moments are needed to specify all the star's properties, and that the pattern of moments is very different from that for black holes. In Chapter 6, we estimate how accurately a gravitational-wave detector can estimate the multipole moments of the central body from the gravitational waves produced by an inspiraling compact object. We find that, typically, a space-based detector such as LISA (as opposed to an Earth-based detector such as LIGO) is necessary to get accurate enough measurements of the multipole moments so as to search for massive, compact, non-black-hole objects. In Chapter 7, as a model for computing the full details of the gravitational waves from an orbital inspiral, we compute the scalar waves produced by a scalar charge in a circular, equatorial orbit around a body with arbitrary multipole moments.

Contents

1 Introduction

Gravitational-wave detectors will provide us with ears to detect events such as stellar collapses, pulsars, the stochastic background of gravitational-wave sources, and the inspirals and collisions of black holes and other compact objects into each other [1, 2]. While experimenters construct these detectors, theorists must construct templates for the expected waveforms, to be used both for searching for the expected sources and, if their waves are detected, for deducing the properties of the source.

Inspiraling-binary sources (consisting of two compact objects such as neutron stars or black holes orbiting around each other while emitting gravitational waves) are of great interest because they give clean and direct information as to the nature of gravity in the strong-field regime. From this viewpoint, there is a special interest in inspiraling binaries with a large mass ratio between the two objects. This is because the characteristics of the smaller-mass member of the binary do not have a significant effect on the gravitational waveforms; the waveforms carry information solely and cleanly about the characteristics of the larger-mass object. In particular, the waves can give a detailed and highly accurate map of the more massive object's gravitational field and other properties as they exist in the absence of the inspiraling object. This is in contrast to the complexities that would arise if the masses were comparable and the waves depended strongly on the properties of both objects and their mutual interactions.

The smaller-mass object serves as a gravitational-wave-producing test probe of the larger-mass object's external gravitational field. The smaller-mass object is often (as in Chapters 2 and 3) referred to as "the particle." For the most part, the properties of the smaller-mass object are insignificant. All that is important about it is the value of its mass μ and the requirement that it is compact enough that it does not tidally disrupt during the inspiral. This object might be a white dwarf, a neutron star, or a small black hole, with a mass typically on the order of $1M_{\odot}$ (one solar mass).

The mass M of the larger-mass object is, of course, subject to the condition that $\mu \ll M$. For the gravitational waves to be in the highly relativistic range of interest, the object must be compact enough that its radius is only a few times $GM/c^2 \equiv M$ (here and throughout this thesis, we use units where Newton's gravitational constant G and the speed of light c are set to unity). For a circular orbit of radius r, the frequency F of the produced gravitational waves will primarily be at twice the orbital frequency: $F \sim 2(M/r^3)^{1/2}/(2\pi) = (M/r^3)^{1/2}/\pi$. Therefore, since we are interested in the strong-gravity case in which r also can become as small as a few times M, then we would want to use a gravitational-wave detector which is highly sensitive in a range from lower frequencies up to, say, $0.1/M \approx 2 \times 10^4 \mathrm{Hz}(M_\odot/M)$.

Several broad-band, laser-interferometer gravitational-wave detectors are under construction or in planning stages. Among them, the Caltech-MIT Laser Interferometer Gravitational-Wave Observatory (LIGO) [3] will measure "high-frequency" waves from $\sim$ 10 Hz to $\sim$ 500 Hz. At such frequencies, our above mentioned application would be well-suited if the mass M were less than $\sim 300 M_\odot$ (but much greater than μ). The European Space Agency's proposed, space-based Laser Interferometer Space Antenna (LISA) [4] will measure "low-frequency" waves, with a sensitivity range from about 10^{-4} Hz to 10^{-1} Hz. This will be best-suited for a central object with mass M in the range $\sim 10^5 M_\odot$ to $\sim 3 \times 10^7 M_\odot$.

A compact object with such a high mass M so as to be in one of the above ranges would likely be a black hole, since ordinary matter of that mass and compactness could not support itself against collapse. We temporarily assume that it is a black hole. As a result of the black-hole no-hair theorem [5], these Kerr (spinning) black holes need only two parameters—their mass and their spin angular momentum—to describe them. Hence, the space of templates for possible inspiral waves would be describable by a small set of parameters.

Despite this, computation of the templates is difficult. It consists of three tasks: computing the motion of the particle in the absence of gravitational radiation by using a set of constants of motion, computing the gravitational waves produced by that motion, and finally, computing how

the radiation reaction associated with those waves modifies the constants of motion. Fortunately, in the limit of $\mu \ll M$, the timescale for the modification of the constants of motion is much longer than an orbital period, so that each task can be solved relatively independently of the others. Here is how one might go about solving each task:

1. Although the orbit is very complex, in general being both elliptical (having a nonzero eccentricity) and out of the black-hole's equatorial plane, the task of computing the motion ignoring radiation is tractable because there exist three constants of motion (see §33.5 of Ref. [6]): the orbital energy, the component of the orbital angular momentum along the black hole's spin axis, and the so-called "Carter constant," which is (roughly speaking) the sum of the squares of the orbital angular momentum along the other two axes. With these constants of motion, computation of the coordinates of the particle along its path reduces to fairly simple integrations.

2. The task of computing the waves can be done using the Teukolsky formalism, which allows for a separation-of-variables solution to the gravitational-wave-generation equations. Although this task is complicated in practice, it is straightforward in principle.

3. The task of computing the effects of radiation reaction on the constants of motion is easy for the energy and the angular momentum along the black hole's spin axis. This is because the sum of the orbital energy and the energy carried in the gravitational waves is conserved, and similarly so for the angular momentum. Therefore, the values of these two constants decay at the rate that energy and angular momentum are carried away by the waves (both to "infinity" and into the hole). However, there is no conservation law to determine the evolution of the Carter constant. Without the ability to compute the Carter constant's evolution, we would only be able to solve the restricted case of the orbital motion being in the spinning black hole's equatorial plane (which is any plane if the black hole is not spinning). In that case, the Carter constant would be and would stay zero.

In Chapter 2 of this thesis (each of Chapters 2 through 7 is a separate, published or submitted paper, corresponding to Refs. [7, 8, 9, 10, 11, 12], respectively), we develop a different method that allows for solving for the evolution of all three constants of motion, even when the orbit is out of the equatorial plane. By computing a radiation reaction force which acts on the particle, we compute how this force changes the three constants. As expected, the computed changes in the first two constants of motion are in agreement with the changes predicted by using conservation laws. Knowledge of the previously uncomputed evolution of the third constant completes the circle of tasks.

Unfortunately, our Chapter 2 calculation is restricted to the limit of large orbits (that is, we compute the first post-Newtonian term in a post-Newtonian series). Moreover, we compute the evolution only for orbits which are initially "circular." These "circular orbits" are ones which have a constant value of (Boyer-Lindquist coordinate) radius r; they are not really circles because the plane of the orbit precesses around the black hole's spin axis. Our result shows that these orbits remain circular under radiation reaction, at least to the leading post-Newtonian order to which the calculation is valid. That is, the initially circular orbit will evolve into another circular orbit at a smaller value of r. Interestingly enough, the orbital angular momentum evolves slightly towards antialignment with the black hole's spin angular momentum.

Chapter 3 is an extension of Chapter 2 to orbits which are elliptical in addition to being out of the equatorial plane. Similar to the case with circular orbits, radiation reaction drives eccentric, large orbits towards antialignment with the black hole's spin. Chapter 3 also contains a proof of a conjecture by Kennefick and Ori (which they have independently proved by a different method [13]) that circular orbits around a Kerr black hole remain circular exactly (not just in the limit of large radius, as shown in Chapter 2). Our proof is based on a property that these circular orbits possess: they are "reflection symmetric" in the sense that the path of the orbit on one side of the equatorial plane is duplicated by the path on the other side during the next half orbit. This symmetry is preserved under radiation reaction. It turns out that slightly elliptical (noncircular) orbits are

never reflection symmetric. Therefore, a circular orbit, which is reflection symmetric and must remain so even as it evolves under radiation reaction, can only evolve into another circular orbit.

Our discussion in Chapters 2 and 3 is based on the assumption that the larger-mass object (the central body) with mass M is a black hole. For the remainder of this thesis (Chapters 4 through 7), we consider how we can use the gravitational waves to determine whether the central body is indeed a black hole or instead some other type of massive, compact object [14]—e.g., a (hypothetical) boson star [17], soliton star [18], or naked singularity. In Chapter 4, we look at how the gravitational waves carry the information to make such a determination. In Chapter 5, we consider boson stars as a concrete example. In Chapter 6, we consider how the noise of the gravitational-wave detectors affects how accurately we can make the determination. In Chapter 7, we develop a numerical scheme that might aid in the construction of the templates needed to search for non-black-hole, compact bodies.

To what extent do the gravitational waves carry information of the exterior gravitational field of the larger-mass object? This question is addressed in Chapter 4 of this thesis. We restrict the gravitational field of the central body to be stationary (unchanging in time), axially symmetric, and reflection symmetric across the equatorial plane. We can describe this exterior gravitational field by two infinite sets of Geroch-Hansen scalar multipole moments [15, 16]. One set consists of the mass moments, which include the mass itself (which is M), the mass quadrupole moment, and an infinite sequence of higher moments. The other set consists of the current moments, which include the spin angular momentum, the current octopole moment, and an infinite sequence of higher moments. For black holes, these moments satisfy simple relations among themselves, as dictated by the black-hole "no-hair" theorem (really "two-hair" theorem): All the moments can be expressed uniquely in terms of the mass and the spin. For other types of candidate objects that we might search for, such as boson stars [17], soliton stars [18], or naked singularities, these moments may satisfy some completely different relations, or may all be independent.

In Chapter 4, we restrict attention to the simplest case of the orbiting object traveling through

vacuum in the central body's equatorial plane in a circle which slowly shrinks in radius as gravitational waves are emitted. We show that all the multipole moments are encoded in these gravitational waves, in fact in (at least) four independent ways:

1. The dominant gravitational-wave frequency F (twice the orbital frequency $F_{\rm orb}$) sweeps upwards as a function of time. If we could measure the cumulative gravitational-wave energy that has been emitted as a function of the dominant gravitational-wave frequency, $E_{\rm GW}(F)$, or equivalently $dE_{\rm GW}/dF$, then we would be able to deduce the moments from this function. This ability arises because each moment first appears in the post-Newtonian expansion for the energy at a different post-Newtonian order. We show how to compute the post-Newtonian expansion for the energy as a function of orbital frequency. We list the first few terms of this series. Unfortunately, we cannot actually measure the cumulative energy, because we can only measure the energy that is emitted in the direction of Earth instead of that emitted in all directions. However, this exercise shows that the waves carry the values of all the moments.

2. If the orbit is not exactly a circle, but rather slightly elliptical, then the orbit will precess at a frequency $F_{\rm prec,1}$ which is a function of the orbital frequency (and correspondingly, a function of the dominant gravitational-wave frequency $F = 2F_{\rm orb}$). This precession law $F_{\rm prec,1}(F)$ can be measured by gravitational-wave detectors. We perform the same type of analysis as we just described for the energy, and conclude that the function $F_{\rm prec,1}(F)$ contains, in an extractable form, all the moments of the central body.

3. If the (almost) circular orbit is slightly out of the equatorial plane (of a non-spherically-symmetric central body), then the orbit will precess with a different type of precession than that described above for elliptical orbits. This precession frequency, which is a function of the gravitational-wave frequency, $F_{\rm prec,2}(F)$, can be measured by the detectors. We show that it contains in extractable form all the body's moments.

4. The most accurate way of determining the moments is by measuring the phase Φ of the dominant gravitational-wave frequency component, as a function of that frequency F. Here too, we show that each moment appears at a different order in the post-Newtonian series and thus can be extracted from measurements of $\Phi(F)$. However, while we do know how each moment first enters into the series, we have not yet calculated how the moment appears at higher orders. That is, we have not solved the (very difficult) equations for wave generation around a body with arbitrary multipole moments. Therefore, we cannot give a complete prescription of how all the moments can be determined, but rather just a proof that if the series were completely known, then all the moments could be deduced from $\Phi(F)$, or equivalently from $d\Phi/dF = 2\pi F/(dF/dt)$.

As mentioned, our analysis in Chapter 4 is performed with some idealizing assumptions (nearly circular orbits, nearly in the equatorial plane) and with a key task left incomplete [computing the full details of $\Phi(F)$]. Let us assume that these gaps are filled by the time that the inspiral sources are detected and analyzed, so that we can measure the multipole moments of the central body. How well can these moments determine what the central body is? First of all, we have to hope that the central body is spinning; for if not, then it would probably be spherically symmetric and all the moments except for the mass would be zero. By measurements of the multipole moments alone, we cannot distinguish a spherically symmetric black hole from, say, a spherically symmetric soliton star. But even if the central body is spinning, it might be the case that the moments of another type of candidate object may satisfy relations among themselves which are indistinguishably close to the relations that a black hole's moments satisfy. To get a feel for whether or not this is so, it would be useful to see how the moments for another type of object are related to each other.

For such an other candidate object, we choose spinning boson stars with large self-interaction. Boson stars are conglomerations of a scalar field ϕ with scalar field mass m, held together by gravity and supported against collapse by the Heisenberg uncertainty principle. Equivalently, they are a condensate of a huge number of zero-spin bosons which interact gravitationally. These "stars"

were first studied by Ruffini and Bonazolla in 1968 [17]. However, the Ruffini-Bonazolla stars had masses far below the range of interest for gravitational-wave detectors. In 1986, Colpi, Shapiro, and Wasserman [19] discovered that by adding a large self-interaction term $\lambda|\phi|^4$ to the scalar field Lagrangian, the mass of the star can be made large. In fact, it can be made large enough so as to be relevant for our purpose. They considered only nonspinning boson stars. Our objective is to generalize their results to the spinning case, for only in that case are the moments (besides the mass) nonzero.

In Chapter 5 of this thesis, we compute the structure of these large-λ boson stars, subject to the plausible condition that the emission of waves has driven the star into a stationary and axially symmetric state. We find that such stars are completely described by three parameters (three "hairs"). (This is analogous to a black hole being described by two "hairs", its mass and spin.) One parameter is $\lambda^{1/2}/m^2$, which sets the overall scale of the star; that is, all quantities with dimensions of length such as the mass of the star and the radius of the star scale with $\lambda^{1/2}/m^2$. Because this first parameter has a rather trivial effect, our computations effectively span a two-dimensional space. The second parameter corresponds to the spin of the star. The third parameter corresponds to the compactness of the star.

For a representative set of "points" in this two-dimensional space, we compute the structure of the star and, from that, the values of the first few multipole moments. Each computation is done by solving Einstein's gravitational-field equations with a method of Komatsu, Eriguchi, and Hachisu [20]. It consists of taking the field equations $G^{\mu\nu} = 8\pi T^{\mu\nu}$ and keeping on the left-hand side terms for which we know the flat-space Green's function while moving to the right-hand side all the other terms. The metric functions can be numerically computed as integrals of the Green's function multiplied by the sum of $8\pi T^{\mu\nu}$ and the terms that were brought over to the right-hand side. Since these terms involve the metric functions themselves, several iterations have to be performed to converge on the solution.

We find that spinning boson stars are shaped like doughnuts, with vacuum along the axis of

symmetry (the spin axis). We also find that for the same mass and spin, a boson star will typically have a much larger quadrupole moment than will a black hole, making the two types of objects distinguishable.

Given values of the three parameters that specify a spinning boson star, we can compute all the moments. These computed moments can be compared with the moments measured by gravitational-wave detectors. For example, we can use the first three measured moments (the mass, the spin angular momentum, and the mass quadrupole moment) to deduce the three boson star parameters. Then, we can use these three values and the results of Chapter 5 to compute the value of the next moment (the current octopole moment). Finally, we can compare this computed value with the measured value of the current octopole moment. If there is good agreement, then we have evidence for a spinning boson star, and we can be sure the object is not a black hole.

The results in this thesis thus far give us (after the detectors are built and the full details of the waves have been computed) the ability to search for black holes and $\lambda|\phi|^4$ boson stars. Expanding this list to include other types of candidate objects will require studies of these objects. For such studies that involve numerical computations, it would be useful to know how accurate those computations have to be. If the gravitational-wave detectors can only measure a certain moment to some accuracy, then for the purpose of searching for that object, the value of that moment would not need to be calculated to much greater accuracy. In Chapter 6 of this thesis, we turn to the data analysis question of the expected accuracies for measuring the multipole moments.

Similar data analysis calculations have been performed by others: Finn [21], Finn and Chernoff [22], Cutler and Flanagan [23], and Poisson and Will [24] have established the data analysis formalism (that we shall use) and have analyzed measurement accuracies for the mass and spin parameters of compact binaries for Earth-based detectors such as LIGO. Poisson [25] has used the same type of data analysis formalism for space-based detectors such as LISA. Our objective is to extend these works to include the measurement accuracies for higher order multipole moments.

Our calculation requires making several assumptions, most significantly that the inspiraling

object travels in a circular orbit in the central body's equatorial plane. We estimate the measurement accuracies by using a simplified model for how the templates depend on the multipole moments, a model consisting of only the leading post-Newtonian order effect of each moment on the waveforms. Although this model might introduce sizable errors in our analysis, we use it for two reasons: First, just knowing the order-of-magnitude accuracy for each moment is useful information for determining to what accuracy various calculations have to be performed. Second, we currently have no choice, because, as mentioned in our discussion of Chapter 4, nobody has yet computed the full details of the gravitational waves produced from an inspiral around a body with arbitrary multipole moments.

If we assume an amplitude signal-to-noise ratio $S/N = 10$ for the measured signals, then it turns out that LIGO cannot give sufficiently accurate measurements of the moments to determine whether the central body is a black hole or some other type of compact object. On the other hand, for the same signal-to-noise ratio, LISA can make this determination with high accuracy. The difference arises from the fact that, typically, a signal measured by LISA (at frequencies $F \sim 10^{-3}$ to 10^{-1} Hz) has many more cycles than one measured by LIGO (at $F \sim 10^{+1}$ to 10^{+3} Hz).

Our analyses in Chapters 4 and 6 are primarily limited by the fact that we do not currently have a good algorithm for solving the equations for wave generation around a body with arbitrary multipole moments and by the fact that we consider only circular orbits in the equatorial plane. For our final chapter, we make an attempt to tackle the former limitation. We would like to compute the full details of the gravitational waves produced when the orbiting particle travels in a circle and the central body has arbitrary multipole moments. This itself involves two difficulties: First, the two-dimensional gravitational-wave-generation differential equations cannot be solved by a separation-of-variables method. Second, the problem is complicated by the gravitational field having many tensor components which are coupled in those equations. (Neither of these difficulties occurs when the central body is a black hole, as Saul Teukolsky showed in his Caltech Ph.D. thesis a quarter-century ago.)

Chapter 7 is an attempt to develop a method that tackles only the first difficulty: we solve the problem with the gravitational-wave-generation equations replaced by the scalar-wave-generation equation and with the object (in a circular, equatorial orbit) given a scalar charge. This toy problem allows for the development of an efficient algorithm for solving a two-dimensional differential equation which is similar to but simpler than the problem we eventually want to solve.

Our method uses a numerical iteration process very similar to that used in Chapter 5 for solving for the structure of boson stars. We take the curved-space scalar field equation and keep on one side of the equation only the flat-space d'Alembertian term (for which we know the Green's function) and place on the other side all other terms. Then we iterate much as is done in Chapter 5. The method turns out to converge very efficiently for orbits of radius greater than about $8M$, but is not that efficient for smaller orbits. The next, yet undone, step would be to replace the scalar-wave generation equation with the gravitational-wave generation equations.

Clearly, there are many tasks left for the future. This thesis may only be a preview of these tasks, but it demonstrates that upon completion of them, upon construction of the detectors, and upon measurements of the signals, we will have the power to confirm the existence of black holes and search for other exotic, compact objects. Although it may be unlikely that any very massive, compact objects besides black holes actually exist in sufficient profusion to be found, any discovery of such an object would be of so high importance as to make these tasks worth pursuing.

References

[1] K. S. Thorne, in *Particle and Nuclear Astrophysics and Cosmology in the Next Millennium: Proceedings of the 1994 Snowmass Summer Study, Snowmass, Colorado, June 29–July 14, 1994*, eds. E. W. Kolb and R. Peccei (World Scientific, Singapore, 1995).

[2] B. F. Schutz, Class. & Quant. Grav. **13**, A219 (1996).

[3] A. Abramovici, W. E. Althouse, R. W. P. Drever, Y. Gürsel, S. Kawamura, F. J. Raab, D. Shoemaker, L. Sievers, R. E. Spero, K. S. Thorne, R. E. Vogt, R. Weiss, S. E. Whitcomb, and M. E. Zucker, *Science* **256**, 325 (1992).

[4] P. Bender, I. Ciufolini, K. Danzmann, W. M. Folkner, J. Hough, D. Robertson, A. Rüdiger, M. C. W. Sandford, R. Schilling, B. Schutz, R. Stebbins, T. Sumner, P. Touboul, S. Vitale, H. Ward, and W. Winkler, *LISA: Laser Interferometer Space Antenna for the detection and observation of gravitational waves*, Pre-Phase A Report (1995).

[5] B. Carter, chapter 6 of *General Relativity: an Einstein Centenary Survey*, eds. S. W. Hawking and W. Israel (Cambridge University Press, Cambridge, 1979).

[6] C. W. Misner, K. S. Thorne, and J. A. Wheeler, *Gravitation* (Freeman, San Francisco, 1973).

[7] F. D. Ryan, Phys. Rev. D **52**, R3159 (1995).

[8] F. D. Ryan, Phys. Rev. D **53**, 3064 (1996).

[9] F. D. Ryan, Phys. Rev. D **52**, 5707 (1995).

[10] F. D. Ryan, to appear in Phys. Rev. D, May 15, 1997.

[11] F. D. Ryan, submitted to Phys. Rev. D.

[12] F. D. Ryan, submitted to Phys. Rev. D.

[13] D. Kennefick and A. Ori, Phys. Rev. D **53**, 4319 (1996).

[14] F. D. Ryan, L. S. Finn, and K. S. Thorne, in preparation.

[15] R. Geroch, J. Math. Phys. **11**, 2580 (1970).

[16] R. O. Hansen, J. Math. Phys. **15**, 46 (1974).

[17] R. Ruffini and S. Bonazolla, Phys. Rev. **187**, 1767 (1969). Discussions of later work concerning spherical boson stars can be found in the following review articles: A. R. Liddle and

M. S. Madsen, Int. J. Mod. Phys. D **1**, 101 (1992). P. Jetzer, Phys. Rep. 220, 163 (1992). T. D. Lee and Y. Pang, Phys. Rep. 221, 251 (1992).

[18] T. D. Lee and Y. Pang, Phys. Rep. **221**, 251 (1992).

[19] M. Colpi, S. L. Shapiro, and I. Wasserman, Phys. Rev. Lett. **57**, 2485 (1986).

[20] H. Komatsu, Y. Eriguchi, and I. Hachisu, Mon. Not. R. Astr. Soc., **237**, 335 (1989).

[21] L. S. Finn, Phys. Rev. D **46**, 5236 (1992).

[22] L. S. Finn and D. F. Chernoff, Phys. Rev. D **47**, 2198 (1993).

[23] C. Cutler and É. E. Flanagan, Phys. Rev. D **49**, 2658 (1994).

[24] E. Poisson and C. M. Will, Phys. Rev. D **52**, 848 (1995).

[25] E. Poisson, Phys. Rev. D **54**, 5939 (1996).

2 Effect of gravitational radiation reaction on circular orbits around a spinning black hole

Abstract

The effect of gravitational radiation reaction on circular orbits around a spinning (Kerr) black hole is computed to leading order in S (the magnitude of the spin angular momentum of the hole) and in the strength of gravity M/r (where M is the mass of the black hole, r is the orbital radius, and $G = c = 1$). The radiation reaction makes the orbit shrink but leaves it circular, and drives the orbital plane very slowly toward antialignment with the spin of the hole: $\tan(\iota/2) = \tan(\iota_0/2)[1+(61/72)(S/M^2)(M/r)^{3/2}]$, *where ι is the angle between the normal to the orbital plane and the spin direction, and ι_0 is the initial value of ι, when r is very large.*

The earth-based LIGO/VIRGO network of gravitational wave detectors (which is now under construction) will be used to search for and study the gravitational waves from "particles," such as neutron stars and small black holes, spiraling into massive black holes (mass M up to $\sim 300M_\odot$); and ESA's planned space-based LISA [1] interferometer will do the same for inspirals into supermassive black holes (M up to $\sim 10^7 M_\odot$). To search for the inspiral waves and extract the information they carry will require templates based on theoretical calculations of the emitted waveforms; and to compute the waveforms requires a detailed understanding of how radiation reaction influences the orbital evolution.

For several years a stumbling block has impeded computations of the evolution, when the orbital plane of the particle is inclined to the equatorial plane of a spinning hole: No practical method has been developed to deduce how radiation reaction influences the evolution of the orbit's "Carter constant" [2, 3], which governs the orbital shape and inclination angle. This paper describes the

first progress on this problem: a "post-Newtonian" gravitational radiation reaction force is used to compute the full orbital evolution to first order in S, the magnitude of the spin angular momentum of the black hole, and leading order in the strength of gravity M/r at the orbital radius r. (Here and throughout, units with $G = c = 1$ are used.) The analysis is restricted to orbits that initially are "circular" (more precisely, orbits which have constant radius r—these orbits are circular in the "orbital plane" discussed below, but this plane precesses). However, the method can readily be extended to noncircular orbits [4] and (with considerably more difficulty) should be extendible to the fully relativistic regime $r \sim M$.

The computation of the evolution presented here proceeds as follows: First, in the absence of radiation reaction, the orbital motion and the associated constants of motion are reviewed. Then, the leading order radiation reaction accelerations that act on the orbiting particle and on the hole are derived and used to compute the radiation-reaction-induced evolution of the constants of motion. Finally, the evolution of the orbit—its shape and inclination angle—is obtained.

The leading order effect of the spin on the (otherwise Newtonian) orbit was deduced long ago by Lense and Thirring [5] (reviewed by Landau and Lifshitz [6])—though, of course, they regarded the central body as a star rather than a black hole. In fact, our analysis does not require the body to be a black hole (rather, it can be any spinning body), but since this is the primary case of physical interest, the discussion is phrased in terms of a black hole.

Let spherical polar coordinates, r, θ, and ϕ, centered on the black hole, be used to describe the location of the particle (these coordinates describe the relative separation of the two bodies), with the hole's spin along the polar axis. The Lagrangian [7] for the motion of the particle (which, for now, does not have to be circular) is given, to linear order in S but otherwise in solely Newtonian theory, by

$$\mathcal{L} = \frac{\mu}{2}\left(\dot{r}^2 + r^2\dot{\theta}^2 + r^2\sin^2(\theta)\dot{\phi}^2\right) + \frac{\mu M}{r} - \frac{2\mu S\sin^2\theta}{r}\dot{\phi}, \tag{1}$$

where μ is the mass of the particle. In general, an overdot represents d/dt. The entire analysis is to leading order in μ. To leading order in S and in M/r, the motion resulting from this Lagrangian

is the same as in the Kerr metric, which describes the gravitational field of a spinning hole. The use of flat space coordinates, which ignores M/r corrections, is adequate to leading order.

Following standard procedure [8], the Hamilton-Jacobi equation associated with the Lagrangian (1) can be shown to have a separation-of-variables (t, ϕ, r, θ) solution, which reveals three constants of motion:

$$E = \frac{\mu}{2}\left(\dot{r}^2 + r^2\dot{\theta}^2 + r^2\sin^2(\theta)\dot{\phi}^2\right) - \frac{\mu M}{r}, \tag{2}$$

$$L_z = \mu r^2 \sin^2(\theta)\dot{\phi} - \frac{2\mu S \sin^2\theta}{r}, \tag{3}$$

$$Q + L_z^2 = \mu^2 r^4\left(\dot{\theta}^2 + \sin^2(\theta)\dot{\phi}^2\right) - 4\mu^2 S r \sin^2(\theta)\dot{\phi}. \tag{4}$$

Comparing these expressions to Eqs. (33.31) of Ref. [3], it is clear that E, L_z, and Q correspond, to leading order in S and in M/r, to the constants of motion for a test particle in the Kerr metric: the energy minus the test particle mass, the z-component (component along the spin axis of the hole) of angular momentum, and the Carter constant, respectively.

The analysis of radiation reaction, below, is in Cartesian coordinates, $x_1 = r\sin\theta\cos\phi$, $x_2 = r\sin\theta\sin\phi$, and $x_3 = r\cos\theta$. In these coordinates, the constants of motion (2)–(4) become (repeated indices are summed)

$$E = \frac{\mu}{2}\dot{x}_j\dot{x}_j - \frac{\mu M}{(x_j x_j)^{1/2}}, \tag{5}$$

$$L_z = \mu\epsilon_{3jk}x_j\dot{x}_k - \frac{2\mu S\left(x_1^2 + x_2^2\right)}{(x_j x_j)^{3/2}}, \tag{6}$$

$$Q + L_z^2 = \mu^2\epsilon_{ijk}x_j\dot{x}_k\epsilon_{ilm}x_l\dot{x}_m - \frac{4\mu^2 S\epsilon_{3jk}x_j\dot{x}_k}{(x_m x_m)^{1/2}}. \tag{7}$$

Let the orbital plane have inclination angle ι (restricted to $0 \le \iota \le \pi$, where $\iota > \pi/2$ corresponds to an orbit counter-rotating relative to the spin), defined as

$$\cos\iota \equiv \frac{L_z}{(Q + L_z^2)^{1/2}}. \tag{8}$$

The constants of motion admit orbits of constant radius, just as for the Kerr metric in Boyer-Lindquist coordinates. One of the Euler-Lagrange equations implies that, for r to be constant,

$\partial\mathcal{L}/\partial r = 0$, which leads to

$$r = My^{-2}\left[1 + 6(S/M^2)y^3\cos\iota\right], \tag{9}$$

$$y \equiv \left(\frac{Q + L_z^2}{\mu^2 M^2}\right)^{-1/2}. \tag{10}$$

The positive root in any square root is always chosen.

The following relationship between the constants of motion for circular orbits is easily derived:

$$E = -\frac{1}{2}\mu y^2\left[1 - 4(S/M^2)y^3\cos\iota\right]. \tag{11}$$

The other two Euler-Lagrange equations predict that $\theta(t)$ and $\phi(t)$ are the same as for a circular orbit in the case when $S = 0$, except that $\dot{\phi}$ is altered to $\dot{\phi} = \dot{\phi}|_{S=0} + 2S/r^3$. By transforming these angular motions to Cartesian coordinates, the following equations for the orbit are obtained:

$$x_1 = r\left[\cos(\Omega_\theta t)\cos\left(\frac{2St}{r^3}\right)\cos\iota - \sin(\Omega_\theta t)\sin\left(\frac{2St}{r^3}\right)\right], \tag{12}$$

$$x_2 = r\left[\sin(\Omega_\theta t)\cos\left(\frac{2St}{r^3}\right) + \cos(\Omega_\theta t)\sin\left(\frac{2St}{r^3}\right)\cos\iota\right], \tag{13}$$

$$x_3 = r\cos(\Omega_\theta t)\sin\iota, \tag{14}$$

where the angular velocity in the x_3 direction is

$$\Omega_\theta \equiv M^{-1}y^3\left[1 - 12(S/M^2)y^3\cos\iota\right]. \tag{15}$$

These equations describe a circular orbit on a plane (the orbital plane, which is inclined at angle ι to the equatorial plane) which precesses around the spin axis of the black hole with angular velocity $2S/r^3$ (the Lense-Thirring precession). Because the particle's motion is the sum of the circular motion and the plane precession, the particle itself does not travel on a fixed plane, nor does it travel in a circle, nor does it cross the equatorial plane at angle ι, but rather at an angle ι' [9].

Turn, now, to the gravitational radiation reaction force (or acceleration) that slowly modifies the above orbital motion. The emitted waves and their associated radiation reaction can be expressed in terms of the multipole moments of the "system" (particle plus hole) [10, 11]. In the absence

of spin, $S = 0$, the reaction, at leading order in M/r, is due to the mass quadrupole moment I_{ij} of the system; when $S \neq 0$, the leading order influence of S on the reaction is due in part to the mass quadrupole moment I_{ij} and in part to the current quadrupole moment J_{ij}. The moments I_{ij} and J_{ij} are usually written as integrals over the mass and momentum densities of the source. For the black hole, however, this cannot be done, and even for a neutron star the standard integrals are invalid because they ignore the star's relativistic gravity. There is an alternative approach, however, that does work for this black-hole-plus-particle system: the moments are defined in terms of the weak, asymptotic gravitational fields far from the hole and particle. When this is done, all the standard formulas of the multipolar gravitational wave formalism remain valid [10].

The standard theory of the radiation reaction force (for example, Ref. [11]) is generally formulated in the center-of-mass Cartesian coordinate system $\{x'_j\}$, which differs from the black-hole-centered coordinates $\{x_j\}$ used above. In the asymptotic, center-of-mass coordinates, the hole (or rather its asymptotically spherical gravitational field [10, 12]) moves along the path $x'_k(t) = -(\mu/M)x_k(t)$ with its spin still pointing in the x_3 direction, and the particle moves along the path $x'_k(t) = [1-(\mu/M)]x_k(t)$. Correspondingly, to leading order in μ/M, the mass and current quadrupole moments are

$$I_{ij} = [\mu x_i x_j]^{STF}, \tag{16}$$

$$J_{ij} = \left[\mu x_i \epsilon_{jkm} x_k \dot{x}_m - \frac{3}{2}(\mu/M) x_i S\delta_{j3}\right]^{STF}. \tag{17}$$

Here, STF means "symmetrize and remove the trace," and $x_i = x_i(t)$ is the trajectory of the particle in the hole-centered coordinates, as given by Eqs. (12)–(14).

Equations (16) and (17) agree with the $\mu \ll M$ limit of the moments given in Kidder, Will, and Wiseman (Ref. [7], Eqs. (14a,c)). The first term of J_{ij} is the standard contribution due to the motion of the particle; the second term arises from the motion of the spin of the hole relative to the asymptotic, center-of-mass inertial frame: when the current dipole moment, due to the hole's spin angular momentum $J_i = S\delta_{i3}$, is displaced from the system's center of mass

by $\delta x_i' = -(\mu/M)x_i$ due to the orbital motion, that displacement produces a current quadrupole moment $J_{ij} = [3/2\delta x_i' J_j]^{STF}$ = [second term in expression (17)], as one can deduce from the asymptotic metric components by which the moments are defined: Eq. (11.1b) of Ref. [10].

Consider, for the moment, the radiation reaction force acting individually on the hole or on the particle. Let the object of interest (hole or particle) have a location x_j' and velocity $\dot{x}_j'$ in the asymptotic, center-of-mass coordinates. Then, for the moment ignoring the object's spin, its radiation reaction acceleration (force divided by mass) is given by

$$a_j^{(react)} = -\frac{2}{5} I_{jk}^{(5)} x_k' + \frac{16}{45}\epsilon_{jpq} J_{pk}^{(6)} x_q' x_k' + \frac{32}{45}\epsilon_{jpq} J_{pk}^{(5)} x_k' \dot{x}_q' + \frac{32}{45}\epsilon_{pq[j} J_{k]p}^{(5)} x_q' \dot{x}_k'. \tag{18}$$

This can be derived from Eqs. (11) and (12) of Blanchet and Damour [11], keeping only the mass quadrupole and current quadrupole moment terms. Here, the brackets denote antisymmetrization: $C_{[jk]} \equiv (C_{jk} - C_{kj})/2$. The number in parentheses to the upper right of a multipole moment indicates taking that number of time derivatives.

The coupling of the object's spin angular momentum J_i to the radiation reaction field due to J_{ij} produces an additional radiation reaction acceleration,

$$a_j^{(react)}|_{spin} = -\frac{8}{15} J_{ij}^{(5)} J_i/m, \tag{19}$$

where m is the mass of the object. If the spinning object were nearly Newtonian, Eq. (19) could be derived by adding up the velocity dependent radiation reaction force [mass×Eq. (18)] on each bit of mass inside the source and then dividing by the total mass m of the object. For the black hole, such a procedure is invalid; however, the result (19) must still be true: The analysis of Thorne and Hartle [12], specifically their Eq. (1.9b), shows that the force on any isolated spinning object in a "gravitomagnetic field" (the type of radiation reaction field that is responsible for this force [11]) is the same as for a spinning mass with only weak self-gravity.

Since the constants of motion, E, L_z, and Q, are defined and expressed in terms of black-hole-centered coordinates rather than center-of-mass coordinates, their evolution must be computed using the radiation reaction acceleration of the particle relative to the black hole, i.e. the difference

of the accelerations of the particle and the hole relative to the center-of-mass:

$$a_j \equiv a_j^{(react)}|_{particle} - a_j^{(react)}|_{black\ hole} \tag{20}$$

$$= -\frac{2}{5}I_{jk}^{(5)}x_k + \frac{16}{45}\epsilon_{jpq}J_{pk}^{(6)}x_q x_k + \frac{32}{45}\epsilon_{jpq}J_{pk}^{(5)}x_k\dot{x}_q + \frac{32}{45}\epsilon_{pq[j}J_{k]p}^{(5)}x_q\dot{x}_k + \frac{8}{15}(S/M)J_{3j}^{(5)}. \tag{21}$$

Here, the moments I_{ij} and J_{ij} are given by Eqs. (16) and (17). There is no contribution to (21) (up to leading order in μ) from the acceleration on the hole except through the spin interaction (19), which gives the fifth term in Eq. (21). For the J_{ij} in the contribution to the acceleration on the particle [the second, third, and fourth terms of Eq. (21)], only the second term of Eq. (17) needs to be kept: the contribution from the first term is not at leading order in M/r for either terms not involving S or terms involving S. Similarly, the J_{3j} in the fifth term of Eq. (21) requires only the contribution from the first term of Eq. (17).

By differentiating Eqs. (5)–(7) with respect to time and using the a_j of Eqs. (20) and (21) as the radiation reaction contribution to $\ddot{x}_j$, we obtain the following evolution of the "constants" of motion:

$$\dot{E} = \mu\dot{x}_j a_j, \tag{22}$$

$$\dot{L}_z = \mu\epsilon_{3jk}x_j a_k, \tag{23}$$

$$\dot{Q + L_z^2} = 2\mu^2\epsilon_{ijk}x_j\dot{x}_k\epsilon_{ilm}x_l a_m - \frac{4\mu^2 S\epsilon_{3jk}x_j a_k}{(x_m x_m)^{1/2}}. \tag{24}$$

While Eqs. (16)–(24) are valid for noncircular orbits as well as circular orbits, we will treat only circular orbits here. Suppose that the orbit initially is circular, so the trajectory of the particle $x_k(t)$ in the hole-centered coordinates is given by Eqs. (12)–(14). Then, the evolution of its constants of motion, E, L_z, and $Q + L_z^2$, can be computed as follows. Insert the trajectory of the particle (12)–(14) into Eqs. (16) and (17) to get the I_{ij} and J_{ij} moments. Then, insert these moments and the trajectory of the particle into Eq. (21) to get the relative radiation reaction acceleration. Insert this acceleration into Eqs. (22)–(24) for the time derivatives of E, L_z, and

$Q + L_z^2$, and average the resulting expressions over an orbit. [The averaging, denoted by $\langle\ \rangle$, can be taken to involve times $-\pi/\Omega_\theta < t < +\pi/\Omega_\theta$, and because of this restriction to small t, for terms in the trajectory (12)–(14) that have argument $2St/r^3$, the cosine can be replaced by 1 and the sine can be replaced by its argument, thereby simplifying the calculation.] The result is [13]

$$\left\langle \dot{E} \right\rangle = -\frac{32}{5}\frac{\mu^2}{M^2}y^{10}\left(1 - \frac{433}{12}\frac{Sy^3}{M^2}\cos\iota\right), \tag{25}$$

$$\left\langle \dot{L}_z \right\rangle = -\frac{32}{5}\frac{\mu^2}{M}y^{7}\left(\cos\iota + \frac{61 - 687\cos^2\iota}{24}\frac{Sy^3}{M^2}\right), \tag{26}$$

$$\left\langle \dot{Q + L_z^2} \right\rangle = -\frac{64}{5}\mu^3 y^6\left(1 - \frac{313}{12}\frac{Sy^3}{M^2}\cos\iota\right). \tag{27}$$

Equations (25) and (26) agree [16] (after trivial conversions of notation) with previous results (Ref. [14], Eqs. (3.13), (3.18) and Ref. [15], Eqs. (4.10), (4.11)).

These time derivatives of the constants of motion have two major implications for the orbital evolution: First, they imply that the orbit, which was assumed initially circular, remains circular; this can be seen from the fact that they preserve the circular-orbit relationship (11). Second, when combined with Eqs. (8), they imply the following evolution of the orbital plane's inclination angle:

$$\left\langle \frac{d\iota}{dt} \right\rangle = \frac{244}{15}\frac{\mu S}{M^4}y^{11}\sin\iota. \tag{28}$$

This equation implies that radiation reaction drives the orbital plane toward antialignment with the spin, as *might* be intuitively expected since that orientation minimizes the energy of spin-orbit coupling [17].

By combining Eq. (28) with the leading order change in r, $\dot{r} = -\frac{64}{5}(\mu/M)y^6$, the following differential equation relating r and ι is obtained:

$$\frac{d\iota}{-d\ln r} = \frac{61}{48}\frac{S}{M^2}\left(\frac{M}{r}\right)^{3/2}\sin\iota. \tag{29}$$

The time-averaging of the left hand side of Eq. (29) is not explicitly written down. Integrating Eq. (29) yields

$$\tan(\iota/2) = \tan(\iota_0/2)[1 + \frac{61}{72}(S/M^2)(M/r)^{3/2}], \tag{30}$$

where ι_0 is the value of the inclination angle when the orbit has large radius.

Equation (30) shows, for example, that for an $S \lesssim M^2$ black hole, if the particle orbits with a small inclination angle ($0 \lesssim \iota \ll \pi$), then ι fractionally changes by 0.06 from its initial value at large radius to its value at $r \approx 6M$. The regime $r \lesssim 6M$ is of special interest; it is there that waves from the final stages of inspiral can give high-accuracy maps of the hole's spacetime geometry [18]. However, when $r \approx 6M$, our leading order analysis breaks down, so that to be able to map the hole's geometry, the analysis must be carried out to higher order in M/r and S.

The above analysis illustrates the power of the radiation reaction force method to reveal the detailed evolution of a system under radiation reaction. The case solved was sufficiently simple to give an easily presented solution. A future paper [4] will give more details of the above calculations, along with the generalization to eccentric orbits. Hopefully, future work with radiation reaction forces will: (1) Generalize the analysis to an arbitrary mass ratio μ/M and the case of both masses having spin. (2) Extend the analysis to higher order in M/r and in S. (3) Achieve a similar calculation of the orbital evolution in the fully relativistic Kerr metric.

Acknowledgments

The author is grateful to Alan Wiseman and Kip Thorne for their advice. This work was supported by NSF grants AST-9114925 and AST-9417371, and by NASA grants NAGW-2897 and NAGW-4268.

References

[1] K. Danzmann, A. Rüdiger, R. Schilling, W. Winkler, J. Hough, G. P. Newton, D. Robertson, N. A. Robertson, H. Ward, P. Bender, J. Faller, D. Hils, R. Stebbins, C. D. Edwards, W. Folkner, M. Vincent, A. Bernard, B. Bertotti, A. Brillet, C. N. Man, M. Cruise, P. Gray, M. Sandford, R. W. P. Drever, V. Kose, M. Kühne, B. F. Schutz, R. Weiss, and H.

Welling, *LISA: Proposal for a Laser-Interferometric Gravitational Wave Detector in Space* (Max-Planck-Institut für Quantenoptik, Garching bei München, Germany, 1993).

[2] B. Carter, Phys. Rev. **174**, 1559 (1968).

[3] C. W. Misner, K. S. Thorne, and J. A. Wheeler, *Gravitation* (Freeman, San Francisco, 1973).

[4] For brevity, our discussion is limited to circular orbits; the more complicated case of eccentric orbits is solved but deferred to a future paper: F. D. Ryan, in preparation.

[5] J. Lense and H. Thirring, Phys. Z. **19**, 156 (1918). English translation in Gen. Rel. & Grav. **16**, 727 (1984).

[6] L. D. Landau and E. M. Lifshitz, *The Classical Theory of Fields*, 4th rev. English ed. (Pergamon, Oxford, 1975).

[7] L. E. Kidder, C. M. Will, and A. G. Wiseman, Phys. Rev. D **47**, R4183 (1993).

[8] H. Goldstein, *Classical Mechanics* (Addison-Wesley, Reading, Massachusetts, 1950).

[9] The angle ι' is defined as the angle between the Newtonian orbital angular momentum $L_{N_i} \equiv \mu\epsilon_{ijk}x_j\dot{x}_k$ and the spin axis, so that when the particle crosses the equator, it does so at angle ι'. However, neither L_{N_i} nor ι' is a constant of the motion. For circular orbits, ι' is given by $\cos\iota' = \cos\iota + 2(S/M^2)y^3(\sin^2\theta - \cos^2\iota)$.

[10] K. S. Thorne, Rev. Mod. Phys. **52**, 299 (1980).

[11] L. Blanchet and T. Damour, Phys. Lett. **104A**, 82 (1984).

[12] K. S. Thorne and J. B. Hartle, Phys. Rev. D **31**, 1815 (1985).

[13] Algebraic manipulations were performed with the aid of Mathematica [S. Wolfram, *Mathematica: A System for Doing Mathematics by Computer* (Addison-Wesley, Redwood City, California, 1988)].

[14] M. Shibata, M. Sasaki, H. Tagoshi, and T. Tanaka, Phys. Rev. D **51**, 1646 (1995).

[15] L. E. Kidder, Washington University preprint WUGRAV 94-6 (1995). The $\hat{L}_N$ in his Eq. (4.11) has to be averaged (see [9]) over an orbit to agree with our Eq. (26).

[16] Refs. [14, 15] do not compute the change in the Carter constant, although making the *assumption* that circular orbits remain circular allows the calculation to be done.

[17] Other definitions of "inclination angle", such as ι' at $\theta = \pi/2$ (see [9]), can lead to such angle decreasing with time.

[18] F. D. Ryan, L. S. Finn, and K. S. Thorne, Phys. Rev. Lett., in preparation.

3 Effect of gravitational radiation reaction on nonequatorial orbits around a Kerr black hole

Abstract

The effect of gravitational radiation reaction on orbits around a spinning black hole is analyzed. Such orbits possess three constants of motion: ι, e, and a, which correspond, in the Newtonian limit of the orbit being an ellipse, to the inclination angle of the orbital plane to the hole's equatorial plane, the eccentricity, and the semi-major axis length, respectively. First, it is argued that circular orbits ($e = 0$) remain circular under gravitational radiation reaction. Second, for elliptical orbits (removing the restriction of $e = 0$), the evolution of ι, e, and a is computed to leading order in S (the magnitude of the spin angular momentum of the hole) and in M/a, where M is the mass of the black hole. As a decreases, ι increases and e decreases.

3.1 Introduction

The Earth-based Laser Interferometer Gravitational Wave Observatory–(LIGO-)VIRGO [1, 2] network of gravitational wave detectors (which is now under construction) and the European Space Agency's planned space-based Laser Interferometer Space Antenna (LISA) [3] will be used to search for and study the gravitational waves from "particles", such as neutron stars and small black holes, spiraling into massive black holes (mass M up to $\sim 300M_\odot$ for LIGO/VIRGO and up to $\sim 10^7 M_\odot$ for LISA). To search for the inspiral waves and extract the information they carry will require templates based on theoretical calculations of the emitted waveforms, which in turn require a detailed understanding of how radiation reaction influences the orbital evolution.

When the orbital plane of the particle is inclined to the equatorial plane of a spinning hole,

only one method has been successfully implemented to deduce how radiation reaction influences the evolution of the orbit's "Carter constant" [4, 5], which governs the orbital shape and inclination angle. This method, which uses a "post-Newtonian" gravitational radiation reaction force, was described in a previous paper [6], but there only applied to "circular orbits" (orbits of constant Boyer-Lindquist radial coordinate r) for simplicity. This follow-up paper has a two-fold purpose: First, in Sec. 3.2, we will argue that circular orbits remain circular under gravitational radiation reaction. Second, in Sec. 3.3, we will compute the evolution of elliptical orbits under radiation reaction, but only to leading order in S, the magnitude of the spin angular momentum of the black hole, and leading order in M/a, where M is the black hole's mass and a is the size of the orbit, as defined more precisely below. (Here and throughout, units with $G = c = 1$ are used.)

3.2 Evolution of circular orbits

Several years ago, Ori [7] put forth the conjecture that circular orbits in the Kerr metric remain circular even under gravitational radiation reaction. Here, we will argue in favor of the conjecture. We will start by reviewing some properties of elliptical and circular orbits in the Kerr metric. Then we will argue that a circular orbit and the reaction force acting on it have a type of reflection symmetry that ensures that the orbit remains circular under radiation reaction, in the limit of the particle's mass being small compared to the hole's mass.

In the absence of gravitational radiation, the geodesic motion of a particle in orbit around a Kerr black hole is well-known and discussed, for example, in Sec. 33.6 of Ref. [5]. The location of the particle can be described in Boyer-Lindquist coordinates r, θ, ϕ, and t. The orbit can be described by three constants of motion: the energy E, the angular momentum along the hole's spin axis L_z, and the Carter constant Q. The particle's rest mass μ can be counted as another constant of the motion. The energy E is defined as the relativistic energy of the particle minus its rest mass, so that "$E - \mu$" in the language of Ref. [5] corresponds to "E" here. We will restrict to bound orbits, that is $E < 0$ and, as a consequence (see Ref. [4]), $Q \geq 0$.

An interesting feature of the Kerr metric in Boyer-Lindquist coordinates is the existence of nonequatorial, circular, geodesic orbits. These orbits are circular in the sense that the particle maintains a constant Boyer-Lindquist coordinate r; however, the plane of the circular orbit is not fixed but rather precesses around the hole's spin axis. Such orbits exist and are stable for values of E, L_z, and Q that give $R = 0$, $\partial R/\partial r = 0$, and $\partial^2 R/\partial r^2 < 0$, where R (see Eq. (33.33c) of Ref. [5]) is defined by

$$\begin{aligned} R &= \left[(E+\mu)(r^2+S^2/M^2) - L_z S/M\right]^2 \\ &\quad -(r^2-2Mr+S^2/M^2)\left[\mu^2 r^2 + (L_z - S\mu/M - SE/M)^2 + Q\right]. \end{aligned} \tag{31}$$

For an arbitrary orbit with constants E, L_z, and Q, there might be some other energy $\bar{E} \leq E$ ($\bar{E}$ depends on L_z and Q) such that, if the orbit had energy $\bar{E}(L_z, Q)$ rather than E, the orbit would be circular and stable. In such a case, as an alternative set of constants to E, L_z, and Q, the constants ι, e, and a can be defined as follows:

$$\cos\iota \equiv \frac{L_z}{(Q+L_z^2)^{1/2}}, \tag{32}$$

$$1-e^2 \equiv \frac{E}{\bar{E}}, \tag{33}$$

$$a \equiv \frac{\bar{E}\bar{r}}{E}. \tag{34}$$

Here $\bar{r} = \bar{r}(L_z, Q)$ is the radius of the circular orbit with constants $\bar{E}$, L_z, and Q. Note that a should not be confused with the conventional notation for the spin of the black hole, which is S here.

The positive root in Eq. (32) or in any other square root is always chosen. We choose the angle ι to lie in the range $0 \leq \iota \leq \pi$, so that $\iota < \pi/2$ corresponds to an orbit co-rotating relative to the spin and $\iota > \pi/2$ to counter-rotating. Also, e is chosen as nonnegative.

This set of constants ι, e, and a has the conceptual advantage that in the Newtonian limit of large a, the orbit of the particle is an ellipse of eccentricity e and semimajor axis length a, on a

plane with inclination angle ι to the hole's equatorial plane. When not in the Newtonian limit, interpreting ι, e, and a as the inclination angle, eccentricity, and semimajor axis length must be done with the caveat that since the orbit is not an ellipse, then words such as "eccentricity" are subject to a modified interpretation and can be misleading.

Even though the particle's motion is complicated when not in the Newtonian limit, some of the parameters that describe the particle's motion need not be specified. For example, we are not concerned with the value of ϕ or t, because making a ϕ or t translation does not change the physics in the axisymmetric, stationary Kerr metric. Another symmetry is that if the orbital motion is flipped over the hole's equatorial plane, i.e., $\theta(t)$ is replaced by $\pi - \theta(t)$, the motion can be considered the same. All such ϕ and t translations and θ reflections leave the shape of the orbit unchanged.

We can think of the particle as undergoing oscillatory, coupled motion in the r and θ directions. We define one *orbital revolution* to be one oscillation cycle as measured by the θ motion. Given any chosen starting point of an orbital revolution with coordinate θ_0, the revolution can be broken into two half revolutions, the first when the particle goes from θ_0 to $\pi - \theta_0$ half a θ-cycle later, and the second when the particle goes from $\pi - \theta_0$ back to θ_0 another half θ-cycle later. [Because of the coupling of the r motion with the θ motion, the θ motion does not peak at the same extrema every cycle. Therefore, $|\pi/2 - \theta_0|$ has to be chosen small enough that the orbit does indeed go through $\pi - \theta_0$ and θ_0 in the following cycle. However, this is a very minor restriction for the rest of Sec. 3.2, where in proving that circular orbits stay circular, we only consider circular and almost circular orbits (we do not have to consider generally eccentric orbits since we know that a circular orbit cannot immediately become generally eccentric without first being slightly eccentric). In such case, the peaks of the θ motion are almost the same every cycle.]

Now we consider the effect of gravitational radiation reaction on an orbit. We assume that the rest mass μ is small enough for the adiabatic approximation to hold: the timescale of gravitational radiation reaction is much longer than any other timescale in the problem. Then the particle moves

very nearly on a geodesic path characterized by the constants of motion ι, e, and a; and only on a very long timescale (which varies like $1/\mu$ as $\mu \to 0$, because the radiation reaction acceleration scales like μ) is this motion substantially modified by gravitational radiation reaction.

We now consider, for an orbit slowly inspiraling due to radiation reaction, an orbital revolution that satisfies the following condition, to which we give the name *reflection symmetry*: Consider the point on the orbit that is at the beginning of the orbital revolution. Denote by r_0, θ_0, $\dot{r}_0$, $\dot{\theta}_0$, and $\dot{\phi}_0$ the Boyer-Lindquist spatial coordinates of that point and their time derivatives. (Here and throughout, an overdot represents d/dt.) Then there are two other locations later on the path with coordinates

$$r_n = r_0 + \mu n \tilde{r} + \text{h.o.}, \tag{35}$$

$$\theta_n - \pi/2 = (-1)^{2n}(\theta_0 - \pi/2 + \mu n \tilde{\theta}) + \text{h.o.}, \tag{36}$$

$$\dot{r}_n = \dot{r}_0 + \mu n \dot{\tilde{r}} + \text{h.o.}, \tag{37}$$

$$\dot{\theta}_n = \dot{\theta}_0 + \mu n \dot{\tilde{\theta}} + \text{h.o.}, \tag{38}$$

$$\dot{\phi}_n = \dot{\phi}_0 + \mu n \dot{\tilde{\phi}} + \text{h.o.}, \tag{39}$$

for $n = 1/2$ (a half revolution after $n = 0$) and $n = 1$ (a full orbital revolution after $n = 0$). The functions with tildes are not functions of μ. The "h.o." terms are any terms that go to zero faster than μ as $\mu \to 0$ (*higher order* in μ than linear).

Because of the initial conditions at the beginning of the first and second half revolutions (at $n = 0$ and $n = 1/2$, respectively), the shape of the first half revolution (the path connecting the $n = 0$ and $n = 1/2$ locations) deviates from the shape of the second half revolution (the path connecting the $n = 1/2$ and $n = 1$ locations) by a path deviation of order μ. Of course, these two paths also differ by a ϕ translation, a t translation, and a reflection across the equatorial plane. But as we discussed above, these are unimportant differences because of the symmetries; the shapes of the paths are the same.

Now that we have written Eqs. (35)–(39), we temporarily (for the remainder of this paragraph)

go back to the case of no radiation reaction, i.e., we set to zero the μ terms and the h.o. terms in Eqs. (35)–(39). Clearly, a circular orbital revolution satisfies Eqs. (35)–(39) for any initial $n = 0$ location chosen on the circular orbit. But could there be an eccentric orbit which also satisfies Eqs. (35)–(39)? The answer is negative, as we shall now show. A slightly eccentric orbit (one with the value of e small enough that e^2 terms are negligible) would have the same $\theta(t)$ and $\phi(t)$ motion regardless of the value of e, but $r - \bar{r}$ would oscillate with an amplitude proportional to e. This can be verified from the Kerr-metric geodesic equations, Eqs. (33.32) of Ref. [5]. In the Newtonian limit, the oscillation of $r - \bar{r}$ would be periodic with the same period that $\theta(t)$ has, but when not in the Newtonian limit the θ and r oscillations would have different periods. If an orbit were to be reflection symmetric, then $r - \bar{r}$ would have to have the same value when the orbital motion is at θ_0 as it does when it is at $\pi - \theta_0$ at the next value of n. This would require that either $r - \bar{r}$ oscillate at a frequency that is an even integer multiple of the θ oscillation frequency, or $r - \bar{r}$ have zero amplitude (a circular orbit). The former is never the case, as can be verified by numerically [8] examining circular orbits in the Kerr metric over the space of possible physically acceptable values of S, L_z and Q. The fact that $r - \bar{r}$ does not resonate with an even multiple of the θ frequency implies that a slightly eccentric orbit cannot be reflection symmetric.

Now we shall return to the case of interest: that with gravitational radiation reaction. What precisely do we refer to when we discuss circular orbital revolutions, when the orbital revolution is not actually circular but is slowly inspiraling? A good, but not unique, definition is one that agrees with the result in the case of no radiation reaction: We define that a circular orbital revolution is one that satisfies Eqs. (35)–(39), while an eccentric orbital revolution is one that does not (at least for slight eccentricity: as mentioned above, we are not considering generally eccentric orbits). An orbital revolution with weak radiation reaction is defined as circular if and only if it is reflection symmetric.

We now consider starting with an initial orbital revolution that is circular, or equivalently, that is reflection symmetric, i.e., that satisfies conditions (35)–(39). For small μ, ignoring the

h.o. (higher than μ) corrections, we would expect that the third half revolution (the first half of the next orbital revolution) would have a shape that deviates from that of the second half revolution by the same amount as the shape of the second half revolution deviates from that of the first. We expect this, because from conditions (35)–(39) above, the initial conditions of the third half revolution differ from those of the second by the same amount (to linear order in μ) as those of the second differ from those of the first; and the acceleration on the particle should similarly be equally (also to linear order in μ) different between corresponding locations on the second and third half revolutions as between corresponding locations on the first and second. The orbit remains circular for the additional half revolution. If there is any eccentricity added, it is in the h.o. terms, but in the $\mu \to 0$ limit, this is ignorable compared to the shrinking of the orbit, which varies like μ (the terms involving tildes).

We can repeat the above argument to get the shape of the fourth half revolution, as well as the fifth, sixth, etc. In fact, the argument can be repeated to any chosen number, $n_{\rm max}$, of orbital revolutions, as long as that chosen number does not go to infinity as $\mu \to 0$; for if it did, then we would not be guaranteed that after the infinite number $n_{\rm max}$ of orbits, the h.o. corrections of the above paragraph would be ignorable. For example, we could choose $n_{\rm max}$ to be 100, but we could not choose it to be $100M/\mu$. The orbit remains reflection symmetric (or equivalently, it remains circular) for n up to $n_{\rm max}$, where n increments by 1/2. In other words, there is a location, with coordinates r_n, θ_n $\dot{r}_n$, $\dot{\theta}_n$, and $\dot{\phi}_n$, satisfying Eqs. (35)–(39) for any n up to $n_{\rm max}$.

The constants of motion E, L_z, and Q (or equivalently, ι, e, and a) evolve in such a way that in going from $n = 0$ to $n = n_{\rm max}$ a circular orbit remains circular. By assigning new values of r_0, θ_0, $\dot{r}_0$, $\dot{\theta}_0$, and $\dot{\phi}_0$ as the old $r_{n_{\rm max}}$, $\theta_{n_{\rm max}}$, $\dot{r}_{n_{\rm max}}$, $\dot{\theta}_{n_{\rm max}}$, and $\dot{\phi}_{n_{\rm max}}$, the argument can be repeated, over and over again. The rates of loss of E, L_z, and Q will then continue at such a rate so as to maintain circularity.

A more intuitive picture of why a circular orbit remains circular was provided by Ori [7], who first pointed out that the incommensurability of the r and θ periods is the key reason why the

argument can be made without knowing the nature of the reaction force: Even if the radiation reaction were to take the bizarre form of somebody with a hammer hitting the particle every time the particle is at some value of θ, there would have to be another person across the equatorial plane at $\pi - \theta$ with a hammer hitting the particle in a corresponding way, as dictated by the orbital symmetries. Since the $r - \bar{r}$ frequency is not an even multiple of the θ frequency, the hammer hits cannot constructively interfere with each other and produce an eccentricity.

If an orbit is circular, then just knowing the rates of change of E and L_z (for example, by knowing the energy and angular momentum carried off in the gravitational waves) is enough to determine the full orbital evolution since the evolution of Q is constrained such that the conditions listed immediately before Eq. (31) are satisfied, for as long as the orbit itself is stable.

3.3 Leading order effect of spin on eccentric orbits

We now wish to consider general, not just circular, orbits around a black hole. But in doing so, we restrict ourselves to only considering the leading order effect of spin. We will use the formalism of a radiation reaction force described in a previous paper [6] and merely state how the method as described in that paper generalizes to orbits with eccentricity.

When one is only interested in leading order in S and in M/r (or equivalently, M/a, in terms of orbit parameters), the effect of the hole's Kerr metric on the particle's motion can be substituted with a spin-orbit interaction in three dimensional flat-space. Let spherical polar coordinates r, θ, and ϕ, centered on the black hole, be used to describe the location of the particle (these coordinates describe the relative separation of the two bodies), with the hole's spin along the polar axis. The Lagrangian (Ref. [9], Eq. (4)) for the motion of the particle is given, to linear order in S but otherwise in solely Newtonian theory, by

$$\mathcal{L} = \frac{\mu}{2}[\dot{r}^2 + r^2\dot{\theta}^2 + r^2\sin^2(\theta)\dot{\phi}^2] + \frac{\mu M}{r} - \frac{2\mu S\sin^2\theta}{r}\dot{\phi}. \tag{40}$$

To leading order in S and in M/r, the motion resulting from this Lagrangian is the same as in

the Kerr metric. The use of flat space coordinates, which ignores M/r corrections, is adequate to leading order. Using the same coordinate variable names r, θ, and ϕ for these coordinates as for the Kerr metric's Boyer-Lindquist coordinates does not cause conflict and should not cause confusion. Alternatively, we can use Cartesian coordinates, $x_1 = r\sin\theta\cos\phi$, $x_2 = r\sin\theta\sin\phi$, and $x_3 = r\cos\theta$.

The Lagrangian (40) admits three constants of motion, called E, L_z, and Q because they are the same constants as we have in the Kerr metric, to leading order in S and in M/r. The values of these constants are:

$$E = \frac{\mu}{2}[\dot{r}^2 + r^2\dot{\theta}^2 + r^2\sin^2(\theta)\dot{\phi}^2] - \frac{\mu M}{r}, \tag{41}$$

$$L_z = \mu r^2\sin^2(\theta)\dot{\phi} - \frac{2\mu S\sin^2\theta}{r}, \tag{42}$$

$$Q + L_z^2 = \mu^2 r^4[\dot{\theta}^2 + \sin^2(\theta)\dot{\phi}^2] - 4\mu^2 S r\sin^2(\theta)\dot{\phi}. \tag{43}$$

The combination $Q + L_z^2$ is a more natural constant to work with than Q. If S were equal to zero, then $Q + L_z^2$ would be the square of the total angular momentum.

The constants of motion ι, e, and a, when considered only to leading order in S and in M/r, are related to E, L_z, and Q by:

$$\cos\iota = \frac{L_z}{(Q + L_z^2)^{1/2}}, \tag{44}$$

$$1 - e^2 = -2\frac{E(Q + L_z^2)}{\mu^3 M^2}\left(1 + 4\frac{SM\mu^3 L_z}{(Q + L_z^2)^2}\right), \tag{45}$$

$$a = -\frac{M\mu}{2E}\left(1 + 2\frac{SM\mu^3 L_z}{(Q + L_z^2)^2}\right). \tag{46}$$

It is easy to verify these, by checking that the $\bar{E}$ and $\bar{r}$ that would make Eqs. (32)–(34) give Eqs. (44)–(46) satisfy (at leading order in S and in M/a) the stable circular orbit constraints listed immediately before Eq. (31). Note that Eqs. (44)–(46) are valid for arbitrary eccentricity e; they do not require $e \ll 1$.

It is possible to express the instantaneous time derivative of each constant of motion, dE/dt, dL_z/dt, or $d(Q + L_z^2)/dt$, as a function of r, x_3, $\dot{r}$, $\dot{x}_3$, and the constants of motion; there is no

occurrence of ϕ (because of the axisymmetry) or $\dot{\phi}$ (as this is determined with L_z, r, and θ known) in any of the expressions. If S were zero then there could be no x_3 dependence, rather only r dependence, since there is no physically preferred direction when spin is absent. Thus, an x_3 or $\dot{x}_3$ can only show up in a term that includes a factor of S. Because of this, to compute the time derivative of each constant of motion to Newtonian order plus the spin correction, $x_3(t)$ only needs to be known to Newtonian order, because the spin correction to x_3 would be an S^2 term in the derivative of the constant of motion. On the other hand, the radial motion $r(t)$ of the particle has to be known to Newtonian order plus the spin correction. The $\phi(t)$ motion does not have to be known at all for computing the evolution of the constants of motion.

Let us, then, compute r and x_3 to the necessary orders. One of the Euler-Lagrange equations yields

$$\ddot{r} = -\frac{M}{r^2} + \frac{Q + L_z^2}{\mu^2 r^3} + 6\frac{SL_z}{\mu r^4}. \tag{47}$$

The solution of this, in terms of a parameter ψ, is

$$r = \frac{(Q + L_z^2)/(\mu^2 M)}{1 + e\cos\psi}\left(1 + \frac{SL_z\mu^3 M}{(Q + L_z^2)^2}(6 + 2e\cos\psi)\right), \tag{48}$$

$$\frac{dt}{d\psi} = \frac{(Q + L_z^2)^{3/2}/(\mu^3 M^2)}{(1 + e\cos\psi)^2}\left(1 + 6\frac{SL_z\mu^3 M}{(Q + L_z^2)^2}\right). \tag{49}$$

In the Newtonian limit of $S = 0$, these are the equations for a Keplerian ellipse, with the true anomaly ψ being the angle on the orbital plane of the particle relative to periastron as seen from the hole.

To Newtonian order, $x_3 = r\cos\theta$ can be expressed as

$$x_3 = r\sin\iota\ \sin(\psi + \psi_0). \tag{50}$$

Here, ψ_0 is some constant that describes the orientation of the ellipse on the orbital plane. As seen from the hole, ψ_0 is the angle between the direction of the periastron and the intersection of the equatorial and orbital planes.

The orbital period, from periastron to periastron, is

$$T = \int_0^{2\pi} d\psi \frac{dt}{d\psi} = 2\pi M \left(\frac{\mu}{-2E}\right)^{3/2}. \tag{51}$$

It happens that T, when written in this form, does not have an explicit S dependence.

This motion we have just described is that in the absence of gravitational radiation reaction; now we will compute the effect of the radiation reaction acceleration. We can take the equations for the rates of change of E, L_z, and Q due to radiation reaction for a particle going around a more massive spinning body from Eqs. (10), (13), and (14) of Ref. [6]. These equations give us formulas for $\dot{E}$, $\dot{L}_z$, and $d(Q + L_z^2)/dt$ as functions of the displacement of the particle relative to the hole in Cartesian coordinates, x_k, and the relative velocity $\dot{x}_k$. There will also be higher order time derivatives of x_k (such as $\ddot{x}_k$, etc.), but these derivatives can be eliminated from the expressions for $\dot{E}$, $\dot{L}_z$, and $Q + L_z^2$ with the aid of the Euler-Lagrange equations [derived from (40) when expressed in Cartesian coordinates—note that repeated indices are summed over 1,2,3]:

$$\ddot{x}_k = -\frac{M}{r^3}x_k + S\left(-\frac{4}{r^3}\epsilon_{3kj}\dot{x}_j + 6\frac{\dot{r}}{r^4}\epsilon_{3kj}x_j + 6\frac{L_z}{\mu r^5}x_k\right). \tag{52}$$

The time evolution of each constant of motion can thereby be expressed in terms of r, $\dot{r}$, x_3, $\dot{x}_3$, and the constants of motion. The trajectory (48)–(51) can be inserted into these expressions, and then time averaged using

$$\left\langle \dot{E} \right\rangle = \frac{1}{T}\int_0^{2\pi} d\psi \frac{dt}{d\psi}\dot{E}, \tag{53}$$

and similarly for L_z and $Q + L_z^2$. The result is [8]

$$\begin{aligned}
\left\langle \dot{E} \right\rangle &= -\frac{32}{5}\frac{\mu^2}{M^2}\left(\frac{M}{a}\right)^5\left(\frac{1}{1-e^2}\right)^{7/2}\left[\left(1 + \frac{73}{24}e^2 + \frac{37}{96}e^4\right)\right. \\
&\quad \left. -\frac{S}{M^2}\left(\frac{M}{a(1-e^2)}\right)^{3/2}\cos\iota\left(\frac{73}{12} + \frac{1211}{24}e^2 + \frac{3143}{96}e^4 + \frac{65}{64}e^6\right)\right], \qquad (54) \\
\left\langle \dot{L}_z \right\rangle &= -\frac{32}{5}\frac{\mu^2}{M}\left(\frac{M}{a}\right)^{7/2}\left(\frac{1}{1-e^2}\right)^2\left[\cos\iota\left(1 + \frac{7}{8}e^2\right) + \frac{S}{M^2}\left(\frac{M}{a(1-e^2)}\right)^{3/2}\right. \\
&\quad \left. \times\left(\left[\frac{61}{24} + \frac{63}{8}e^2 + \frac{95}{64}e^4\right] - \cos^2\iota\left[\frac{61}{8} + \frac{109}{4}e^2 + \frac{293}{64}e^4\right]\right.\right.
\end{aligned}$$

$$- \cos(2\psi_0) \sin^2 \iota \left[\frac{5}{4}e^2 + \frac{13}{16}e^4\right]\Bigg)\Bigg], \tag{55}$$

$$\left\langle Q + \dot{L}_z^2 \right\rangle = -\frac{64}{5}\mu^3 \left(\frac{M}{a}\right)^3 \left(\frac{1}{1-e^2}\right)^{3/2} \left[\left(1 + \frac{7}{8}e^2\right) - \frac{S}{M^2}\left(\frac{M}{a(1-e^2)}\right)^{3/2} \cos\iota \left(\frac{97}{12} + 22e^2 + \frac{99}{32}e^4\right)\right]. \tag{56}$$

The evolution of these constants can be converted, using Eqs. (44)–(46), to the other set of constants:

$$\left\langle \dot{\iota} \right\rangle = \frac{\mu S}{M^4}\left(\frac{M}{a}\right)^{11/2}\left(\frac{1}{1-e^2}\right)^4 \sin\iota \left[\frac{244}{15} + \frac{252}{5}e^2 + \frac{19}{2}e^4 - \cos(2\psi_0)\left(8e^2 + \frac{26}{5}e^4\right)\right], \tag{57}$$

$$\left\langle \dot{a} \right\rangle = -\frac{64}{5}\frac{\mu}{M}\left(\frac{M}{a}\right)^3 \left(\frac{1}{1-e^2}\right)^{7/2} \left[\left(1 + \frac{73}{24}e^2 + \frac{37}{96}e^4\right) - \frac{S}{M^2}\left(\frac{M}{a(1-e^2)}\right)^{3/2} \cos\iota \left(\frac{133}{12} + \frac{337}{6}e^2 + \frac{2965}{96}e^4 + \frac{65}{64}e^6\right)\right], \tag{58}$$

$$\left\langle \dot{e} \right\rangle = -\frac{\mu}{M^2}\left(\frac{M}{a}\right)^4 \left(\frac{1}{1-e^2}\right)^{5/2} e\left[\frac{304 + 121e^2}{15} - \frac{S}{M^2}\left(\frac{M}{a(1-e^2)}\right)^{3/2} \cos\iota \left(\frac{1364}{5} + \frac{5032}{15}e^2 + \frac{263}{10}e^4\right)\right]. \tag{59}$$

After trivial conversions of notation, Eqs. (54)–(56) agree with previous results: Eqs. (15) of Ref. [6] and (the first line of) Eq. (3.14) of Ref. [10], each of which is a special case of Eqs. (54)–(56).

In most cases, the terms with the $\cos(2\psi_0)$ can be dropped because they average to zero; to see when this can be done, consider the following: The Newtonian approximation to the motion is that the particle travels in an ellipse. The first correction to this motion is, as Einstein computed for Mercury, that the periastron position of the ellipse shifts on a timescale of

$$T_{\rm prec} \sim M(M/a)^{-5/2}(1-e^2). \tag{60}$$

The radiation reaction timescale for terms that involve ψ_0, as computed by evaluating

$$\frac{\sin\iota}{\langle\dot{\iota}\rangle_{\psi_0 \text{ terms}}}, \tag{61}$$

is

$$T_{\rm rad} \sim M\left(\frac{M}{a}\right)^{-11/2}\left(\frac{S}{M^2}\right)^{-1}\left(\frac{\mu}{M}\right)^{-1}\frac{(1-e^2)^4}{e^2}. \tag{62}$$

(There are also factors of order unity that involve e which were ignored. If $T_{\rm rad}$ were computed differently, for example by evaluating $L_z/\langle \dot{L}_z \rangle_{\psi_0 \text{ terms}}$, it would contain factors of ι as well.)

In the Newtonian limit, ψ_0 is fixed, but with the periastron precession, ψ_0 changes slightly after each orbit, by a post-Newtonian correction that was ignorable until now: When $T_{\rm rad} \gg T_{\rm prec}$, the $\cos(2\psi_0)$ in Eqs. (55) and (57) averages to zero, and the terms with that factor can be dropped. For extremely eccentric orbits, $T_{\rm rad}$ might not be much greater than $T_{\rm prec}$, so the ψ_0 terms must be kept. In all other respects, the periastron precession can be ignored because it just gives terms higher order in M/a (terms we have neglected). The only effect of the precession, to which our analysis is sensitive, is the averaging away of ψ_0 in the case that $T_{\rm rad} \gg T_{\rm prec}$.

From Eq. (57), it is clear that the angle ι changes such as to become antialigned with the spin. In Ref. [6], this conclusion was reached for circular orbits; finite eccentricity does not change, but only enhances, this result. However, the statement that "the inclination angle antialigns with the spin" is subject to the warning that we mentioned above when introducing ι: With the orbit not confined to a fixed plane, the angle ι is not the only way we could define "inclination angle" [6].

Equation (59) has two important consequences: First, to leading order, orbits tend to circularize, as is a well-known fact. Second, if an orbit is circular, then $e = 0$ and $\langle \dot{e} \rangle = 0$, so the orbit remains circular. This is expected, since this is the leading order limit of the general result in Sec. 3.2.

The above analysis is just one step in a general program for understanding the effects of radiation reaction on orbiting, spinning bodies. Future steps in this program include: generalizing the analysis to an arbitrary mass ratio μ/M and to the case of both masses having spin, extending the analysis to higher order in M/r and in S, and achieving a similar calculation of the orbital evolution in the fully relativistic Kerr metric.

Acknowledgements

The author is grateful to Daniel Kennefick, Alan Wiseman, and Kip Thorne for their advice. This work was supported by NSF Grant AST-9417371, and by NASA Grant NAGW-4268.

References

[1] A. Abramovici, W. E. Althouse, R. W. P. Drever, Y. Gürsel, S. Kawamura, F. J. Raab, D. Shoemaker, L. Sievers, R. E. Spero, K. S. Thorne, R. E. Vogt, R. Weiss, S. E. Whitcomb, and M. E. Zucker, Science **256**, 325 (1992).

[2] C. Bradaschia, E. Calloni, M. Cobal, R. Del Fasbro, A. Di Virgilio, A. Giazotto, L. E. Holloway, H. Kautzky, B. Michelozzi, V. Montelatici, D. Pascuello, and W. Velloso, in *Gravitation: a Banff Summer Institute*, ed. R. Mann and P. Wesson (World Scientific, Singapore, 1991).

[3] K. Danzmann, A. Rüdiger, R. Schilling, W. Winkler, J. Hough, G. P. Newton, D. Robertson, N. A. Robertson, H. Ward, P. Bender, J. Faller, D. Hils, R. Stebbins, C. D. Edwards, W. Folkner, M. Vincent, A. Bernard, B. Bertotti, A. Brillet, C. N. Man, M. Cruise, P. Gray, M. Sandford, R. W. P. Drever, V. Kose, M. Kühne, B. F. Schutz, R. Weiss, and H. Welling, *LISA: Proposal for a Laser-Interferometric Gravitational Wave Detector in Space* (Max-Planck-Institut für Quantenoptik, Garching bei München, Germany, 1993).

[4] B. Carter, Phys. Rev. **174**, 1559 (1968).

[5] C. W. Misner, K. S. Thorne, and J. A. Wheeler, *Gravitation* (Freeman, San Francisco, 1973).

[6] F. D. Ryan, Phys. Rev. D **52**, R3159 (1995).

[7] Ori's original argument is unpublished, but a revised argument will be: A. Ori and D. Kennefick (in preparation). The author has also recently become aware of another argument that circular orbits remain circular by Y. Mino (in preparation).

[8] Algebraic manipulations were performed with the aid of MATHEMATICA [S. Wolfram, *Mathematica: A System for Doing Mathematics by Computer* (Addison-Wesley, Redwood City, California, 1988)].

[9] L. E. Kidder, C. M. Will, and A. G. Wiseman, Phys. Rev. D **47**, R4183 (1993).

[10] M. Shibata, Phys. Rev. D **50**, 6297 (1994).

4 Gravitational waves from the inspiral of a compact object into a massive, axisymmetric body with arbitrary multipole moments

Abstract

The gravitational waves, emitted by a compact object orbiting a much more massive central body, depend on the central body's spacetime geometry. This paper is a first attempt to explore that dependence. For simplicity, the central body is assumed to be stationary, axially symmetric (but rotating), and reflection symmetric through an equatorial plane, so its (vacuum) spacetime geometry is fully characterized by two families of scalar multipole moments M_l and S_l with $l = 0, 1, 2, 3, \ldots$; and it is assumed not to absorb any orbital energy (e.g., via waves going down a horizon or via tidal heating). Also for simplicity, the orbit is assumed to lie in the body's equatorial plane and to be circular, except for a gradual shrinkage due to radiative energy loss. For this idealized situation, it is shown that several features of the emitted waves carry, encoded within themselves, the values of all the body's multipole moments M_l, S_l (and thus, also the details of its full spacetime geometry). In particular, the body's moments are encoded in the time evolution of the waves' phase $\Phi(t)$ (the quantity that can be measured with extremely high accuracy by interferometric gravitational-wave detectors); and they are also encoded in the gravitational-wave spectrum $\Delta E(f)$ (energy emitted per unit logarithmic frequency interval). If the orbit is slightly elliptical, the moments are also encoded in the evolution of its periastron precession frequency as a function of wave frequency, $\Omega_\rho(f)$; if the orbit is slightly inclined to the body's equatorial plane, then they are encoded in its inclinational precession frequency as a function of wave frequency, $\Omega_z(f)$. Explicit algorithms are derived for deducing the moments from $\Delta E(f)$, $\Omega_\rho(f)$ and $\Omega_z(f)$. However, to deduce the moments explicitly from the (more accurately measurable) phase evolution $\Phi(t)$ will require a very difficult, explicit

analysis of the wave generation process—a task far beyond the scope of this paper.

4.1 Introduction

For some years, Thorne [1] has been arguing that it should be possible to extract, from the gravitational waves produced by a small object spiraling into a massive black hole, a map of the massive hole's spacetime geometry. This paper is a first attempt to develop the mathematical foundations for such a map extraction. As we shall see, the key to the map extraction is a theorem (proved in this paper) that—at least in certain idealized circumstances—the waves emitted by a small object spiraling into a massive body carry, encoded in themselves, the values of all the body's multipole moments [2, 3], which characterize the vacuum spacetime geometry outside any stationary body (black hole or otherwise).

A separate paper by this author, Finn, and Thorne [4] discusses semiquantitatively the implementation of this paper's results in the analysis of future gravitational-wave data. As is discussed there, the goals of such a data analysis would be (i) to extract from the observed waves the values of the central body's lowest few multipole moments, (ii) to see whether those moments are in accord with the black-hole "no-hair" theorem (which states that the hole's spacetime geometry and thence all its moments are fully determined by its mass and its spin angular momentum), and (iii) via observed violations of the no-hair theorem, to search for unexpected types of massive, compact bodies (e.g. soliton stars and naked singularities) into which are spiraling small objects (white dwarfs, neutron stars, or small-mass black holes).

Such interesting observational studies can be carried out with moderate precision by the Earth-based network of laser-interferometer gravitational-wave detectors [LIGO, VIRGO, GEO600, TAMA] [5], which is now under construction and which can study central bodies with masses up to $\sim 300 M_\odot$. Much higher precision will be achieved by the Laser Interferometer Space Antenna

(LISA) [6], which is likely to fly in 2014 or sooner and can study central bodies with masses $\sim 3 \times 10^5$ to $3 \times 10^7 M_\odot$. See Ref. [4] for details.

For this paper's first analysis of extracting the central body's moments from gravitational-wave data, we make the following idealizing assumptions:

(i) The central body has a vacuum, external gravitational field which is stationary, axisymmetric, reflection symmetric across the equatorial plane, and asymptotically flat. Correspondingly, the body's multipole moments turn out to be scalars: The spacetime geometry can be characterized by mass multipole moments M_l and mass-current multipole moments S_l [3], and the odd-M moments and even-S moments vanish—i.e., the nonvanishing moments are the mass $M_0 \equiv M$, the mass quadrupole moment M_2, M_4, M_6, ... , and the spin angular momentum S_1, the current octopole moment S_3, S_5, S_7, ...

(ii) The inspiraling object is sufficiently compact and has a sufficiently small mass that its orbit evolves slowly and adiabatically from one geodesic orbit to another; and on the timescale of one orbital period, the orbit can be regarded as geodesic.

(iii) The geodesic orbits, through which the inspiral evolves, lie in the equatorial plane, or very nearly so, and are circular, or very nearly so. (For the $M \lesssim 300 M_\odot$ central bodies that can be studied by earth-based interferometers, radiation reaction is likely, in fact, to have circularized the orbit long ago; but for the $M \sim 10^6 M_\odot$ central bodies studied by LISA, the orbit is likely to be highly noncircular due to recent perturbations by other orbiting objects [7]. This should be a warning that the analysis of this paper is only a first treatment of what must ultimately be a much more complicated problem.)

(iv) The central body does not absorb any of the inspiraling object's orbital energy; i.e., we can neglect any energy that goes down the central body's horizon (if it has a horizon), and we can neglect tidal heating. This implies that all of the energy lost from the orbit gets deposited into outgoing gravitational waves.

For a system that satisfies our idealizing circular-orbit assumption (iii), the gravitational waves are emitted primarily (but not solely) at twice the orbital frequency, and correspondingly the dominant gravitational "spectral line" is at the frequency

$$f = \frac{2\Omega}{2\pi} = \frac{\Omega}{\pi}, \tag{63}$$

where Ω is the orbital angular frequency.

As time passes, radiation reaction will cause the orbit to shrink gradually; and correspondingly, f will be a slowly varying function of time t. There will also be emissions at frequencies $\frac{1}{2}f$, $\frac{3}{2}f$, $2f$, ...

In this paper we shall focus on aspects of the waves that can be computed without facing any serious complications of the theory of wave emission. We avoid analyzing wave emission in detail because, for a body with arbitrary multipole moments, such an analysis will be very complex. Fortunately, we can make considerable progress by focusing almost solely on gravitational-wave quantities that depend only on the properties of the central body's circular geodesic orbits.

One such quantity is a gravitational-wave spectrum $\Delta E(f)$, defined as follows: During a short interval of time when the waves' principal frequency is evolving from f to $f + df$, we take all the energy emitted into the principal spectral line, plus all being emitted into all the other lines nf with $n = \frac{1}{2}, \frac{3}{2}, 2, \frac{5}{2}, \ldots$; and we add all that energy together to obtain a total emitted energy $dE_{\rm wave}$. By our idealizing assumption (iv), this is equal to the energy lost from the orbit $-dE$ as the orbital angular frequency varies from $\Omega = \pi f$ to $\Omega + d\Omega = \pi(f + df)$. The quantity $\Delta E(f)$ is the corresponding amount of gravitational-wave energy per logarithmic interval of frequency:

$$\Delta E \equiv f\frac{dE_{\rm wave}}{df} = -\Omega\frac{dE}{d\Omega}\,. \tag{64}$$

Two other gravitational-wave quantities that can be computed without facing the complications of wave-emission theory [as well as without requiring assumption (iv) above] are the frequencies of wave modulation that result from orbital precession. There are two types of precession and corresponding two wave modulations: (i) if the orbit is slightly elliptical, then the ellipse can

precess (a "precession of the orbit's periastron") at some angular frequency Ω_ρ that depends in some way on the orbital radius and thence on the waves' primary frequency f; (ii) if the orbit is slightly inclined to the central body's equator, then the orbital plane will precess at some angular frequency Ω_z that also depends on f. These orbital precessions will modulate the emitted waves at the angular frequencies $\Omega_\rho(f)$ and $\Omega_z(f)$.

In Sec. III of this paper, we shall develop algorithms for computing these three gravitational-wave quantities, ΔE, Ω_ρ, and Ω_z, as power series in f, or equivalently in the dimensionless parameter

$$v = (\pi M f)^{1/3} = (M\Omega)^{1/3} . \tag{65}$$

In the Newtonian limit, v is the orbiting object's linear velocity.

In Sec. II [Eqs. (79)–(81)], we will write down the first few terms of those power series. As is suggested by the forms of those explicit series, our algorithms enable us to express the power series' coefficients entirely in terms of the central body's multipole moments M_l and S_l. Moreover, if (via idealized measurements) we could learn any one of the wave functions $\Delta E(f)$, $\Omega_\rho(f)$, or $\Omega_z(f)$, then by expanding that function as a power series in $v = (\pi M f)^{1/3}$ and examining the numerical values of the coefficients, we would be able to read off the values of all the multipole moments M_l, S_l.

This result is not of great practical interest, because a system of interferometers can achieve only a modest accuracy in any attempt to measure the functions $\Delta E(f)$, $\Omega_\rho(f)$, and $\Omega_z(f)$ (and also because of the idealizing assumptions that have been made). Of greater practical interest will be measurements of the time evolution $\Phi(t)$ of the waves' phase, since via the method of "matched filters" this quantity can be measured with very high accuracy ($\sim 1/10^4$ to $\sim 1/10^7$ depending on the system [4, 8]). This phase evolution $\Phi(t)$ actually contains contributions from all the waves' spectral lines as well as from precessional modulations. In discussing $\Phi(t)$, we shall assume, for simplicity, that the orbit is precisely circular and equatorial so there are no precessions; and we shall focus solely on the portion of $\Phi(t)$ that is associated with the primary

frequency, $\Phi_2(t) = 2\pi \int f dt = 2 \int \Omega dt$. A knowledge of this primary phase evolution is equivalent to a knowledge of the number of cycles ΔN that the primary waves spend in a logarithmic interval of frequency,

$$\Delta N(f) \equiv \frac{f^2}{df/dt} = \frac{f \Delta E(f)}{dE_{\rm wave}/dt} \,. \tag{66}$$

Here $dE_{\rm wave}/dt$ is the gravitational-wave luminosity, or equivalently the rate of loss of orbital energy, $-dE/dt$.

To compute $dE_{\rm wave}/dt$ fully, even with our idealizing assumptions, would require dealing with all the complexities of wave-emission theory. Fortunately, however, we can compute the leading-order contribution of each central-body multipole M_l or S_l to $dE_{\rm wave}/dt$ using fairly elementary wave-generation considerations. We do so in Sec. IV, and we then use Eq. (66) to deduce each multipole's leading-order contribution to the power-series expansion of $N(f)$ [Eq. (135) below]. Just as was the case for our other three wave functions $\Delta E(f)$, $\Omega_\rho(f)$, and $\Omega_z(f)$, each multipole appears first at a different order in the series: M_l at order v^{2l} (beyond where $M_0 = M$ enters at leading order), and S_l at v^{2l+1}. This guarantees that, from the power series expansion of the (accurately measurable) phase evolution $\Delta N(f)$, one (in principle) can read off the values of all the central-body multipole moments. However, to produce a full algorithm for doing so would require dealing with the full complexities of wave-emission theory.

Our derivation and presentation of these results is organized as follows: In Sec. II, we write down the spacetime metric for the central body; we derive equations describing the metric's nearly equatorial and nearly circular geodesic orbits, through which the inspiraling object moves; we use those orbital equations to derive expressions for our gravitational-wave functions ΔE, Ω_ρ, and Ω_z [Eqs. (79)–(81)] in terms of the central body's metric; and we state (with the proof to follow in Sec. 4.3) the first few terms of the expansions of these quantities in powers of $v = (\pi M f)^{1/3}$ with coefficients depending on the central body's multipole moments. In Sec. III, we briefly review key portions of the Ernst formalism for solving the axisymmetric, vacuum Einstein field equations and of the Geroch-Hansen multipole-moment formalism [2, 3] by which the resulting solutions can be

expressed in terms of multipole moments; and then we devise algorithms for computing the power series expansions of ΔE, Ω_ρ, and Ω_z. The explicit power series of Sec. II are derived from those algorithms. In Sec. IV, we digress briefly from the main thread of the paper, to discuss an issue of principle that can be delicate: how to deduce the mass M from the power series expansion $\Omega_z(v)$. Finally, in Sec. V, we use elementary wave-generation arguments to compute the leading-order contribution of each central-body multipole to the gravitational luminosity, and thence to the waves' phase-evolution function $\Delta N(f)$.

4.2 Functions of the multipole moments

In this section, we will review the foundations for analyzing the three functions $\Delta E(f)$, $\Omega_\rho(f)$, and $\Omega_z(f)$ that contain full information of the multipole moments of the central body. The metric produced by the central body, ignoring the effects of the much less massive orbiting object, can be written in terms of (t,ϕ,ρ,z) as (units where $G = c = 1$ are used throughout)

$$ds^2 = -F(dt - \omega d\phi)^2 + \frac{1}{F}\left[e^{2\gamma}(d\rho^2 + dz^2) + \rho^2 d\phi^2\right], \tag{67}$$

where F, ω, and γ are functions of ρ and $|z|$. Instead of specifying these functions, it is more convenient to classify the metric by the Geroch-Hansen [2, 3] multipole moments associated with it. Because of the axisymmetry, specifying the $2l + 1$ independent components of the l-th tensor multipole moment is equivalent to specifying the scalar multipole moment formed by the product of the tensor moment with l symmetry axis vectors, and then dividing by $l!$. As discussed and defined in Hansen [3], these scalar multipole moments can be classified into two families, corresponding to mass and mass current (i.e. momentum density), parametrized by integer values of $l \geq 0$. Because of the reflection symmetry across the equatorial plane, the mass multipole moments can be nonzero only for even l: M, M_2, M_4, ... , M_l, ... The mass monopole moment is the mass itself, so the "0" subscript of M_0 is omitted. Similarly, the current multipole moments can be nonzero only for odd l: S_1, S_3, ... , S_l, ... For example, the Kerr metric with mass m and spin

a has $M_l + iS_l = m(ia)^l$ [Ref. [3], Eq. (3.14)]. The letters M and S are used here to refer to the multipole moments of the central body alone, as opposed to the letters I and J which will be used in Sec. 4.5 when discussing the multipole moments of the entire system, including the orbiting object.

When radiation reaction is neglected, the orbit of the small object is governed by three conservation laws. The first follows from the standard normalization condition for the object's four-velocity:

$$-1 = g_{tt}\left(\frac{dt}{d\tau}\right)^2 + 2g_{t\phi}\left(\frac{dt}{d\tau}\right)\left(\frac{d\phi}{d\tau}\right) + g_{\phi\phi}\left(\frac{d\phi}{d\tau}\right)^2 + g_{\rho\rho}\left(\frac{d\rho}{d\tau}\right)^2 + g_{zz}\left(\frac{dz}{d\tau}\right)^2. \tag{68}$$

The lack of t-dependence in the metric implies that the energy per mass μ of the small object is a conserved quantity. It has value

$$\frac{E}{\mu} = -g_{tt}\left(\frac{dt}{d\tau}\right) - g_{t\phi}\left(\frac{d\phi}{d\tau}\right). \tag{69}$$

Similarly, the "z-component" of angular momentum per mass of the small object,

$$\frac{L_z}{\mu} = g_{t\phi}\left(\frac{dt}{d\tau}\right) + g_{\phi\phi}\left(\frac{d\phi}{d\tau}\right), \tag{70}$$

is conserved because of the lack of ϕ-dependence in the metric.

If the object is moving in a circle along the equator $z = 0$, then the orbital angular velocity (or "angular frequency" as we shall call it) is

$$\Omega = \frac{d\phi}{dt} = \frac{-g_{t\phi,\rho} + \sqrt{(g_{t\phi,\rho})^2 - g_{tt,\rho}g_{\phi\phi,\rho}}}{g_{\phi\phi,\rho}}. \tag{71}$$

This is easily obtained from the geodesic equation and by imposing the conditions of constant orbital radius, that $d\rho/d\tau = 0$ and $d^2\rho/d\tau^2 = 0$.

A circular orbit also implies that $d\rho/d\tau = 0$ and $dz/d\tau = 0$ in Eq. (68), while $d\phi/d\tau = \Omega\, dt/d\tau$, so that solving for $dt/d\tau$ in Eq. (68) and substituting in Eq. (69) gives:

$$\frac{E}{\mu} = \frac{-g_{tt} - g_{t\phi}\Omega}{\sqrt{-g_{tt} - 2g_{t\phi}\Omega - g_{\phi\phi}\Omega^2}}. \tag{72}$$

Similarly, a circular orbit implies, from Eq. (70), that

$$\frac{L_z}{\mu} = \frac{g_{t\phi} + g_{\phi\phi}\Omega}{\sqrt{-g_{tt} - 2g_{t\phi}\Omega - g_{\phi\phi}\Omega^2}}. \tag{73}$$

The orbit might also be slightly different from a circle in the equatorial plane: it might be slightly elliptical or slightly out of the equatorial plane. In this case, Eqs. (69) and (70) can be solved for $dt/d\tau$ and $d\phi/d\tau$, which can be inserted into Eq. (68) to get

$$-1+\left(\frac{g_{\phi\phi}}{\rho^2}\right)\frac{E^2}{\mu^2}+2\left(\frac{g_{t\phi}}{\rho^2}\right)\frac{EL_z}{\mu^2}+\left(\frac{g_{tt}}{\rho^2}\right)\frac{L_z^2}{\mu^2}=g_{\rho\rho}\left(\frac{d\rho}{d\tau}\right)^2+g_{zz}\left(\frac{dz}{d\tau}\right)^2, \tag{74}$$

where the fact that

$$\rho^2=g_{t\phi}^2-g_{tt}g_{\phi\phi} \tag{75}$$

was used. When the left-hand side of Eq. (74) is expanded in powers of z and of $\delta\rho \equiv$ (radial displacement from the value of ρ which, along with $z=0$, maximizes the left hand side), and when only the leading-order (quadratic) terms in z and $\delta\rho$ are kept, then Eq. (74) becomes the law of energy conservation for a two-dimensional harmonic oscillator. The vanishing of the mixed ρz derivative of the left hand side (because of the reflection symmetry, taking a single z derivative gives zero) implies that the motions in the ρ and z directions are independent of each other. These motions correspond to the periastron precession and the orbital plane precession, which are at frequencies Ω_ρ and Ω_z, respectively. The precession frequencies are

$$\begin{aligned}\Omega_\alpha \;=\; \Omega-\Bigg(-\frac{g^{\alpha\alpha}}{2}\Bigg[&(g_{tt}+g_{t\phi}\Omega)^2\left(\frac{g_{\phi\phi}}{\rho^2}\right)_{,\alpha\alpha}\\ &-2\left(g_{tt}+g_{t\phi}\Omega\right)\left(g_{t\phi}+g_{\phi\phi}\Omega\right)\left(\frac{g_{t\phi}}{\rho^2}\right)_{,\alpha\alpha}+\left(g_{t\phi}+g_{\phi\phi}\Omega\right)^2\left(\frac{g_{tt}}{\rho^2}\right)_{,\alpha\alpha}\Bigg]\Bigg)^{1/2},\end{aligned} \tag{76}$$

where α is ρ or z, and the expression is evaluated at $z=0$. The "$_{,\alpha\alpha}$" signifies double partial differentiation with respect to the α index. Eq. (76) was derived by evaluating the second derivative, with respect to either ρ or z, of the left hand side of Eq. (74). Then, the values of E and L_z were substituted from Eqs. (72) and (73). This substitution is valid only in the limit of small deviations of the orbit from a circle in the equatorial plane. The second derivatives were then used to determine the frequencies of the harmonic oscillators in the ρ and z directions which, when subtracted from Ω, give the precession frequencies of Eq. (76).

The metric functions and their derivatives, when evaluated at $z=0$, can all be expressed as

power series in $1/\rho$. From Eq. (71), Ω can be expressed as

$$\Omega = (M/\rho^3)^{1/2}(1 + \text{series in } \rho^{-1/2}) \tag{77}$$

so that

$$\begin{aligned} 1/\rho &= (M/\Omega^2)^{1/3}(1 + \text{series in } \rho^{-1/2}) \\ &= (M/\Omega^2)^{1/3}(1 + \text{series in } \Omega^{1/3}). \end{aligned} \tag{78}$$

Since $\Delta E/\mu$, Ω_ρ/Ω, and Ω_z/Ω are all functions of $1/\rho$ and Ω, then they too can be expressed as power series in $\Omega^{1/3}$. We shall see that the coefficients of these power series can be used to obtain the moments.

These power series have the following forms, as can be derived by an algorithm described in Sec. 4.3 below. Listing just the first few terms, which are functions of the lowest three mass moments M, M_2, and M_4 and the lowest two current moments S_1 and S_3, the functions are [using $v \equiv (M\Omega)^{1/3}$]:

$$\begin{aligned} \frac{\Delta E}{\mu} &= \frac{1}{3}v^2 - \frac{1}{2}v^4 + \frac{20}{9}\frac{S_1}{M^2}v^5 + \left(-\frac{27}{8} + \frac{M_2}{M^3}\right)v^6 + \frac{28}{3}\frac{S_1}{M^2}v^7 \\ &\quad + \left(-\frac{225}{16} + \frac{80}{27}\frac{S_1^2}{M^4} + \frac{70}{9}\frac{M_2}{M^3}\right)v^8 + \left(\frac{81}{2}\frac{S_1}{M^2} + 6\frac{S_1 M_2}{M^5} - 6\frac{S_3}{M^4}\right)v^9 \\ &\quad + \left(-\frac{6615}{128} + \frac{115}{18}\frac{S_1^2}{M^4} + \frac{935}{24}\frac{M_2}{M^3} + \frac{35}{12}\frac{M_2^2}{M^6} - \frac{35}{12}\frac{M_4}{M^5}\right)v^{10} \\ &\quad + \left(165\frac{S_1}{M^2} + \frac{1408}{243}\frac{S_1^3}{M^6} + \frac{968}{27}\frac{S_1 M_2}{M^5} - \frac{352}{9}\frac{S_3}{M^4}\right)v^{11} + \left(-\frac{45927}{256} - \frac{123}{14}\frac{S_1^2}{M^4}\right. \\ &\quad \left. + \frac{9147}{56}\frac{M_2}{M^3} + \frac{93}{4}\frac{M_2^2}{M^6} + 24\frac{S_1^2 M_2}{M^7} - 24\frac{S_1 S_3}{M^6} - \frac{99}{4}\frac{M_4}{M^5}\right)v^{12} + \dots, \end{aligned} \tag{79}$$

$$\begin{aligned} \frac{\Omega_\rho}{\Omega} &= 3v^2 - 4\frac{S_1}{M^2}v^3 + \left(\frac{9}{2} - \frac{3}{2}\frac{M_2}{M^3}\right)v^4 - 10\frac{S_1}{M^2}v^5 + \left(\frac{27}{2} - 2\frac{S_1^2}{M^4} - \frac{21}{2}\frac{M_2}{M^3}\right)v^6 \\ &\quad + \left(-48\frac{S_1}{M^2} - 5\frac{S_1 M_2}{M^5} + 9\frac{S_3}{M^4}\right)v^7 + \left(\frac{405}{8} + \frac{2243}{84}\frac{S_1^2}{M^4} - \frac{661}{14}\frac{M_2}{M^3}\right. \\ &\quad \left. - \frac{21}{8}\frac{M_2^2}{M^6} + \frac{15}{4}\frac{M_4}{M^5}\right)v^8 + \left(-243\frac{S_1}{M^2} - 16\frac{S_1^3}{M^6} + 4\frac{S_1 M_2}{M^5} + 45\frac{S_3}{M^4}\right)v^9 + \left(\frac{1701}{8}\right. \\ &\quad \left. + \frac{8443}{28}\frac{S_1^2}{M^4} - \frac{1545}{7}\frac{M_2}{M^3} - \frac{95}{8}\frac{M_2^2}{M^6} - \frac{85}{3}\frac{S_1^2 M_2}{M^7} + 12\frac{S_1 S_3}{M^6} + 30\frac{M_4}{M^5}\right)v^{10} + \dots, \end{aligned} \tag{80}$$

$$\begin{aligned}\frac{\Omega_z}{\Omega} &= 2\frac{S_1}{M^2}v^3 + \frac{3}{2}\frac{M_2}{M^3}v^4 + \left(7\frac{S_1^2}{M^4} + 3\frac{M_2}{M^3}\right)v^6 + \left(11\frac{S_1 M_2}{M^5} - 6\frac{S_3}{M^4}\right)v^7 \\ &+ \left(\frac{153}{28}\frac{S_1^2}{M^4} + \frac{153}{28}\frac{M_2}{M^3} + \frac{39}{8}\frac{M_2^2}{M^6} - \frac{15}{4}\frac{M_4}{M^5}\right)v^8 + \left(26\frac{S_1^3}{M^6} + 31\frac{S_1 M_2}{M^5} - 15\frac{S_3}{M^4}\right)v^9 \\ &+ \left(\frac{69}{7}\frac{S_1^2}{M^4} + \frac{69}{7}\frac{M_2}{M^3} + \frac{41}{2}\frac{M_2^2}{M^6} + \frac{389}{6}\frac{S_1^2 M_2}{M^7} - 41\frac{S_1 S_3}{M^6} - 15\frac{M_4}{M^5}\right)v^{10} + \ldots . \qquad (81)\end{aligned}$$

These expressions give some indication as to why all the multipole moments are obtainable from any one of the functions $\Delta E(v)$, $\Omega_\rho(v)$, or $\Omega_z(v)$ [with $v = (M\Omega)^{1/3} = (\pi M f)^{1/3}$]. The current moment S_l ($l = 1, 3, 5, \ldots$) always first appears in the coefficient of $\Omega^{(2l+3)/3}$ in $\Delta E/\mu$, and of $\Omega^{(2l+1)/3}$ in Ω_ρ/Ω and Ω_z/Ω. The mass moment M_l ($l = 2, 4, 6, \ldots$) always first appears in the coefficient of $\Omega^{(2l+2)/3}$ in $\Delta E/\mu$, and of $\Omega^{2l/3}$ in Ω_ρ/Ω and Ω_z/Ω. Since each multipole moment makes its first appearance at a different order, then one would expect that all the moments can be obtained from these functions.

In $\Delta E/\mu$, the first two powers of Ω have coefficients that involve only M, but to different powers. This allows not only for the determination of the mass, but also if $\Delta E/\mu$ is only measurable up to a proportionality constant (for example, because μ or the distance to the source is not known exactly), this constant can be determined. In Ω_ρ/Ω, the mass M can be determined from the first term. In Ω_z/Ω, there is no term that involves only the mass. If all the terms in the Ω_z/Ω expansion are zero (because $M_l = S_l = 0$ for $l \geq 1$), then the mass M cannot be determined at all from Ω_z/Ω. This case corresponds to the gravitational field of the more massive object being spherically symmetric, so that there is no orbital plane precession possible. If some of the terms in the Ω_z/Ω expansion are nonzero, then it is possible to determine M from this expansion, as we shall see in Sec. 4.4.

4.3 Determination of the multipole moments

In this section we shall develop an algorithm by which the power series expansions (79)–(81) can be derived, to all orders; and we shall show that each moment S_l or M_l first appears in that expansion at the order described in Sec. 4.2. The appearance of each moment at a unique order guarantees

that the multipole moment can be determined from knowledge of the power series.

We will divide this presentation into five parts. In part A, we will review the Ernst potential and its relation to the metric. We will show that the Ernst potential is completely determined everywhere by a set of coefficients called a_{j0} and a_{j1} which describe the metric on the equatorial plane. In part B, we will show that all the a_{j0} and a_{j1} can be determined from $\Delta E/\mu$, Ω_ρ/Ω, or Ω_z/Ω. In part C, the algorithm described in part B to do this will be summarized. In part D, we will show how to go from the a_{j0} and a_{j1} to the multipole moments M_l and S_l. In part E, we will show how Eqs. (79)–(81) can be derived.

In Secs. 4.3 and 4.4, we assume that any one of the dimensionless functions, $\Delta E/\mu$, Ω_ρ/Ω, or Ω_z/Ω, is known exactly to all orders in Ω. In addition, in Sec. 4.3, we assume that M is known—if $\Delta E/\mu$ or Ω_ρ/Ω is the known function, then M is easily extracted from the first term in either series (79) or (80); if Ω_z/Ω is the known function, then M can be determined from the algorithm described below in Sec. 4.4.

4.3.1 The Ernst potential

Fodor, Hoenselaers, and Perjés [9] give details of the computation of the multipole moments from the complex potential $\tilde{\xi}$, a function of ρ and z. This $\tilde{\xi}$ is related to the Ernst potential [10] $\mathcal{E}$ by

$$\mathcal{E} = F + i\psi = \frac{\sqrt{\rho^2+z^2}-\tilde{\xi}}{\sqrt{\rho^2+z^2}+\tilde{\xi}}, \tag{82}$$

where F is related to the metric by [see Eq. (67)]

$$g_{tt} = -F, \tag{83}$$

and ψ is related to the metric by [Ref. [11], Eq. (I.3b)]

$$g_{t\phi} = F\int_\rho^\infty \frac{\rho'}{F^2}\frac{\partial\psi}{\partial z}d\rho'\bigg|_{\text{constant } z}. \tag{84}$$

The Ernst potential $\mathcal{E}$ is powerful for generating stationary, axisymmetric solutions to the gravitational field equations. It contains all the information of the spacetime geometry in a single, complex function, and thus so also does $\tilde{\xi}$.

The potential $\tilde{\xi}$ has the property that it can be expanded as [Ref. [9], Eq. (15)]

$$\tilde{\xi} = \sum_{j,k=0}^{\infty} a_{jk} \frac{\rho^j z^k}{(\rho^2 + z^2)^{j+k}}. \tag{85}$$

The a_{jk} can be nonzero only for nonnegative, even j and nonnegative k. Because of the reflection symmetry across the equatorial plane, a_{jk} is real for even k and imaginary for odd k.

Since the measured function, any one of $\Delta E/\mu$, Ω_ρ/Ω, or Ω_z/Ω, is directly related to the metric in the region around the equatorial plane $z = 0$, then it is most convenient to convert the measured function into the coefficients that contain information of the equatorial plane metric, namely, a_{j0} and a_{j1}.

Assume for the moment that for any positive, even integer m, all the a_{j0} with $j = 0, 2, \ldots, m$ and the a_{j1} with $j = 0, 2, \ldots, m-2$ are known; and assume that for any positive, odd integer m, all the a_{j0} with $j = 0, 2, \ldots, m-1$ and a_{j1} with $j = 0, 2, \ldots, m-1$ are known.

From these a_{j0} and a_{j1}, all the a_{jk} for $j + k \leq m$ can be computed from [Ref. [9], Eq. (16)]

$$\begin{aligned} a_{r,s+2} \;=\; & \frac{1}{(s+2)(s+1)} \Bigg(-(r+2)^2 a_{r+2,s} + \\ & \sum_{k,l,p,q} a_{kl} a^*_{r-k-p,s-l-q} \Big[a_{pq}(p^2 + q^2 - 4p - 5q - 2pk - 2ql - 2) \\ & + a_{p+2,q-2}(p+2)(p+2-2k) + a_{p-2,q+2}(q+2)(q+1-2l) \Big] \Bigg). \end{aligned} \tag{86}$$

The sum is over all integer values of k, l, p, and q that give nonzero contributions, namely $0 \leq k \leq r$, $0 \leq l \leq s+1$, $0 \leq p \leq r-k$, $-1 \leq q \leq s-l$, and k and p even.

All the coefficients a_{jk} that are within the summation sign in Eq. (86) have the property that $j+k < r+s+2$. Thus, $a_{r,s+2}$ (with $s \geq 0$) is a function of the a_{j0} and $a_{j-1,1}$ with $j \leq r+s+2$, but no higher order a_{j0} or $a_{j-1,1}$. This shows explicitly that $\tilde{\xi}$, and thence also the entire spacetime metric, are fully determined by a knowledge of the a_{j0} and $a_{j-1,1}$, or equivalently a knowledge of the equatorial plane metric.

4.3.2 Computing a_{j0} and a_{j1}

The process [12] of determining the a_{j0} and a_{j1} from $\Delta E/\mu$, Ω_ρ/Ω, or Ω_z/Ω occurs in iterations, each stage labeled by $n = 0, 1, 2, \ldots$. For now, assume that it is $\Delta E/\mu$ that is known, rather than Ω_ρ/Ω or Ω_z/Ω. Assume that the a_{j0} are known up to order $j = 2n$, and the a_{j1} are known up to order $j = 2n-2$. That is, a_{00}, a_{20}, a_{40}, $\ldots$, $a_{2n,0}$ and a_{01}, a_{21}, a_{41}, $\ldots$, $a_{2n-2,1}$ are known. (At the $n = 0$ stage, only $a_{00} = M$ is known.) All unknown a_{j0} and a_{j1} are set to zero at this nth stage. The goal of this nth stage is to figure out what $a_{2n+2,0}$ and $a_{2n,1}$ must be in order to reproduce the observed functional form for $\Delta E/\mu$.

From the known values of a_{j0} and a_{j1}, the metric functions g_{tt} and $g_{t\phi}$ on the equatorial plane can be computed with Eqs. (82)–(85). Then, the metric function $g_{\phi\phi}$ can be obtained from Eq. (75).

Therefore, with the a_{j0} known up to $j = 2n$, the a_{j1} known up to $j = 2n-2$, and all other a_{j0} and a_{j1} (temporarily) set to zero, the three metric functions g_{tt}, $g_{t\phi}$, and $g_{\phi\phi}$ can be expressed as power series in $1/\rho$ on the equatorial plane $z = 0$. Then, Ω can be computed as a power series in $1/\rho$ using Eq. (71). This series can be inverted to have $1/\rho$ as a series in Ω, so that the metric functions are power series in Ω. With Eqs. (64) and (72), we can compute $\Delta E/\mu$ as a power series in Ω; we will call this computed function $(\Delta E/\mu)_n$. The n subscript denotes the fact that this is as computed only using the known a_{j0} and a_{j1} at stage n, and setting all unknown a_{j0} and a_{j1} to zero. In particular, $a_{2n+2,0}$ and $a_{2n,1}$ were set to zero in calculating $(\Delta E/\mu)_n$, and we will remedy this situation below.

We can express these two functions—the actual, measured $\Delta E/\mu$ that is being deciphered, and the computed $(\Delta E/\mu)_n$—as power series in $\Omega^{1/3}$:

$$\Delta E/\mu = \sum_\alpha A_\alpha \Omega^{\alpha/3}, \tag{87}$$

$$(\Delta E/\mu)_n = \sum_\alpha B_\alpha \Omega^{\alpha/3}. \tag{88}$$

It is easy to verify that if $a_{2n,1}$ (which is unknown at this nth stage) were changed from zero

to a nonzero value, then to leading order in Ω, $(\Delta E/\mu)_n$ would change by

$$-i\frac{16n+20}{9}a_{2n,1}M^{-(2n+1)/3}\Omega^{(4n+5)/3}. \tag{89}$$

The $\Omega^{(4n+6)/3}$ term would not change if $a_{2n,1}$ were changed; however, if the $a_{2n+2,0}$ term were changed from zero to a nonzero value, then $(\Delta E/\mu)_n$ would change to lowest order by

$$-\frac{(4n+3)(4n+6)}{9}a_{2n+2,0}M^{-(2n+3)/3}\Omega^{(4n+6)/3}. \tag{90}$$

Based on these facts, then the $a_{2n,1}$ and $a_{2n+2,0}$ terms can be computed at the nth iteration stage, by simply setting the $a_{2n,1}$ and $a_{2n+2,0}$ seen in Eqs. (89) and (90) to the values that would have made $(\Delta E/\mu)_n$ agree with $\Delta E/\mu$ to order $\Omega^{(4n+6)/3}$ (rather than setting $a_{2n,1}$ and $a_{2n+2,0}$ to zero as was done at the beginning of the nth stage): we set

$$a_{2n,1} = i\frac{9M^{(2n+1)/3}}{16n+20}(A_{4n+5}-B_{4n+5}), \tag{91}$$

$$a_{2n+2,0} = -\frac{9M^{(2n+3)/3}}{(4n+3)(4n+6)}(A_{4n+6}-B_{4n+6}). \tag{92}$$

Then the process can be repeated at the $(n+1)$th iteration stage.

Now, we will repeat the above argument of part B for what to do at the nth stage if instead of $\Delta E/\mu$, it is Ω_ρ/Ω that is known. A similar procedure as in the $\Delta E/\mu$ case can be followed, except that instead of Eq. (72), Eq. (76) must be used. To compute the $g^{\rho\rho}$ function that appears in this equation, it is necessary to compute the γ function that appears in the metric (67) evaluated on the equatorial plane [see, for example, Ref. [11], Eq. (I.4a) or Ref. [13], Eq. (7.1.26)]:

$$\gamma = -\frac{1}{4}\int_\rho^\infty \left[\frac{\rho'}{g_{tt}^2}\left(\frac{dg_{tt}}{d\rho'}\right)^2 - \frac{g_{tt}^2}{\rho'}\left(\frac{d(g_{t\phi}/g_{tt})}{d\rho'}\right)^2\right]d\rho'. \tag{93}$$

Following a similar argument as in the $\Delta E/\mu$ case, at the iteration labeled by n,

$$(\Omega_\rho/\Omega)_n = \sum_\alpha D_\alpha \Omega^{\alpha/3} \tag{94}$$

can be computed to order $\Omega^{(4n+4)/3}$ and compared to

$$\Omega_\rho/\Omega = \sum_\alpha C_\alpha \Omega^{\alpha/3}. \tag{95}$$

It is easily verifiable that the leading order effect of an $a_{2n,1}$ on $(\Omega_\rho/\Omega)_n$ is

$$i(2n+4)a_{2n,1}M^{-(2n+3)/3}\Omega^{(4n+3)/3}, \tag{96}$$

and $a_{2n,1}$ has no effect on the $\Omega^{(4n+4)/3}$ term. The leading order effect of an $a_{2n+2,0}$ on $(\Omega_\rho/\Omega)_n$ is

$$(n+1)(2n+3)a_{2n+2,0}M^{-(2n+5)/3}\Omega^{(4n+4)/3}. \tag{97}$$

From these facts, the next two coefficients should be set to

$$a_{2n,1} = -i\frac{M^{(2n+3)/3}}{2n+4}(C_{4n+3}-D_{4n+3}), \tag{98}$$

$$a_{2n+2,0} = \frac{M^{(2n+5)/3}}{(n+1)(2n+3)}(C_{4n+4}-D_{4n+4}). \tag{99}$$

If it is Ω_z/Ω that is known, then it is also necessary to compute the second derivatives of the metric functions $g_{tt,zz}$, $g_{t\phi,zz}$, and $g_{\phi\phi,zz}$, evaluated on $z=0$. These require the a_{j2} and a_{j3} terms, which can be obtained from Eq. (86). At the iteration labeled by n,

$$(\Omega_z/\Omega)_n = \sum_\alpha H_\alpha \Omega^{\alpha/3} \tag{100}$$

can be computed to order $\Omega^{(4n+4)/3}$ and compared to

$$\Omega_z/\Omega = \sum_\alpha F_\alpha \Omega^{\alpha/3}. \tag{101}$$

Following the same type of argument as in the case of $\Delta E/\mu$ and Ω_ρ/Ω, the effects of $a_{2n,1}$ and $a_{2n+2,0}$ on $(\Omega_z/\Omega)_n$ are:

$$-i(2n+2)a_{2n,1}M^{-(2n+3)/3}\Omega^{(4n+3)/3}, \tag{102}$$

$$-(n+1)(2n+3)a_{2n+2,0}M^{-(2n+5)/3}\Omega^{(4n+4)/3}, \tag{103}$$

respectively, and $a_{2n,1}$ has no effect on the $\Omega^{(4n+4)/3}$ term. The next two coefficients therefore should be set to:

$$a_{2n,1} = i\frac{M^{(2n+3)/3}}{2n+2}(F_{4n+3} - H_{4n+3}), \tag{104}$$

$$a_{2n+2,0} = -\frac{M^{(2n+5)/3}}{(n+1)(2n+3)}(F_{4n+4} - H_{4n+4}). \tag{105}$$

Whether analyzing $\Delta E/\mu$, Ω_ρ/Ω, or Ω_z/Ω, this iteration can be repeated up to an indefinite order.

4.3.3 Summary of above

To summarize the iterative process that allows for the determination of the a_{j0} and the a_{j1}:

Stage n, Step 1: With the a_{j0} up to $j = 2n$ and the a_{j1} up to $j = 2n-2$, and the higher order a_{j0} and a_{j1} set to zero, use Eqs. (82)–(85) and (75) to compute g_{tt}, $g_{t\phi}$, and $g_{\phi\phi}$ as functions of $1/\rho$ on the equatorial plane.

Stage n, Step 2: From these g_{tt}, $g_{t\phi}$, and $g_{\phi\phi}$, compute $(\Delta E/\mu)_n$ [with the help of Eqs. (64) and (72)], $(\Omega_\rho/\Omega)_n$ [with Eqs. (76) and (93)], or $(\Omega_z/\Omega)_n$ [with Eqs. (76), (86), and (93)] as a function of Ω [with the aid of Eq. (71) to get $1/\rho$ as a function of Ω].

Stage n, Step 3: Set the values of $a_{2n,1}$ and $a_{2n+2,0}$ using Eqs. (91) and (92) for $\Delta E/\mu$, Eqs. (98) and (99) for Ω_ρ/Ω, or Eqs. (4.3.2) for Ω_z/Ω.

Stage n, Step 4: Go to Stage $n+1$, Step 1.

4.3.4 Computing the moments

After as many as desired of the a_{j0} and a_{j1} terms have been computed, the a_{jk} can be computed with Eq. (86). Then, using the algorithm in Ref. [9], the multipole moments can be computed from the a_{jk}: in terms of

$$\bar{\rho} = \frac{\rho}{\rho^2 + z^2}, \quad \bar{z} = \frac{z}{\rho^2 + z^2}, \tag{106}$$

the multipole moments are

$$M_l + iS_l = \left.\frac{S_0^{(l)}}{(2l-1)!!}\right|_{\bar{\rho}=0,\bar{z}=0} \tag{107}$$

where these $S_a^{(n)}$, not to be confused with the S_l, are recursively computed by

$$S_0^{(0)} = \tilde{\xi},\ S_0^{(1)} = \frac{\partial\tilde{\xi}}{\partial\bar{z}},\ S_1^{(1)} = \frac{\partial\tilde{\xi}}{\partial\bar{\rho}}, \tag{108}$$

$$\begin{aligned} S_a^{(n)} \;=\; & \frac{1}{n}\Bigg[a\frac{\partial}{\partial\bar{\rho}}S_{a-1}^{(n-1)} + (n-a)\frac{\partial}{\partial\bar{z}}S_a^{(n-1)} + a\left([a+1-2n]\gamma_1 - \frac{a-1}{\bar{\rho}}\right)S_{a-1}^{(n-1)} \\ & +(a-n)(a+n-1)\gamma_2 S_a^{(n-1)} + (n-a)(n-a-1)\left(\gamma_1 - \frac{1}{\bar{\rho}}\right)S_{a+1}^{(n-1)} \\ & +a(a-1)\gamma_2 S_{a-2}^{(n-1)} - \Big[a(a-1)\tilde{R}_{11}S_{a-2}^{(n-2)} + 2a(n-a)\tilde{R}_{12}S_{a-1}^{(n-2)} \\ & +(n-a)(n-a-1)\tilde{R}_{22}S_a^{(n-2)}\Big]\left(n-\frac{3}{2}\right)\Bigg], \end{aligned} \tag{109}$$

in which $\tilde{R}_{11}$, $\tilde{R}_{12}$, and $\tilde{R}_{22}$ are given by

$$\tilde{R}_{ij} = \left[(\bar{\rho}^2+\bar{z}^2)|\tilde{\xi}|^2 - 1\right]^{-2}\left(G_iG_j^* + G_i^*G_j\right), \tag{110}$$

with

$$G_1 = \bar{z}\frac{\partial\tilde{\xi}}{\partial\bar{\rho}} - \bar{\rho}\frac{\partial\tilde{\xi}}{\partial\bar{z}},\ G_2 = \bar{\rho}\frac{\partial\tilde{\xi}}{\partial\bar{\rho}} + \bar{z}\frac{\partial\tilde{\xi}}{\partial\bar{z}} + \tilde{\xi}, \tag{111}$$

and from these $\tilde{R}_{ij}$,

$$\gamma_1 = (\bar{\rho}/2)(\tilde{R}_{11} - \tilde{R}_{22}),\ \gamma_2 = \bar{\rho}\tilde{R}_{12}. \tag{112}$$

Therefore, knowledge of the mass M and $\Delta E/\mu$, Ω_ρ/Ω, or Ω_z/Ω allows for determination of the M_l and S_l.

We have seen that each a_{l0} and $a_{l-1,1}$ is determined from $\Delta E/\mu$, Ω_ρ/Ω, or Ω_z/Ω by the value of a certain coefficient in the power series expansion. Then, with Eq. (86), all the a_{rs} with $r+s=l$ are determined, and with Eqs. (106)–(112), it can be verified that a variation of $\tilde{\xi}$ by $\sum_{r+s=l} a_{rs}\bar{\rho}^r\bar{z}^s$ leads to a variation in $M_l + iS_l$ such that

$$a_{0l} = M_l + iS_l + L.O.M. \tag{113}$$

"L.O.M." is an abbreviation for lower order moments: some combination of M_j and S_k with $j < l$ and $k < l$. Equivalently by virtue of Eq. (86),

$$a_{l0} = (-1)^{l/2}\frac{(l-1)!!}{l!!}M_l + L.O.M., \tag{114}$$

$$a_{l-1,1} = i(-1)^{(l-1)/2}\frac{l!!}{(l-1)!!}S_l + L.O.M. \tag{115}$$

Given an integer m, for even m, knowing the a_{j0} up to a_{m0} and the a_{j1} up to $a_{m-2,1}$ is equivalent to knowing $M, S_1, M_2, S_3, M_4, \ldots, S_{m-1}, M_m$; for odd m, knowing the a_{j0} up to $a_{m-1,0}$ and the a_{j1} up to $a_{m-1,1}$ is equivalent to knowing $M, S_1, M_2, S_3, M_4, \ldots, M_{m-1}, S_m$. Thus there is a unique term in the power series expansion of any one of the functions $\Delta E/\mu$, Ω_ρ/Ω, or Ω_z/Ω where each multipole moment appears to leading order, and there is a prescribed algorithm for obtaining the moments.

4.3.5 Deriving expansions for $\Delta E/\mu$, Ω_ρ/Ω, and Ω_z/Ω

Finally, Eqs. (79)–(81) can be derived as follows: First, use the method of part D above to compute M_l as a function of $a_{00}, a_{20}, \ldots, a_{l0}$, and $a_{01}, a_{21}, \ldots, a_{l-2,1}$ (or S_l as a function of $a_{00}, a_{20}, \ldots, a_{l-1,0}$, and $a_{01}, a_{21}, \ldots, a_{l-1,1}$). Then, by inverting the series, obtain a_{l0} as a function of M_0, S_1, $M_2, \ldots, S_{l-1}$, M_l, (or $a_{l-1,1}$ as a function of M_0, S_1, $M_2, \ldots, M_{l-1}$, S_l). Inverting is trivial as long as the problem is solved for the $l-1$ case before trying to solve for the l case. The metric functions and from these, $\Delta E/\mu$, Ω_ρ/Ω, or Ω_z/Ω, can then be expressed as functions of the a_{j0} and a_{j1} using the equations in part A. Then inserting the values of these a_{j0} and a_{j1} in terms of the multipole moments, we obtain Eqs. (79)–(81).

Alternatively, we can derive the expansions by simply figuring out how the different combinations of the multipole moments appear in the expansions. First of all, each term has as many powers of M as are required to produce the correct dimensions. Then, for example, to find the S_1S_3 dependence in the Ω_ρ/Ω function, an Ω_ρ/Ω can be chosen (by varying the function order by order as needed) such that when the above algorithm to compute the multipole moments is performed

on this chosen Ω_ρ/Ω, all the multipole moments except S_1 and S_3 are zero, while S_1 and S_3 take on different nonzero values. Then, looking at the $(\Omega_\rho/\Omega)_n$ function as computed in Step 2 of the above iterative process, the dependencies of Ω_ρ/Ω on S_1S_3, $S_1^2S_3$, $S_1S_3^2$, etc., can be inferred by examining how $(\Omega_\rho/\Omega)_n$ changes as S_1 and S_3 change values. For brevity, shown in Eqs. (79)–(81) are the first few terms only, but additional ones are not hard to compute. The calculation was verified by checking that when the moments take on their Kerr values, Eqs. (79)–(81) give the correct expressions that can be computed independently, directly from the Kerr metric.

4.4 Determination of the mass for Ω_z/Ω

With $\Delta E/\mu$ or Ω_ρ/Ω known as a function of Ω, it is easy to determine the mass M since it appears in the first term in either expansion, Eq. (79) or (80). For Ω_z/Ω, it will be shown in this section that M can be determined in the case that there is some precession (Ω_z/Ω is not zero for all Ω). This is possible because up to any order in the Ω expansion of $\Omega_z/\Omega = \sum_\alpha F_\alpha \Omega^{\alpha/3}$, there are roughly twice as many terms as multipole moment variables, and information of the mass is contained in the redundant terms.

If the coefficient of the Ω term in the expansion of Ω_z/Ω is nonzero ($F_3 \neq 0$), then a method to determine M can be derived by examining Eq. (81). If $F_4 \neq 0$, then the mass is

$$M = \left(\frac{4F_6 - 7F_3^2}{8F_4}\right)^{3/2}, \tag{116}$$

while if $F_4 = 0$, then the mass is

$$M = \left(\frac{2F_8}{3F_3^2} + \sqrt{\frac{4F_8^2}{9F_3^4} + \frac{41F_7}{36F_3} - \frac{F_{10}}{3F_3^2}}\right)^{3/2}. \tag{117}$$

In the case that the coefficient of the Ω term in the Ω_z/Ω expansion is zero ($F_3 = 0$), there is a general procedure that can be followed to obtain the mass. With the equations of Sec. 4.3, specifically, those leading up to Expressions (102) and (103) but carrying the process out to one more order, the next-to-leading order effects of the $a_{2n,1}$ (for $n \geq 1$) and $a_{2n+2,0}$ (for $n \geq 0$) on

$(\Omega_z/\Omega)_n$ are

$$-2in(2n+3)a_{2n,1}M^{-(2n+1)/3}\Omega^{(4n+5)/3}, \tag{118}$$

$$-2(n+1)^2(2n+3)a_{2n+2,0}M^{-(2n+3)/3}\Omega^{(4n+6)/3}. \tag{119}$$

Comparing these with Expressions (102) and (103), the mass can be determined by looking at the first nonzero term in the Ω_z/Ω expansion. If the first nonzero term is an $\Omega^{(4n+3)/3}$ term for integer $n \geq 1$, then the mass is

$$M = \left(\frac{(n+1)F_{4n+5}}{n(2n+3)F_{4n+3}}\right)^{3/2}. \tag{120}$$

If the first nonzero term is an $\Omega^{(4n+4)/3}$ term for integer $n \geq 0$, then the mass is

$$M = \left(\frac{F_{4n+6}}{(2n+2)F_{4n+4}}\right)^{3/2}. \tag{121}$$

After M is determined, then the multipole moments can be determined as described in Sec. 4.3, where it is assumed that M is known.

4.5 Leading order effect of the multipole moments on the gravitational-wave phase evolution

Another interesting but much more accurately measurable function of Ω is the gravitational-wave phase evolution for circular orbits in the equatorial plane, expressed as ΔN as a function of Ω, as defined in Eq. (66).

Unfortunately, a similar analysis cannot be conducted for ΔN as was done for the other functions, because the dE_{wave}/dt that appears in ΔN cannot be computed from the Ernst formalism. Rather $dE_{\text{wave}}/dt = -dE/dt$ can only be computed by solving wave equations to compute the wave generation: equations which (apparently) will not decouple from each other nor allow a separation-of-variables solution. These hindrances make the calculation much more difficult than solving perturbations of the Kerr metric, for which decoupling and separation-of-variables do in

fact occur and simplify the problem. To make the situation in the general case even more difficult, ΔN depends also on the inner boundary conditions for the gravitational-wave equations and on the amount of energy absorbed by the central body through, for example, a horizon or tidal heating of matter. These inner conditions are not, in general, determined from just the multipole moments. However, at least in the case of a Schwarzshild black hole, the effects of the horizon do not appear until a very high order [14]. It is perhaps possible that just as we made the idealizing assumption (iv) of energy balance when computing ΔE, we can also make some type of simplicity assumption (such as regularity of the wave functions at the origin), and get an accurate enough answer, but this is not clear. Despite this uncertainty, if in the future the task were undertaken to determine ΔN as a function of at least the lowest few multipole moments, the potential to experimentally test the "no-hair" theorem for black holes would be very promising [4]. It will be shown below that if we once again make our four idealizing assumptions, then ΔN contains full information of all the multipole moments. While we cannot yet construct a general algorithm to actually extract all the multipole moments from ΔN, we can, it turns out, extract M, S_1, and M_2 (enough, in principle, to test the no-hair theorem). The following is just a limited discussion of how each multipole moment appears to leading order in ΔN, which in turn depends on how each multipole moment appears to leading order in ΔE and in the gravitational-wave luminosity.

We will divide the discussion in three parts. In part A, we will show a simple way, based on the mass quadrupolar radiation formalism, to compute how central-body multipole moments with $l \geq 2$ (M_2, S_3, M_4, ...) show up to leading order in the gravitational-wave luminosity, $-dE/dt$. For example, we will see how M_2 first shows up at v^4 order (beyond where M first appears) in the luminosity. However, while we can compute this $M_2 v^4$ term, we cannot compute, for example, $M_2 v^6$ or $M_2 v^8$ terms. In part B, we will show that there is another effect which must be taken into account when calculating the leading order influence of S_1 (at v^3 order) on the luminosity. Moreover, we will calculate the leading order occurrence of not only S_1 but also S_1^2 (which shows up at v^4 order) in the series expansion for the luminosity. The $S_1^2 v^4$ term is calculated for its

usefulness in part C, where the leading order effect of the multipole moments M_l, S_l, and S_1^2 on ΔN are computed. From these leading order effects, and some well-known terms derived elsewhere, we also infer the entire series for ΔN up through v^4 order (including $S_1 v^3$, $S_1^2 v^4$, and $M_2 v^4$). From this fully known part of the series we get a simple way of testing the no-hair theorem. Incidentally, we could also, for example, calculate the leading order effect of M_2^2 on the luminosity, which is an $M_2^2 v^8$ term, but this would be of little practical value since we cannot calculate $M_2 v^8$ terms at present anyway. Therefore, we will limit this discussion to just the leading order effects of M_l, S_l, and S_1^2 on ΔN, and save the more general discussion of higher order terms and combinations of multipole moments [such as an expression similar to Eqs. (79)–(81)] for future work.

4.5.1 The dominant contribution to $-dE/dt$

The luminosity $dE_{\rm wave}/dt = -dE/dt$ can be determined by computing the symmetric trace-free radiative multipole moments [15] that determine the gravitational field of the source. The mass multipole moments I_L and current multipole moments J_L are those of the entire source (including the orbiting object of small mass μ), as opposed to the M_l and S_l moments which are the moments of the central body alone. The L subscript is shorthand for l indices: L means $a_1 a_2 \ldots a_l$. Because the entire source is not axisymmetric, these I_L and J_L are not reducible to scalar moments, as the M_l and S_l moments are. For nearly-Newtonian sources, in terms of an integral over the mass density $\tilde{\rho}$ of the source and Cartesian coordinates y_k, these moments are given by [Ref. [15], Eqs. (5.28)]

$$I_L(t) = \left[\int d^3\mathrm{y}\,\tilde{\rho}(\mathrm{y},t) y_L\right]^{STF}, \tag{122}$$

$$J_L(t) = \left[\int d^3\mathrm{y}\,\tilde{\rho}(\mathrm{y},t) y_{L-1}\epsilon_{a_l km} y_k u_m,\right]^{STF}. \tag{123}$$

The STF superscript means that the expression is to be symmetrized and made trace-free on its l free indices. Repeated indices are summed. The u_m is the material's velocity, so that $\tilde{\rho}u_m$ is the mass-current density. The expression y_L means $y_{a_1} y_{a_2} \cdots y_{a_l}$ and y_{L-1} means $y_{a_1} y_{a_2} \cdots y_{a_{l-1}}$.

In terms of these radiative multipole moments, the gravitational-wave luminosity is [Ref. [15], Eq. (4.16')]

$$-\frac{dE}{dt} = \sum_{l=2}^{\infty} \frac{(l+1)(l+2)}{(l-1)l} \frac{1}{l!(2l+1)!!} \langle I_L^{(l+1)} I_L^{(l+1)} \rangle + \sum_{l=2}^{\infty} \frac{4l(l+2)}{(l-1)} \frac{1}{(l+1)!(2l+1)!!} \langle J_L^{(l+1)} J_L^{(l+1)} \rangle. \tag{124}$$

The brackets indicate averaging over time. A number in parentheses to the above right of a moment indicates taking that many time derivatives of that radiative moment.

The leading order contribution comes from the mass quadrupole radiative moment I_{ij}. This quadrupolar contribution to the energy loss for a mass μ moving in a circle of radius ρ at angular frequency Ω is [see, for example, Ref. [16], Eq. (3.6)]

$$-\left.\frac{dE}{dt}\right|_{I_{ij}} = \frac{32}{5} \mu^2 \rho^4 \Omega^6. \tag{125}$$

It turns out that for all central-body moments except S_1, the leading order correction to Eq. (125) arises from a modification of the orbital radius ρ as a function of Ω. Each mass moment M_l ($l > 0$) or current moment S_l changes ρ by the following [where $v = (M\Omega)^{1/3}$]:

$$\rho = M v^{-2} \left(1 + \frac{(-1)^{l/2} \, (l+1)!! \, M_l \, v^{2l}}{3 \, l!! \, M^{l+1}} \right), \tag{126}$$

$$\rho = M v^{-2} \left(1 - \frac{2(-1)^{(l-1)/2} \, l!! \, S_l \, v^{2l+1}}{3 \, (l-1)!! \, M^{l+1}} \right). \tag{127}$$

Equations (126) and (127) are derived by using Eqs. (114) and (115), (82)–(85), (75), and (71). Inserting Eqs. (126) and (127) into Eq. (125) gives the following leading order effects of the central-body moments on the energy loss, due to the mass quadrupole radiation contribution:

$$-\left.\frac{dE}{dt}\right|_{I_{ij}} = \frac{32}{5} \left(\frac{\mu}{M}\right)^2 v^{10} \left[1 + \sum_{l=2,4,\ldots} \frac{4(-1)^{l/2} \, (l+1)!! \, M_l \, v^{2l}}{3 \, l!! \, M^{l+1}} - \sum_{l=1,3,\ldots} \frac{8(-1)^{(l-1)/2} \, l!! \, S_l \, v^{2l+1}}{3 \, (l-1)!! \, M^{l+1}} \right]. \tag{128}$$

4.5.2 Additional contributions from S_1 and S_1^2

In this section, we discuss another contribution to the radiated power $-dE/dt$ which arises for all central body moments—but which is negligible compared to the ρ-change contribution (128) in all cases except for S_1. For S_1, the second effect together with (128), comprises the full leading order $-dE/dt$.

In computing this second contribution, it will be sufficient to treat each radiative moment in its Newtonian sense: the gravitational field is the sum of the field due to the small mass and the field due to the large mass. The contribution from the small mass comes directly from using Eqs. (122) and (123). The contribution of the large mass can be computed as follows.

If the orbiting object of mass μ were absent, then the radiative moments would be determined from just the moments of the central body: $I_L \propto M_l$ and $J_L \propto S_l$. These moments are stationary and therefore do not radiate. However, in the presence of the orbiting object, the large mass moves along a path $-(\mu/M)x_k$, where x_k is the path of the small mass ($x_1 = \rho\cos(\Omega t)$, $x_2 = \rho\sin(\Omega t)$, and $x_3 = 0$). Therefore, the multipole moments due to the large mass are what the stationary moments would be in a Cartesian coordinate system displaced by $(\mu/M)x_k$. The changes in the $l+1$ radiative multipole moments, due to this displacement, are

$$\delta I_{L+1} = \left[-(l+1)I_L(\mu/M)x_{a_{l+1}}\right]^{STF}, \tag{129}$$

$$\delta J_{L+1} = \left[-\frac{(l+2)l}{l+1}J_L(\mu/M)x_{a_{l+1}}\right]^{STF}. \tag{130}$$

These can be derived from simply applying a coordinate displacement to the metric of Eqs. (11.1) of Ref. [15].

For example, the current quadrupole radiative moment J_{ij} picks up a contribution from the $J_j = S_1\delta_{j3}$ moment of the large mass, and when added to the direct contribution from the orbiting object, it produces for the total radiative current quadrupole moment

$$J_{ij} = \left[\mu x_i\epsilon_{jkm}x_k\frac{dx_m}{dt} - \frac{3}{2}\frac{\mu}{M}x_iS_1\delta_{j3}\right]^{STF}. \tag{131}$$

This result for J_{ij} is given in Kidder, Will, and Wiseman [17].

Eq. (131) inserted into Eq. (124) leads to a contribution to the luminosity of

$$-\left.\frac{dE}{dt}\right|_{J_{ij}} = \frac{32}{5}\left(\frac{\mu}{M}\right)^2 v^{10}\left[\frac{1}{36}v^2 - \frac{1}{12}\frac{S_1}{M^2}v^3 + \frac{1}{16}\frac{S_1^2}{M^4}v^4\right]. \tag{132}$$

The $S_1 v^3$ term is of the same magnitude as the leading-order S_1 term in Eq. (128). However, it is easy to verify that no other central-body moment, M_2, S_3, M_4, S_5, ... , contributes to ΔN by this means, through Eqs. (124) and (130), at the same leading order as in Eq. (128). This is because the time derivatives in Eq. (124) each contribute a factor of Ω, enough factors that the contributions of the I_L ($l > 2$) and J_L moments end up being suppressed sufficiently that they do not appear in the luminosity at leading order.

Now, to finish computing the gravitational-wave luminosity $-dE/dt$: We want the leading order occurrence of each multipole moment, but in addition, to facilitate a discussion below of testing the no-hair theorem, we also want the entire series through order v^4. Eq. (132) can be added to Eq. (128), since both are contributions to $-dE/dt$, and this gives us the first appearances of the multipole moments. But to get the series through order v^4, we also need to add in additional contributions to the luminosity: these terms, which do not involve any multipole moments except for M_0, are derived elsewhere [see, for example, Ref. [16], Eq. (3.13)]. Adding all these terms up, we get:

$$\begin{aligned}
-\frac{dE}{dt} &= \frac{32}{5}\left(\frac{\mu}{M}\right)^2 v^{10}\left[1 - \frac{1247}{336}v^2 + 4\pi|v|^3 - \frac{44711}{9072}v^4\right. \\
&\quad -\frac{11}{4}\frac{S_1}{M^2}v^3 + \frac{1}{16}\frac{S_1^2}{M^4}v^4 - 2\frac{M_2}{M^3}v^4 \\
&\quad + \sum_{l=4,6,\ldots} \frac{4(-1)^{l/2}\,(l+1)!!\;M_l\;v^{2l}}{3\;l!!\;M^{l+1}} \\
&\quad \left. - \sum_{l=3,5,\ldots} \frac{8(-1)^{(l-1)/2}\;l!!\;S_l\;v^{2l+1}}{3\;(l-1)!!\;M^{l+1}}\right].
\end{aligned} \tag{133}$$

Above, the first line has the terms that were derived elsewhere. The second line shows the remaining terms that appear through v^4 order (the M_2 term is explicitly written out, rather than including

it in the summation of the third line, which could have also been done). The third and fourth lines show the leading order occurrences of the higher ($l > 3$) moments. The $-11/4 S_1 M^{-2} v^3$ term from Eq. (133) is well-known [17, 18]. The $(1/16 S_1^2 M^{-4} - 2 M_2 M^{-3}) v^4$ term agrees with previous work [Ref. [16], Eq. (3.13), the $33/16 q^2 v^4$ term] for the Kerr metric.

4.5.3 Computation of ΔN

Finally, we want to compute, from Eq. (66), the leading order effects of the central-body multipole moments on ΔN. This computation requires, in addition to the leading order effects on $-dE/dt = dE_{\rm wave}/dt$, also the leading order effects of the moments on ΔE. By combining Eq. (90) with Eq. (114), as well as combining Eq. (89) with Eq. (115), and using Eq. (79) to get the contributions through v^4 order, we get:

$$\begin{aligned}
\frac{\Delta E}{\mu} &= \frac{1}{3} v^2 \Bigg[1 - \frac{3}{2} v^2 - \frac{81}{8} v^4 \\
&\quad - \sum_{l=2,4,\ldots} \frac{(-1)^{l/2}\, (4l-2)\, (l+1)!!\, M_l\, v^{2l}}{3\, l!!\, M^{l+1}} \\
&\quad + \sum_{l=1,3,\ldots} \frac{(-1)^{(l-1)/2}\, (8l+12)\, l!!\, S_l\, v^{2l+1}}{3\, (l-1)!!\, M^{l+1}} \Bigg] .
\end{aligned} \tag{134}$$

(There is no S_1^2 contribution at v^4 order.)

Combining Eqs. (66), (133), and (134), we get all the terms in ΔN through v^4 order, as well as the leading order effects of the higher moments M_l, S_l ($l \geq 3$):

$$\begin{aligned}
\Delta N &= \frac{5}{96\pi} \left(\frac{M}{\mu} \right) v^{-5} \Bigg[1 + \frac{743}{336} v^2 - 4\pi |v|^3 + \frac{113}{12} \frac{S_1}{M^2} v^3 \\
&\quad + \left(\frac{3058673}{1016064} - \frac{1}{16} \frac{S_1^2}{M^4} + 5 \frac{M_2}{M^3} \right) v^4 \\
&\quad - \sum_{l=4,6,\ldots} \frac{(-1)^{l/2}\, (4l+2)\, (l+1)!!\, M_l\, v^{2l}}{3\, l!!\, M^{l+1}} \\
&\quad + \sum_{l=3,5,\ldots} \frac{(-1)^{(l-1)/2} (8l+20) l!!\, S_l\, v^{2l+1}}{3\, (l-1)!!\, M^{l+1}} \Bigg] .
\end{aligned} \tag{135}$$

Since each multipole moment makes its first appearance at a different order, then ΔN does contain full information of the multipole moments.

It should be stressed that Eqs. (133)–(135) ignore many higher order terms—only the first appearance of each multipole moment is shown.

If ΔN can be measured and written as a series expansion in powers of $\Omega^{1/3}$, and the coefficients of the $\Omega^{-5/3}$, Ω^{-1}, $\Omega^{-2/3}$ and $\Omega^{-1/3}$ terms [i.e. the terms on the first two lines of Eq. (135)] can be determined, then from the four coefficient values, it would be possible to solve for the four unknowns: μ, M, S_1, and M_2. Then by checking to see whether $M_2 = -S_1^2/M$ or not, we could see whether the moments of the larger object correspond to those of a Kerr black hole satisfying the no-hair theorem or not. In reality, as the orbiting object nears its last stable circular orbit, the v parameter in Eq. (135) becomes close to unity, so that many more terms in the series would need to be known for a high accuracy test of the no-hair theorem, as well as to look at higher order moments such as S_3.

There is still much work that is required even after a complete series for ΔN is developed. Some of our four idealizing assumptions made at the beginning of this paper need to be removed: We have considered only circular and equatorial orbits, but should generalize to all orbits. There is also the issue of how ΔN depends on the inner boundary conditions, that is, how it depends on whether or not the central body absorbs energy through a horizon, through tidal heating, etc. Traveling through an accretion disk would also change the orbiting object's energy and angular momentum, thereby affecting ΔN.

However, seeing that the information of the multipole moments is contained in many ways in the gravitational waves is encouragement that even after the problem is solved for the general case, we most likely will still have the ability to determine the central body's spacetime geometry from future gravitational-wave measurements.

Acknowledgments

The author would like to thank Kip Thorne for suggesting this project and for valuable discussions. This work was supported by NSF grant AST-9417371 and by NASA grant NAGW-4268.

References

[1] See, e.g., A. Abramovici, W. E. Althouse, R. W. P. Drever, Y. Gürsel, S. Kawamura, F. J. Raab, D. Shoemaker, L. Sievers, R. E. Spero, K. S. Thorne, R. E. Vogt, R. Weiss, S. E. Whitcomb, and M. E. Zucker, *Science* **256**, 325 (1992).

[2] R. Geroch, J. Math. Phys. **11**, 2580 (1970).

[3] R. O. Hansen, J. Math. Phys. **15**, 46 (1974). In Hansen's paper, S_l is called J_l, and "current" is called "angular momentum".

[4] F. D. Ryan, L. S. Finn, and K. S. Thorne, Phys Rev. Lett., in preparation.

[5] K. S. Thorne, in *Proceedings of Snowmass 94 Summer Study on Particle and Nuclear Astrophysics and Cosmology*, eds. E. W. Kolb and R. Peccei (World Scientific, Singapore), in press.

[6] K. Danzmann, A. Rüdiger, R. Schilling, W. Winkler, J. Hough, G. P. Newton, D. Robertson, N. A. Robertson, H. Ward, P. Bender, J. Faller, D. Hils, R. Stebbins, C. D. Edwards, W. Folkner, M. Vincent, A. Bernard, B. Bertotti, A. Brillet, C. N. Man, M. Cruise, P. Gray, M. Sandford, R. W. P. Drever, V. Kose, M. Kühne, B. F. Schutz, R. Weiss, and H. Welling, *LISA: Proposal for a Laser-Interferometric Gravitational Wave Detector in Space* (Max-Planck-Institut für Quantenoptik, Garching bei München, Germany, 1993).

[7] D. Hils and P. L. Bender, ApJ **445**, L7 (1995).

[8] C. Cutler, T. A. Apostolatos, L. Bildsten, L. S. Finn, E. E. Flanagan, D. Kennefick, D. M. Markovic, A. Ori, E. Poisson, G. J. Sussman, and K. S. Thorne, Phys. Rev. Lett. **70**, 2984 (1993).

[9] G. Fodor, C. Hoenselaers, and Z. Perjés, J. Math. Phys. **30**, 2252 (1989). Be aware that the ρ and z used above correspond to the first, not the second, definitions of ρ and z given in Fodor

et al. The $\bar{\rho}$ and $\bar{z}$ used above correspond to the second definitions of ρ and z (as well as $\bar{\rho}$ and $\bar{z}$) used in their paper.

[10] F. J. Ernst, Phys. Rev. **167**, 1175 (1968).

[11] W. Dietz, in *Solutions of Einstein's Equations, Techniques and Results*, C. Hoenselaers and W. Dietz, eds. (Springer, Heidelberg, 1984).

[12] Algebraic manipulations were performed with the aid of Mathematica [S. Wolfram, *Mathematica: A System for Doing Mathematics by Computer* (Addison-Wesley, Redwood City, California, 1988)].

[13] R. M. Wald, *General Relativity*, (University of Chicago Press, Chicago, 1984).

[14] M. Sasaki, Prog. Theor. Phys. **92**, 17 (1994).

[15] K. S. Thorne, Rev. Mod. Phys. **52**, 299 (1980). The relation between the moments of Thorne and the moments of Geroch and Hansen is discussed in Y. Gürsel, Gen. Rel. & Grav. **15**, 737 (1983).

[16] M. Shibata, M. Sasaki, H. Tagoshi, and T. Tanaka, Phys. Rev. D **51**, 1646 (1995).

[17] L. E. Kidder, C. M. Will, and A. G. Wiseman, Phys. Rev. D **47**, R4183 (1993).

[18] E. Poisson, Phys Rev. D. **48**, 1860 (1993).

5 Spinning boson stars with large self-interaction

Abstract

A rapidly spinning boson star of many solar masses, consisting of a gravitationally bound, massive scalar field with a large self-interaction parameter, may be detectable by gravitational-wave detectors if a particle (a neutron star or a small black hole) were to spiral into the boson star. Necessary for such detection is a knowledge of the boson star's structure. This paper derives the equations governing that structure assuming the star to be stationary and axisymmetric. It is shown that the macroscopic structure of such a star is completely determined by only three parameters, which are related (probably by a one-to-one mapping for spinning stars) to its mass, spin, and quadrupole moment. The structure equations are solved numerically, and the resulting structure and stellar multipole moments are plotted in Figs. 5.4.4–5.4.4. From these figures and from gravitational-wave measurements of a candidate boson star's mass, spin, quadrupole moment, and spin octopole moment, one can in principle confirm the existence of a boson star and determine all three of its parameters. Also discussed is the possibility of the particle inspiraling in the interior of the boson star.

5.1 Introduction

One exciting use for future gravitational-wave detectors is searching for unexpected stellar objects [1]. If a "particle" with mass $\sim 1M_\odot$, such as a small black hole or a neutron star, is observed to be spiraling into an object with a much larger mass M (greater than several solar masses at least) and a radius comparable to GM/c^2, then conventional wisdom would indicate that the larger object must be a black hole. This prediction could be tested, because from the emitted gravitational waves, one can extract the values of the lowest few multipole moments of

the object (its mass M, its spin angular momentum S_1, its mass quadrupole moment M_2, etc., as defined below) [2]. If the object were a black hole, then the moments would satisfy a relation specified by the black-hole no-hair theorem (really, "two-hair" theorem): all the hole's multipole moments are uniquely determined by its lowest two (M and S_1); for example, the quadrupole moment is determined by $M_2 = -S_1^2/M$. But what if the measured moments did not satisfy such a relation, indicating that the object is not a black hole? Some understanding of other candidate objects—and the relations between the multipole moments of such objects when they are rapidly spinning—would be of considerable interest.

This paper examines one such candidate: spinning boson stars. Spherically symmetric (non-spinning) boson stars have been investigated by many authors [3]. There is also some work on spinning boson stars, when slowly spinning in general relativity [4], and in the Newtonian approximation [5]. A boson star is an equilibrium configuration of a scalar field held together by its own gravity while supported against collapse due to the Heisenberg uncertainty principle. With scalar fields often used to model early Universe physics, there is the possibility that such fields could condense to form boson stars. If one were to plot the energy density as a function of radius for a spherically symmetric boson star, the graph would qualitatively resemble the sech(radius/r_0) function. There is a tail region (radius $> r_0$) where the energy density decays approximately exponentially with radius. Most of the mass of the star is located in the "interior", non-tail region.

We are interested in a special type of boson star, when the scalar field ϕ is complex and has a strong self-interaction term $-(1/4)\lambda|\phi|^4$ in the Lagrangian, in addition to the mass term $-(1/2)m^2|\phi|^2$. Colpi, Shapiro, and Wasserman [6] have studied nonspinning, spherical boson stars with such a self-interaction term. They found that a boson star can have a mass comparable to that of a neutron star, or even larger for reasonable values of the boson's rest mass m and self-interaction parameter λ: In the limit of $\lambda \gg m^2/m_{\rm Planck}^2$, the maximum mass of the boson star is $0.1 M_\odot \lambda^{1/2}/(m/\mathrm{GeV})^2$. Since we are interested in the case when the total star mass is greater than several solar masses, then we would hope that λ is significantly larger than one, so that the star

would be massive enough even if m were significantly larger than a GeV. Without self-interaction, the mass of the star would generally be much smaller, and not useful for the aforementioned gravitational-wave application.

Besides being a necessity for boson stars to be observed with gravitational-wave detectors, having a large self-interaction term also leads to convenient simplifications. Colpi, Shapiro, and Wasserman have shown that as λ increases, the size of the tail region decreases relative to the size of the remaining, interior region. Because of this, the interesting macroscopic properties of the star such as its mass can be determined by neglecting the tail region (treating that region as a vacuum). Colpi, Shapiro, and Wasserman found that the non-tail region can be analyzed by changing coordinates and other variables to ones which scale with m and λ, so that neither m nor λ enters explicitly into calculations, except at the end when converting back to the physical variables. They also found that the scalar field varies on such a large spatial scale in the interior region that the spatial derivatives of the scalar field can be ignored, greatly simplifying the analysis.

We wish to generalize the findings of Ref. [6] to the spinning case, because only when spinning are the star's multipole moments (other than the mass) nonzero, thereby allowing gravitational-wave measurements to distinguish the boson star from a black hole. In Sec. 5.2, we will set up the problem of computing the structure and multipole moments of rotating boson stars with strong self-interaction, following the steps of Ref. [6], but for a spinning solution. In Sec. 5.3, we will describe the two-dimensional numerical analysis used to solve the problem, with additional details in the appendix. In Sec. 5.4, *which can be largely understood without first reading Secs. 5.2 and 5.3*, we will give the results of the calculations. We will see that among the more interesting results are how bosons stars are characterized by only three parameters (much like black holes are characterized by two: mass and spin) and how spinning boson stars are shaped like doughnuts with a hole along the axis of spin. We will also briefly discuss how gravitational-wave measurements can be used to search for boson stars and measure their parameters.

5.2 Equations governing a spinning boson star

As is described in Ref. [6], the scalar field Lagrangian density is

$$\mathcal{L} = -\frac{1}{2}g^{\sigma\nu}\phi^*_{,\sigma}\phi_{,\nu} - \frac{1}{2}m^2|\phi|^2 - \frac{1}{4}\lambda|\phi|^4, \tag{136}$$

where m is the mass of the scalar field particle (the boson), and λ is the self-interaction parameter. The $(-,+,+,+)$ sign convention for the metric is used. Natural units, where $G = \hbar = c = 1$, will be used throughout this paper. Thus the mass m is in units of the Planck mass. Since the Planck mass is extraordinarily large, 2.2×10^{-5} grams, then m is extraordinarily small. For the rest of this paper, we consider only the strong self-interaction limit of $\lambda \gg m^2$.

Without gravity, the scalar field would disperse away; with gravity there are bound solutions. We are primarily interested in compact boson stars, which have masses on the order of their radii, because only when the star is compact are the gravitational waves from an inspiraling body in the right frequency band and strong enough for detection, and only then will the waves depend sensitively on the features that distinguish boson stars from other types of stars. For these compact stars, general relativity must be used for the gravitational equations. Einstein's equations take the form $G_{\sigma\nu} = 8\pi T_{\sigma\nu}$, where $T_{\sigma\nu}$ can be derived from the Lagrangian density (136):

$$\begin{aligned} T_{\sigma\nu} &= \frac{1}{2}(\phi^*_{,\sigma}\phi_{,\nu} + \phi_{,\sigma}\phi^*_{,\nu}) \\ &\quad -\frac{1}{2}g_{\sigma\nu}(g^{\xi\zeta}\phi^*_{,\xi}\phi_{,\zeta} + m^2|\phi|^2 + \frac{1}{2}\lambda|\phi|^4). \end{aligned} \tag{137}$$

We will restrict the metric, with coordinates r, θ, φ, and t, to be stationary (not a function of t), axisymmetric (not a function of φ), and reflection symmetric across the equatorial plane (the same at θ as at $\pi - \theta$). The coordinate $\mu \equiv \cos\theta$ will often be used instead of θ.

To achieve stationarity and axisymmetry of the metric and correspondingly of the stress-energy tensor, the scalar field must have the form

$$\phi = \Phi(r,\theta)e^{i(s\varphi - \Omega t)}, \tag{138}$$

where s is an integer [7] and Ω is some constant. It is likely that, in nature, a boson star would be found (if found at all!) in a pure state as in (138), as opposed to a mixed state as the sum over modes of different s. The latter case would not yield a stationary, axially symmetric stress-energy tensor, because if ϕ were the sum of terms like Eq. (138) with different values of s (and as one would naturally expect, each value of $|s|$ has a different value of Ω), then the stress-energy tensor would be time-changing, due to cross terms of ϕ in Eq. (137). It seems reasonable to expect that the gravitational waves produced would remove energy from the higher s modes and drive the star into a pure state, although the details of such a radiation reaction process would be hard to calculate. In any case, we will only consider states with stationary, axisymmetric metrics and thus assume that Eq. (138) holds true.

Let us, for this paragraph only, ignore the tail region. As we mentioned in Sec. 5.1, in the interior, non-tail region the spatial gradient of ϕ (or Φ) can be ignored in the spherical case [6]. We might be tempted to think that the same must be true even when s is nonzero; however, such is not the case because s can be made to scale with λ in such a way (and this will be seen at the end of this section) that the variations of ϕ in the φ-direction cannot be ignored. Indeed, terms like $\phi_{,\varphi}$ in Eq. (137) correspond to a rotating stress-energy tensor. But it is evident from intuition (and we therefore assume) that the stress-energy tensor should vary on the same distance scale when the star is rotating as when the star is not. This implies that $\phi_{,r}$ and $\phi_{,\theta}$ must be ignorable, as they are in the spherical case. Substituting Eq. (138) into Eq. (137) and setting $\Phi_{,r}$ and $\Phi_{,\theta}$ to zero yields

$$T_{\sigma\nu} = (\epsilon + P)u_\sigma u_\nu + P g_{\sigma\nu}, \tag{139}$$

where

$$(u_t, u_\varphi, u_r, u_\theta) = \frac{(-\Omega, s, 0, 0)}{(-g^{tt}\Omega^2 + 2g^{t\varphi}\Omega s - g^{\varphi\varphi}s^2)^{1/2}}, \tag{140}$$

$$\epsilon + P = (-g^{tt}\Omega^2 + 2g^{t\varphi}\Omega s - g^{\varphi\varphi}s^2)|\Phi|^2, \tag{141}$$

$$P = \frac{1}{2}(-g^{tt}\Omega^2 + 2g^{t\varphi}\Omega s - g^{\varphi\varphi}s^2 - m^2)|\Phi|^2 - \frac{1}{4}\lambda|\Phi|^4. \tag{142}$$

Now, for this paragraph, we consider the tail region. Equations (140)–(142) are not valid in the tail region. However, $|\Phi|$ there is so small that it can be ignored (treated as zero), so that for our purpose of looking at macroscopic properties of the star, the stress-energy tensor is zero (we can treat ϵ and P as being zero).

From the previous two paragraphs, we see that the stress-energy tensor is (everywhere, non-tail or tail region) one of a perfect fluid with flow velocity in the axial and time directions. The metric for such a matter configuration can always be written in the form:

$$\begin{aligned} ds^2 &= -e^{\gamma+\rho}dt^2 + e^{2\alpha}(dr^2 + r^2 d\theta^2) \\ &\quad + e^{\gamma-\rho}r^2\sin^2\theta(d\varphi - \omega dt)^2. \end{aligned} \tag{143}$$

Next, let us compute the value of $|\Phi|$ that appears in Eqs. (141) and (142). From the Lagrangian density, we can derive the scalar field equation:

$$g^{\sigma\nu}\phi_{;\sigma\nu} - m^2\phi - \lambda|\phi|^2\phi = 0. \tag{144}$$

In the star's interior region, the r and θ derivatives of the scalar field can be ignored, so Eq. (144) becomes

$$(-g^{tt}\Omega^2 + 2g^{t\varphi}\Omega s - g^{\varphi\varphi}s^2 - m^2)\Phi - \lambda|\Phi|^2\Phi = 0. \tag{145}$$

Anywhere that $|\Phi|$ is small (i.e., the tail region), we can just ignore $|\Phi|$ by setting it to zero. Thus in any region, including the tail, we can say that

$$|\Phi|^2 = \mathrm{Max}[0, (-g^{tt}\Omega^2 + 2g^{t\varphi}\Omega s - g^{\varphi\varphi}s^2 - m^2)/\lambda] \tag{146}$$

or, if we substitute in the metric coefficients,

$$|\Phi|^2 = \mathrm{Max}\left[0, \frac{1}{\lambda}\left(\frac{(\Omega - s\omega)^2}{e^{\gamma+\rho}} - \frac{e^{\rho-\gamma}s^2}{r^2\sin^2\theta} - m^2\right)\right]. \tag{147}$$

Observing Eq. (147), we can see that the tail region (where $|\Phi|^2$ is set to zero) will include all large values of r [all solutions have $\Omega < m$, so the negative m^2 term in Eq. (147) dominates at large r]

and will also include small values of $\sin^2\theta$. Thus spinning boson stars look like doughnuts, because the scalar field is essentially zero in a region around the polar axis, due to the term in Eq. (147) that has $r^2\sin^2\theta$ in the denominator.

Now, combining Eq. (146) with Eqs. (140)–(142), we can write

$$(u_t, u_\varphi, u_r, u_\theta) = \frac{(-\Omega, s, 0, 0)}{(\lambda|\Phi|^2 + m^2)^{1/2}}, \tag{148}$$

$$\epsilon = m^2|\Phi|^2 + \frac{3}{4}\lambda|\Phi|^4, \tag{149}$$

$$P = \frac{1}{4}\lambda|\Phi|^4, \tag{150}$$

where $|\Phi|^2$ is given by Eq. (147).

Equation (148) shows that the boson star perfect-fluid matter is differentially rotating with an angular velocity $d\varphi/dt$ determined by the metric coefficients and the constants Ω and s:

$$\frac{d\varphi}{dt} = \frac{u^\varphi}{u^t} = \omega + \frac{s\, e^{2\rho}}{(\Omega - s\omega)r^2\sin^2\theta}. \tag{151}$$

It is easy to verify from Eqs. (149) and (150) that the star's perfect fluid has an equation of state $P = P(\epsilon)$ given by

$$P = \frac{m^4}{9\lambda}\left[\left(1 + 3\frac{\epsilon\lambda}{m^4}\right)^{1/2} - 1\right]^2; \tag{152}$$

this is the same relation as deduced for nonspinning stars in Ref. [6] [their Eqs. (16) and (17)].

So our task is to solve Einstein's equations for the metric of Eq. (143) with a perfect-fluid stress-energy tensor (139) where 4-velocity, energy, and pressure are expressed in terms of $|\Phi|^2$ by Eqs. (148)–(150), and $|\Phi|^2$ in turn depends upon the metric functions as in Eq. (147). Note that we do not have to worry about which region is the tail region and which is not, because when $|\Phi|^2$ is written as it is in Eq. (146) or (147), both cases are automatically covered.

We can make one more simplification. Following Ref. [6], we can completely eliminate λ and m from the numerical task, because both m and λ always enter in as trivial scale factors in the various quantities. We can remove these two parameters by changing to a different set of variables, with tildes:

$$t = \frac{\lambda^{1/2}}{m^2}\tilde{t}, \tag{153}$$

$$r = \frac{\lambda^{1/2}}{m^2}\tilde{r}, \tag{154}$$

$$s = \frac{\lambda^{1/2}}{m}\tilde{s}, \tag{155}$$

$$\Omega = m\tilde{\Omega}, \tag{156}$$

$$|\Phi|^2 = \frac{m^2}{\lambda}|\tilde{\Phi}|^2, \tag{157}$$

$$\epsilon = \frac{m^4}{\lambda}\tilde{\epsilon}, \tag{158}$$

$$P = \frac{m^4}{\lambda}\tilde{P}, \tag{159}$$

$$\omega = \frac{m^2}{\lambda^{1/2}}\tilde{\omega}. \tag{160}$$

The other metric functions, α, ρ, and γ, are dimensionless in cgs units and do not scale with m or λ, so we do not need to introduce tilded variables for them. Remember that $\tilde{s}$ and $\tilde{\Omega}$ are constants (not functions of $\tilde{r}$ or θ). The other quantities, $|\tilde{\Phi}|^2$, $\tilde{\epsilon}$, $\tilde{P}$, $\tilde{\omega}$, α, ρ and γ are all functions of $\tilde{r}$ and θ.

Rather than solving the problem with factors of m and λ cluttering up the equations, we can solve the Einstein equations for the following metric $d\tilde{s}$ with the following stress-energy tensor $\tilde{T}_{\sigma\nu}$, which are in terms of these new scaled functions (153)–(160):

$$\begin{aligned} d\tilde{s}^2 = & -e^{\gamma+\rho}d\tilde{t}^2 + e^{2\alpha}(d\tilde{r}^2 + \tilde{r}^2 d\theta^2) \\ & + e^{\gamma-\rho}\tilde{r}^2\sin^2\theta(d\varphi - \tilde{\omega}d\tilde{t})^2, \end{aligned} \tag{161}$$

$$\tilde{T}_{\sigma\nu} = (\tilde{\epsilon} + \tilde{P})\tilde{u}_\sigma\tilde{u}_\nu + \tilde{P}g_{\sigma\nu}, \tag{162}$$

$$(\tilde{u}_{\tilde{t}}, \tilde{u}_\varphi, \tilde{u}_{\tilde{r}}, \tilde{u}_\theta) = \frac{(-\tilde{\Omega}, \tilde{s}, 0, 0)}{(|\tilde{\Phi}|^2 + 1)^{1/2}}, \tag{163}$$

$$\tilde{\epsilon} = |\tilde{\Phi}|^2 + \frac{3}{4}|\tilde{\Phi}|^4, \tag{164}$$

$$\tilde{P} = \frac{1}{4}|\tilde{\Phi}|^4, \tag{165}$$

where $|\tilde{\Phi}|^2$ is given by

$$|\tilde{\Phi}|^2 = \mathrm{Max}\left[0, \frac{(\tilde{\Omega} - \tilde{s}\tilde{\omega})^2}{e^{\gamma+\rho}} - \frac{e^{\rho-\gamma}}{\tilde{r}^2 \sin^2\theta}\tilde{s}^2 - 1\right]. \tag{166}$$

The solutions to Einstein's equations applied to the above equations (161)–(166) can then be converted to solutions of the physical problem by reinserting factors of m and λ (and G, $\hbar$, and c). When $\tilde{s}$ is set to zero, then Eqs. (161)–(166) agree with their spherical counterparts: the equations in Ref. [6], such as their Eqs. (12) and (15).

We recall that we are only considering extraordinarily large values of $\lambda^{1/2}/m$, because m is extraordinarily small. We will be considering values of $\tilde{s}$ on the order of a few percent so as to be in the regime of significant centrifugal flattening, so that from Eq. (155), s is very large. Thus even though s can only be an integer, we can think of $\tilde{s}$ as being a continuous parameter since the spacing of allowed values is extremely small. This fact that s is very large also explains why we can [and did, in the paragraph preceding Eq. (139)] ignore $\phi_{,r}$ and $\phi_{,\theta}$ but not $\phi_{,\varphi}$: for fixed $\tilde{s}$, s scales so that the variations of ϕ in the φ direction remain large.

We can see how simple the model, embodied in Eqs. (161)–(166), has become. Once we made the assumption of Eq. (138) to guarantee stationarity and axisymmetry, and once we scaled out λ and m because they are trivial scale factors, a boson star can be computed with only two parameters to be specified: $\tilde{\Omega}$ and $\tilde{s}$. Let us do such computations, next.

5.3 Numerical analysis

Solving the Einstein equations for the metric (161) and stress-energy tensor (162)–(166) can be performed using the method of Komatsu, Eriguchi, and Hachisu [9]. They used a Green's function approach to compute the structure of uniformly rotating polytropic stars. Their Green's function

method essentially consists of taking the Einstein equations $G^{\mu\nu} = 8\pi T^{\mu\nu}$ and keeping on the left-hand side terms for which we know the flat-space Green's function while moving to the right-hand side all the other terms. Thus the metric functions are determined, at each iteration, by an integral of the product of a Green's function and a source term which includes the stress-energy tensor and the other terms that were brought over to the right-hand side.

The same Green's function method will be used here, except with the fluid described by Eqs. (163)–(166). The metric potentials ρ, γ, and $\tilde{\omega}$ can be determined from iterating the following equations [Ref. [9], Eqs. (10)–(12) and (33)–(36); see Secs. 2.1 and 2.3 of Ref. [9] for the derivations and explanations of the following equations]:

$$\rho(\tilde{r},\mu) = -e^{-\gamma/2}\sum_{n=0}^{\infty} P_{2n}(\mu)\left[\frac{1}{\tilde{r}^{2n+1}}\int_0^{\tilde{r}} d\tilde{r}'(\tilde{r}')^{2n+2}\int_0^1 d\mu' P_{2n}(\mu')S_\rho(\tilde{r}',\mu') + \tilde{r}^{2n}\int_{\tilde{r}}^{\infty} d\tilde{r}'\frac{1}{(\tilde{r}')^{2n-1}}\int_0^1 d\mu' P_{2n}(\mu')S_\rho(\tilde{r}',\mu')\right], \tag{167}$$

$$\gamma(\tilde{r},\mu) = -\frac{2}{\pi}e^{-\gamma/2}\sum_{n=1}^{\infty}\frac{\sin[(2n-1)\theta]}{(2n-1)\sin\theta}\left[\frac{1}{\tilde{r}^{2n}}\int_0^{\tilde{r}} d\tilde{r}'(\tilde{r}')^{2n+1}\int_0^1 d\mu'\sin[(2n-1)\theta']S_\gamma(\tilde{r}',\mu') + \tilde{r}^{2n-2}\int_{\tilde{r}}^{\infty} d\tilde{r}'\frac{1}{(\tilde{r}')^{2n-3}}\int_0^1 d\mu'\sin[(2n-1)\theta']S_\gamma(\tilde{r}',\mu')\right], \tag{168}$$

$$\tilde{\omega}(\tilde{r},\mu) = -e^{\rho-\gamma/2}\sum_{n=1}^{\infty}\frac{P^1_{2n-1}(\mu)}{2n(2n-1)\sin\theta}\left[\frac{1}{\tilde{r}^{2n+1}}\int_0^{\tilde{r}} d\tilde{r}'(\tilde{r}')^{2n+2}\int_0^1 d\mu'\sin\theta' P^1_{2n-1}(\mu')S_{\tilde{\omega}}(\tilde{r}',\mu') + \tilde{r}^{2n-2}\int_{\tilde{r}}^{\infty} d\tilde{r}'\frac{1}{(\tilde{r}')^{2n-3}}\int_0^1 d\mu'\sin\theta' P^1_{2n-1}(\mu')S_{\tilde{\omega}}(\tilde{r}',\mu')\right], \tag{169}$$

where the $P_{2n}(\mu)$ and $P^1_{2n-1}(\mu)$ are the Legendre and associated Legendre polynomials, respectively. Again, $\mu = \cos\theta$ and $\mu' = \cos\theta'$. The source terms are given by

$$S_\rho(\tilde{r},\mu) = e^{\gamma/2}\left\{8\pi e^{2\alpha}(\tilde{\epsilon}+\tilde{P})\frac{1+v^2}{1-v^2} + \tilde{r}^2(1-\mu^2)e^{-2\rho}\left(\tilde{\omega}^2_{,\tilde{r}} + \frac{1-\mu^2}{\tilde{r}^2}\tilde{\omega}^2_{,\mu}\right) + \frac{1}{\tilde{r}}\gamma_{,\tilde{r}} - \frac{\mu}{\tilde{r}^2}\gamma_{,\mu} + \frac{1}{2}\rho\left[16\pi e^{2\alpha}\tilde{P} - \gamma_{,\tilde{r}}\left(\frac{1}{2}\gamma_{,\tilde{r}} + \frac{1}{\tilde{r}}\right) - \frac{1}{\tilde{r}^2}\gamma_{,\mu}\left(\frac{1-\mu^2}{2}\gamma_{,\mu} - \mu\right)\right]\right\}, \tag{170}$$

$$S_\gamma(\tilde{r},\mu) = e^{\gamma/2}\left[16\pi e^{2\alpha}\tilde{P} + \frac{\gamma}{2}\left(16\pi e^{2\alpha}\tilde{P} - \frac{1}{2}\gamma^2_{,\tilde{r}} - \frac{1-\mu^2}{2\tilde{r}^2}\gamma^2_{,\mu}\right)\right], \tag{171}$$

$$
\begin{aligned}
S_{\tilde{\omega}}(\tilde{r},\mu) \;=\; & e^{\gamma/2-\rho}\Big\{ -16\pi e^{2\alpha+\rho}\frac{v(\tilde{\epsilon}+\tilde{P})}{(1-v^2)\tilde{r}\sin\theta} + \tilde{\omega}\Big[-8\pi e^{2\alpha}\frac{(1+v^2)\tilde{\epsilon}+2v^2\tilde{P}}{1-v^2} \\
& -\frac{1}{\tilde{r}}(2\rho_{,\tilde{r}}+\frac{1}{2}\gamma_{,\tilde{r}}) + \frac{\mu}{\tilde{r}^2}(2\rho_{,\mu}+\frac{1}{2}\gamma_{,\mu}) + \rho_{,\tilde{r}}^2 - \frac{1}{4}\gamma_{,\tilde{r}}^2 + \frac{1-\mu^2}{\tilde{r}^2}(\rho_{,\mu}^2-\frac{1}{4}\gamma_{,\mu}^2) \\
& -\tilde{r}^2(1-\mu^2)e^{-2\rho}\Big(\tilde{\omega}_{,\tilde{r}}^2+\frac{1-\mu^2}{\tilde{r}^2}\tilde{\omega}_{,\mu}^2\Big)\Big]\Big\}. \qquad (172)
\end{aligned}
$$

Here, v is given by [see Eqs. (13) and (14) of Ref. [9], with the velocity profile of Eq. (163) above]

$$
v = \frac{\tilde{s}}{\tilde{\Omega}-\tilde{s}\tilde{\omega}}\frac{e^{\rho}}{\tilde{r}\sin\theta}. \qquad (173)
$$

The fourth metric potential can be determined from setting $\alpha = \frac{1}{2}(\gamma-\rho)$ at the pole ($\mu = 1$), and integrating with

$$
\begin{aligned}
\alpha_{,\mu} \;=\; & -\frac{1}{2}(\rho_{,\mu}+\gamma_{,\mu}) - \Big\{\frac{1}{2}[\tilde{r}^2(\gamma_{,\tilde{r}\tilde{r}}+\gamma_{,\tilde{r}}^2)-(1-\mu^2)(\gamma_{,\mu\mu}+\gamma_{,\mu}^2)][-\mu+(1-\mu^2)\gamma_{,\mu}] \\
& +\tilde{r}\gamma_{,\tilde{r}}[\frac{1}{2}\mu+\mu\tilde{r}\gamma_{,\tilde{r}}+\frac{1}{2}(1-\mu^2)\gamma_{,\mu}]+\frac{3}{2}\gamma_{,\mu}[-\mu^2+\mu(1-\mu^2)\gamma_{,\mu}] \\
& -\tilde{r}(1+\tilde{r}\gamma_{,\tilde{r}})(1-\mu^2)(\gamma_{,\tilde{r}\mu}+\gamma_{,\tilde{r}}\gamma_{,\mu}) - \frac{1}{4}\mu\tilde{r}^2(\rho_{,\tilde{r}}+\gamma_{,\tilde{r}})^2 \\
& -\frac{1}{2}\tilde{r}(1+\tilde{r}\gamma_{,\tilde{r}})(1-\mu^2)(\rho_{,\tilde{r}}+\gamma_{,\tilde{r}})(\rho_{,\mu}+\gamma_{,\mu}) + \frac{1}{4}\mu(1-\mu^2)(\rho_{,\mu}+\gamma_{,\mu})^2 \\
& +\frac{1}{4}(1-\mu^2)\gamma_{,\mu}[\tilde{r}^2(\rho_{,\tilde{r}}+\gamma_{,\tilde{r}})^2-(1-\mu^2)(\rho_{,\mu}+\gamma_{,\mu})^2] \\
& +(1-\mu^2)e^{-2\rho}\Big(\frac{1}{4}\tilde{r}^4\mu\tilde{\omega}_{,\tilde{r}}^2+\frac{1}{2}\tilde{r}^3(1-\mu^2)\tilde{\omega}_{,\tilde{r}}\tilde{\omega}_{,\mu}-\frac{1}{4}\tilde{r}^2\mu(1-\mu^2)\tilde{\omega}_{,\mu}^2 \\
& +\frac{1}{2}\tilde{r}^4(1-\mu^2)\gamma_{,\tilde{r}}\tilde{\omega}_{,\tilde{r}}\tilde{\omega}_{,\mu}-\frac{1}{4}\tilde{r}^2(1-\mu^2)\gamma_{,\mu}[\tilde{r}^2\tilde{\omega}_{,\tilde{r}}^2-(1-\mu^2)\tilde{\omega}_{,\mu}^2]\Big)\Big\} \\
& \Big/\Big\{(1-\mu^2)(1+\tilde{r}\gamma_{,\tilde{r}})^2+[\mu-(1-\mu^2)\gamma_{,\mu}]^2\Big\}. \qquad (174)
\end{aligned}
$$

We have solved Eqs. (167)–(174) numerically for α, ρ, γ, and $\tilde{\omega}$ as functions of $\tilde{r}$ and θ, using an iteration scheme described in the appendix. We now describe the results of those calculations.

5.4 Results: the structures and multipole moments of spinning boson stars

5.4.1 Overview of results

The structure of any boson star—governed by the Lagrangian (136) with large self-interaction and having the stationary, axially symmetric form of Eq. (138)—is completely characterized by three

parameters: the values of $\lambda^{1/2}/m^2$, $\tilde{\Omega}$, and $\tilde{s}$. The value of $\lambda^{1/2}/m^2$ simply sets the scale—for this reason, it was scaled out of the numerical task via Eqs. (153)–(160). Every macroscopic variable with units of (mass)^n (when G and c but not $\hbar$ are set to 1) will scale like $(\lambda^{1/2}/m^2)^n$; for example, the mass and radius of the star scale like $\lambda^{1/2}/m^2$, the spin of the star scales like $(\lambda^{1/2}/m^2)^2$, and the quadrupole moment scales like $(\lambda^{1/2}/m^2)^3$. Given a fixed value of $\lambda^{1/2}/m^2$, then $\tilde{\Omega}$ and $\tilde{s}$ together specify the shape and structure of the star, with the spin angular momentum of the star being approximately linearly dependent upon $\tilde{s}$.

So we see that any stationary, axisymmetric, strongly self-interacting boson star is completely specified by three parameters, which is one more parameter than just the mass and spin that it takes to specify a black hole. It is probably true that for spinning stars there is a one-to-one correspondence between values of $\lambda^{1/2}/m^2$, $\tilde{\Omega}$, and $\tilde{s}$, and values of the star's lowest three moments: its mass M, its spin S_1, and its quadrupole moment M_2. [We do not have a proof that there is such a correspondence. However, it will become fairly evident later when we view Fig. 5.4.4 that the curves in that figure do not cross (at least in the range shown), so that since the three moments pick out one point on one curve and since $\tilde{s}$ increases from left to right along each curve and $\tilde{\Omega}$ decreases from uppermost to lowermost curve, then $\lambda^{1/2}/m^2$, $\tilde{\Omega}$, and $\tilde{s}$ can all be determined uniquely from the moments.] The lowest three moments are more macroscopically interesting than the other set of quantities, as far as describing the star is concerned. Thus, if we know the star's mass, spin, and quadrupole moment, then all the higher order moments are determined, so that in principle one could use gravitational-wave measurements to determine whether the central object in a binary inspiral is a boson star or not by comparing these higher order moments with the predictions based on the lowest three moments.

Although $\lambda^{1/2}/m^2$ may be an uninteresting parameter in terms of a discussion of boson star structure, $\lambda^{1/2}/m^2$ is interesting because it may agree (or disagree) with high energy physics theory or experiment, either of which could possibly give a candidate value of $\lambda^{1/2}/m^2$. If a boson star were believed to have been found, then from three measurements of the star (such as its mass, its

spin, and its quadrupole moment), $\lambda^{1/2}/m^2$ presumably could be inferred.

Let us assume that the $\lambda^{1/2}/m^2$ parameter is fixed, and look at the characteristics of the boson star as a function of its mass and spin. First, to get a qualitative feel for what a boson star looks like, we will present a graph of the energy density of a typical boson star as a function of location in Sec. 5.4.2. It is known [6] that the masses of nonrotating spherical boson stars can range from zero to about $0.06\lambda^{1/2}/m^2$. As might be expected, the maximum mass of a spinning boson star can be greater, as we will see in Sec. 5.4.2. The radius of the star decreases slightly as the mass increases; thus, the ratio of the mass of the star to the radius increases as the mass increases, as we will see in Sec. 5.4.2. Because gravitational waves are strongest and can give the most information when in the strong gravity regime of the star's mass being comparable to its radius, boson stars having a mass close to the maximum mass are of greatest interest for detection with gravitational waves.

How can one detect these boson stars? More specifically, how can one distinguish a boson star from a black hole or other massive, compact, stellar object? Imagine a neutron star, small black hole, or other small, compact "particle" inspiraling into the boson star of, we assume, much greater mass. When the particle is outside the surface of the star, the emitted gravitational waves carry off information about the multipole moment structure of the star [2]. If we could infer from these waves the lowest few moments—the mass, spin, mass quadrupole moment, and spin octopole moment—with sufficient accuracy, then we would be able to deduce all the information about that boson star (three measurements are needed to parameterize the boson star and the fourth measurement is needed to confirm that the object is indeed a boson star). In Sec. 5.4.3, we will compute the mass quadrupole moment and spin octopole moment as functions of the mass and spin.

There is another way to obtain information about boson stars, which we will briefly discuss in Sec. 5.4.4. This method is applicable to easier-to-compute nonspinning boson stars as well. When the particle penetrates the surface of the star, it may reveal details of the boson field

matter. If the particle is a neutron star, then its subsequent behavior would reveal information of the cross section between neutron-star matter and boson-star matter. One could imagine that the interaction between the two is so weak that the neutron star might continue to travel on an inspiral path dictated solely by gravitation, thereby revealing information of the interior of the star. In fact, any particle, even a black hole, that is much less massive than the boson star could map out the boson star's interior: Since both the mass and radius of the boson star scale as $\lambda^{1/2}/m^2$, then the density of the boson field matter decreases like $(\lambda^{1/2}/m^2)^{-2}$. Thus the effect of the immediately surrounding matter on the particle would presumably become small as $\lambda^{1/2}/m^2$ becomes large.

5.4.2 Shape, mass, and size of boson stars

To convey to the reader an idea of the interior structure of spinning boson stars, we map out a typical star, one with mass $0.05\lambda^{1/2}/m^2$ and spin $S_1 = M^2$. A three-dimensional plot of the energy density as a function of location is shown in Fig. 5.4.4. Notice that the energy density goes to zero in the region around the polar axis (at the bottom-left part of the figure). This implies that the star is shaped like a torus, a fact we mentioned in the paragraph following Eq. (147).

Figure 5.4.4 shows the maximum mass of a boson star as a function of its spin in units of M^2. Each point on the curve was computed by holding $\tilde{s}$ constant and then slowly increasing the specified value for the maximum value of $|\tilde{\Phi}|^2$ (as discussed in the appendix) until the numerical computation became unstable, which is presumably at the maximum mass of the star.

Figure 5.4.4 shows, as a function of mass and spin, the star's equatorial circumference, in units of $2\pi M$. Each curve is for a constant mass, and each point on each curve corresponds to a different value of spin.

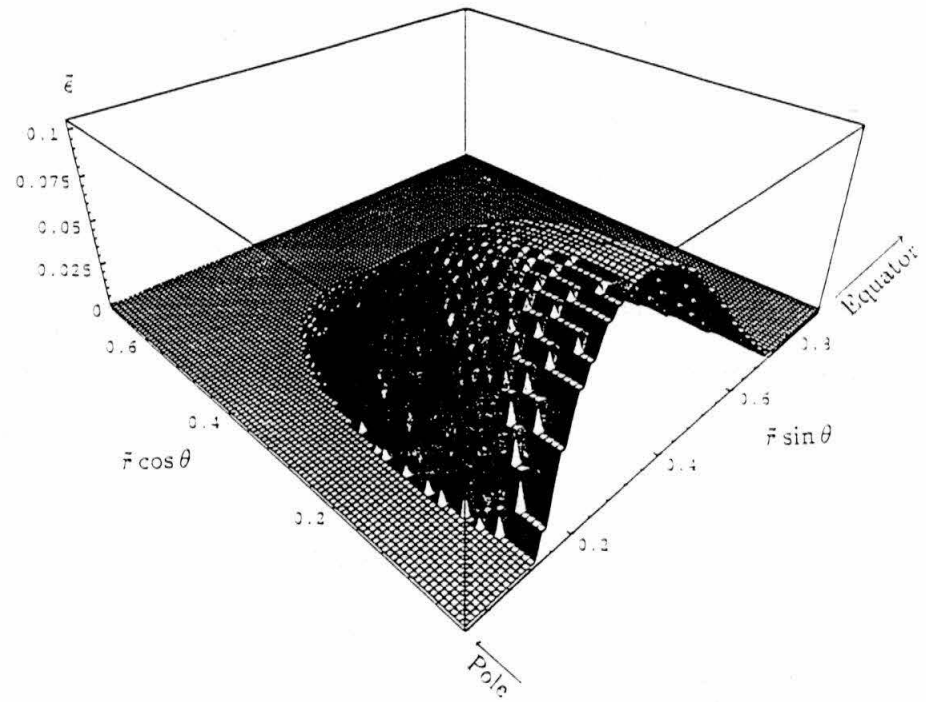

FIG. 1. A three-dimensional plot, prepared using MATHEMATICA, showing the energy density $\bar{\epsilon}$ as a function of location for a quarter of a cross section of a boson star. The vertical axis is the energy density in units of m^4/λ, while the other two axes are (in units of $\lambda^{1/2}/m^2$) the values of $r\cos\theta$ and $r\sin\theta$. The region where the energy density is zero is the tail region. This graph was computed for a star of mass $0.05\lambda^{1/2}/m^2$, with $S_1/M^2=1$, corresponding to $\bar{\Omega}=0.929$ and $\bar{s}=0.0485$.

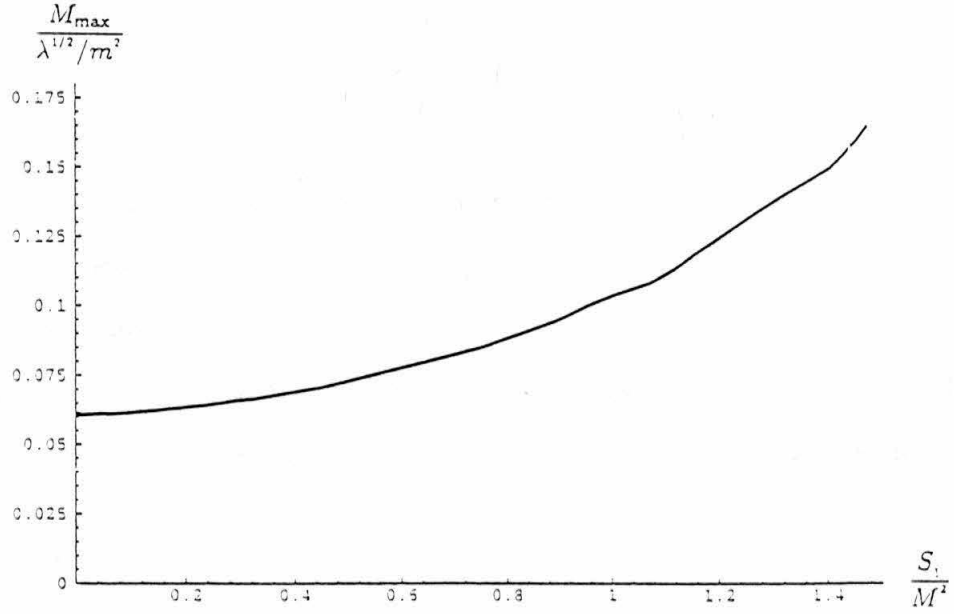

FIG. 2. The maximum mass M of a boson star (beyond which it will collapse to a black hole) as a function of the star's spin angular momentum S_1. The horizontal axis is S_1/M^2 while the vertical axis is the maximum mass M, in units of $\lambda^{1/2}/m^2$, that a star with such spin can have.

5.4.3 Multipole moments

If the metric outside an object is stationary, axisymmetric, reflection symmetric across the equatorial plane, and asymptotically flat, then it can be characterized by two sets of scalar multipole moments: the mass moments M_0, M_2, M_4, ..., and the current moments S_1, S_3, S_5, ...[2, 10]. The moment M_0 is just the mass (so the subscript can be dropped), S_1 is the spin angular momentum, and M_2 is the mass quadrupole moment. These moments affect the gravitational-wave patterns produced when a particle inspirals into the body: The M_n moment first shows up at post^n-Newtonian order and the S_n moment first shows up at post$^{n+1/2}$-Newtonian order. A moment M_n or S_n scales with λ and m like $(\lambda^{1/2}/m^2)^{n+1}$.

The multipole moments are encoded in the asymptotic form of the metric coefficients:

$$\begin{aligned} \rho &= \sum_{n=0}^{\infty} -2\frac{M_{2n}}{r^{2n+1}}P_{2n}(\mu) + \text{higher order}, \\ \omega &= \sum_{n=1}^{\infty} -\frac{2}{2n-1}\frac{S_{2n-1}}{r^{2n+1}}\frac{P^1_{2n-1}(\mu)}{\sin\theta} + \text{higher order}. \end{aligned} \tag{175}$$

Equations (175) and (175) just show the lowest order (in terms of a power series in $1/r$) appearance of each moment. By comparing with Eqs. (167) and (169), it is clear that Eqs. (175) and (175) have the correct angular dependence and correct dependence on the number of powers of $1/r$. The numerical coefficients can be verified by evaluating the above forms for ρ and ω on the equator, and noting their agreement with how the metric on the equator should depend to leading order on the multipole moments, as computed with Eqs. (20)–(23) and (43) of Ref. [2].

The double integral (for each value of n) on the first line of Eq. (167) can be used to get the values of the mass moments: M_{2n} = integral/2. The double integral on the first line of Eq. (169) can be used to get the values of the current moments: S_{2n-1} = integral/$(4n)$. These formulas were derived by comparing Eqs. (167)–(169), (175), and (175).

Figure 5.4.4 shows $-M_2M/S_1^2$ versus S_1/M^2 for a few different constant mass curves (in which, once again, $\lambda^{1/2}/m^2$ is held fixed). Figure 5.4.4 shows $-S_3M^2/S_1^3$ versus S_1/M^2 for some constant mass curves. For Kerr black holes, both $-M_2M/S_1^2$ and $-S_3M^2/S_1^3$ always take on the value of

one, but as Fig. 5.4.4 and Fig. 5.4.4 show us, these ratios are much larger for boson stars. The ratios increase as the mass of the star decreases, corresponding to the stars becoming less compact. For slow spin, the curves are at a constant value. For example, for a slowly spinning star of mass $0.05\lambda^{1/2}/m^2$, the mass quadrupole moment is about 24 times what a black hole of the same mass and spin would have, and the spin octopole moment about 19 times.

Therefore, as an example, if one were to extract from gravitational-wave measurements the lowest four moments M, S_1, M_2, and S_3, and notice that $S_1/M^2 = 0.01$, $-M_2M/S_1^2 = 24$, and $-S_3M^2/S_1^3 = 19$, then one would have good reason to believe that a boson star has been found, with boson field parameters satisfying $\lambda^{1/2}/m^2 = M/0.05$. If instead of 24 and 19, the numbers were 1 and 1, then a black hole has probably been found. If instead of 24 and 19, the numbers were 24 and something significantly different than 19, then most likely, still something else besides a black hole or a boson star has been found.

5.4.4 A map of the star's interior

Let us return to the same star as in Fig. 5.4.4, that of mass $0.05\lambda^{1/2}/m^2$ and $S_1 = M^2$. We can imagine a test particle of unit rest mass orbiting (in the corotating direction) the boson star on a circular geodesic in the equatorial plane. In Fig. 5.4.4, we plot the energy of the particle as a function of its orbital frequency $d\varphi/dt$ times the mass of the star, which corresponds to πMf, where f is the fundamental gravitational-wave frequency. The energy starts out at unity when the frequency is zero, corresponding to when the orbital radius is large. As the radius decreases, one moves clockwise around the curve. When $Md\varphi/dt$ is about 0.018, the particle has reached the star's surface. If the particle continues to travel on a geodesic (even in the presence of the boson star matter), then the frequency continues to increase for a while but then decreases. Circular geodesics are possible and stable all along the curve, up to the point where the curve ends. There, which is at about 5/3 times the radius of the doughnut hole, a circular orbit is no longer a possible solution to the geodesic equation.

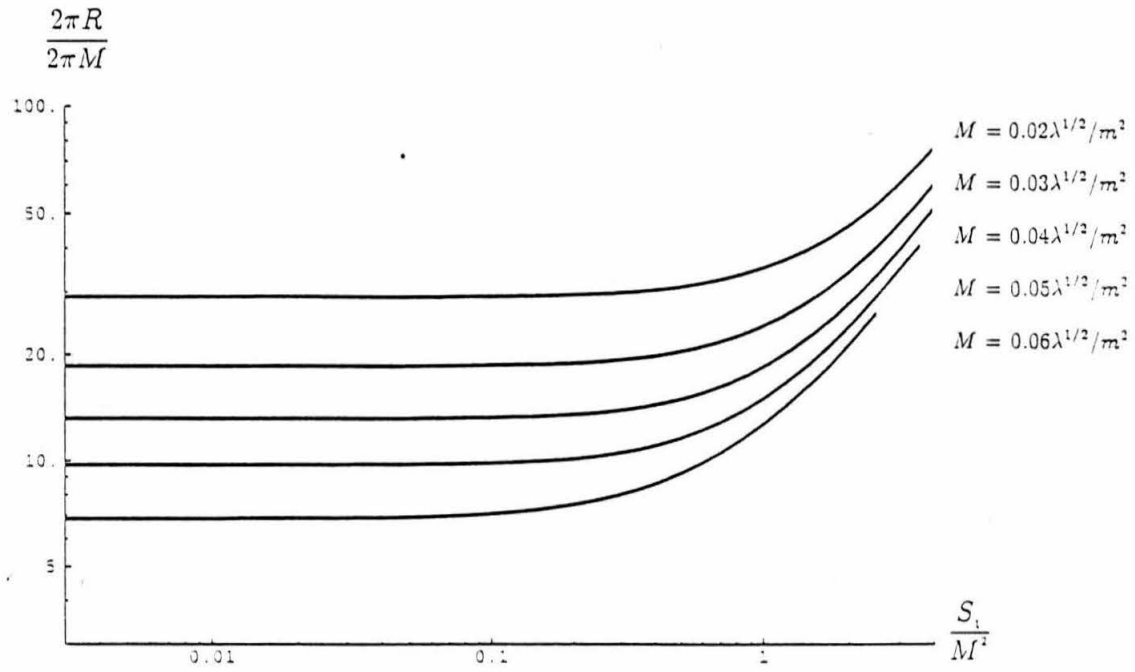

FIG. 3. The equatorial circumference $2\pi R$ of a boson star, in units of $2\pi M$, plotted as a function of the mass M (separate curves) and of the star's spin S_1. From bottom to top, the curves are for boson star masses of 0.02, 0.03, 0.04, 0.05, and 0.06, all in units of $\lambda^{1/2}/m^2$.

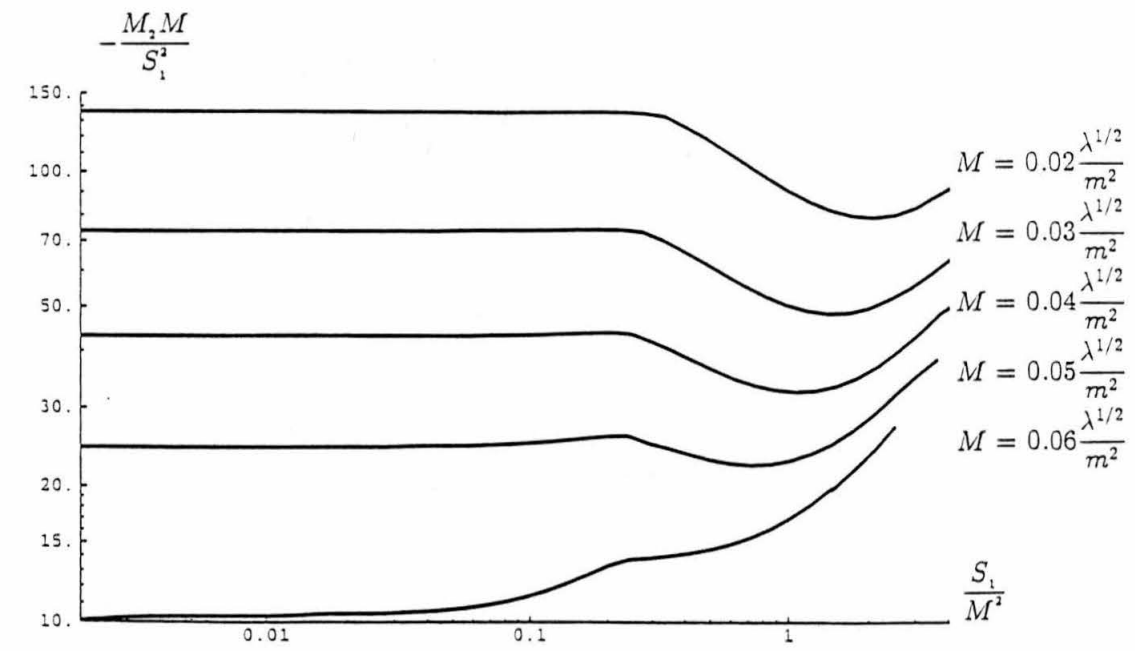

FIG. 4. A graph showing the mass quadrupole moment of a boson star as a function of the star's mass M and spin S_1. The horizontal axis is S_1/M^2 while the vertical axis is $-M_2 M/S_1^2$. From top to bottom, the curves are for boson star masses of 0.02, 0.03, 0.04, 0.05, and 0.06, all in units of $\lambda^{1/2}/m^2$. Note that for a black hole $-M_2 M/S_1^2 = 1$.

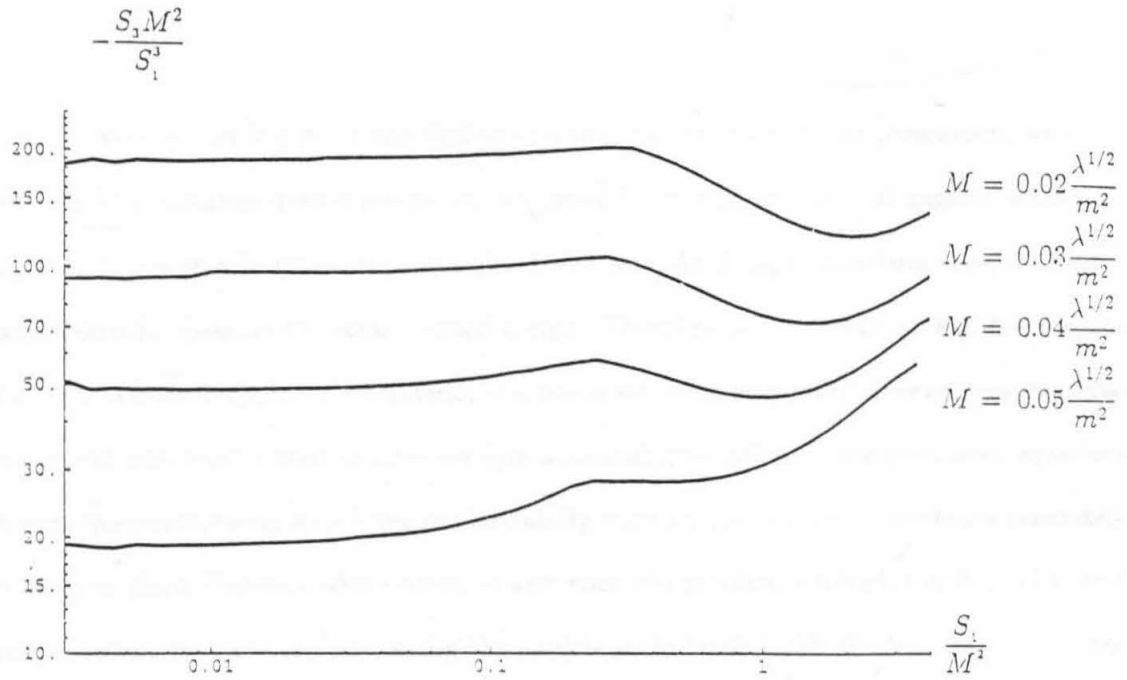

FIG. 5. A graph showing the spin octopole moment of a boson star as a function of the star's mass M and spin S_1. The horizontal axis is S_1/M^2 while the vertical axis is $-S_3M^2/S_1^3$. From top to bottom, the curves are for boson star masses of 0.02, 0.03, 0.04, and 0.05, all in units of $\lambda^{1/2}/m^2$. Note that for a black hole $-S_3M^2/S_1^3 = 1$.

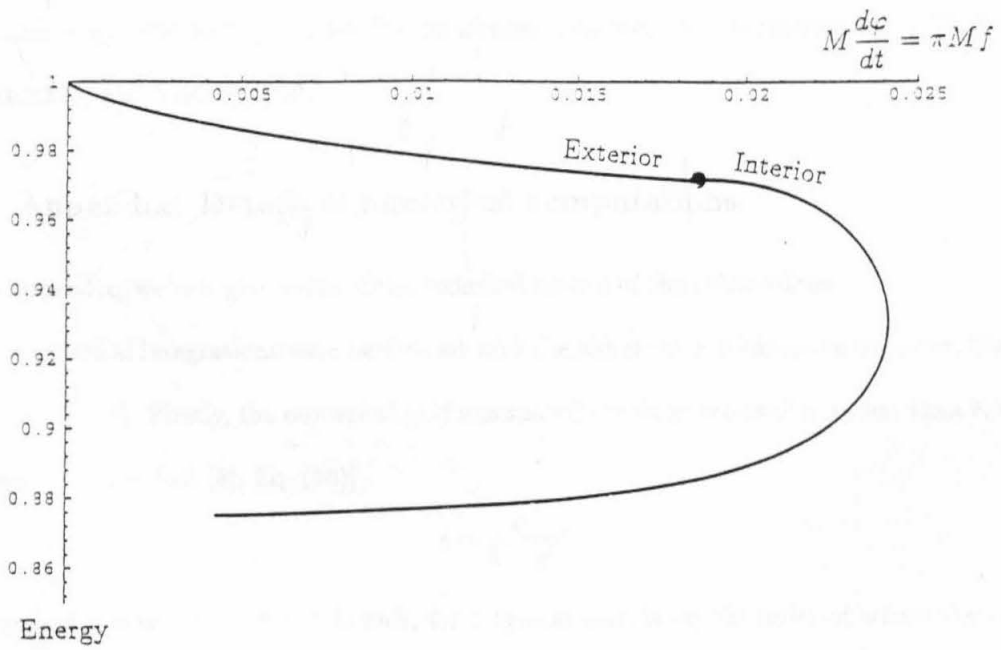

FIG. 6. A plot showing how the energy of a test particle of unit mass (plotted on the vertical axis) varies with the orbital angular frequency, when the particle is in a circular, corotating orbit in the equatorial plane of a boson star. The boson star has a mass of $M = 0.05\lambda^{1/2}/m^2$ and a spin of $S_1 = M^2$. The horizontal axis is the mass of the boson star multiplied by the angular frequency $d\varphi/dt$ of the particle, or equivalently πMf where f is the fundamental-mode frequency of the emitted gravitational waves. Note that 1 − (vertical axis) is the cumulative amount of gravitational-wave energy that has been emitted.

From the curve in Fig. 5.4.4 and similar ones to it for other boson star parameters, we know the emitted gravitational-wave energy per frequency band, summed over all angular directions. However, this energy is not necessarily emitted with some fixed angular pattern; thus, a detector cannot directly measure the total emitted energy. Therefore, a curve such as Fig. 5.4.4 is not enough to allow a mapping of the interior of a boson star from gravitational-wave measurements. One would additionally need to solve the (yet unsolved) gravitational-wave generation equations to know the gravitational waveforms and luminosity, from which one could compute the accurately measurable phase evolution of the waves. If and when this problem is solved, and if gravitational wave detectors find a boson star, and if the particle could travel inside the boson star, then one would be able to map out the boson star's interior.

Acknowledgements

The author is grateful to Kip Thorne for his advice. This work was supported by AST-9417371, PHY-9424337, and NAGW-4268.

5.5 Appendix: Details of numerical computations

In this appendix, we will give some of the technical details of the calculations.

The numerical integrations were performed with the aid of some tricks given by Cook, Shapiro, and Teukolsky [8]. Firstly, the numerical grid was spaced evenly in terms of q, rather than $\tilde{r}$, where q is defined as [see Ref. [8], Eq. (26)]

$$\tilde{r} = \frac{q}{1-q}. \tag{176}$$

This maps $\tilde{r} = 0$ to $q = 0$, $\tilde{r} = 1$ (which, for a typical star, is on the order of where the surface is) to $q = 1/2$, and $\tilde{r} = \infty$ to $q = 1$. The computational grid went from $q = 0$ to $q = 1$ in 1600

(evenly spaced) steps, and from $\mu = 0$ to $\mu = 1$ in 160 steps. Secondly, the angular integrations were improved by using the identities [see Ref. [8], Eqs. (34)–(38)] in Eqs. (167)–(169)

$$\begin{aligned}
P_{2n}(\mu)d\mu &= \frac{1}{2n+1}d[\mu P_{2n}(\mu) - P_{2n-1}(\mu)] \qquad \text{for } n > 0, \\
\sin[(2n-1)\theta]d\mu &= d\left\{\frac{1}{4n}\sin[2n\theta] - \frac{1}{4(n-1)}\sin[2(n-1)\theta]\right\} \qquad \text{for } n > 1, \\
\sin\theta d\mu &= d[\frac{1}{4}\sin(2\theta) - \frac{1}{2}\theta] \quad \text{for } n = 1, \\
\sin\theta P^1_{2n-1}(\mu)d\mu &= \frac{1}{4n-1}d\left[\frac{2n-1}{2n+1}\sin\theta P^1_{2n}(\mu) - \frac{n}{n-1}\sin\theta P^1_{2n-2}(\mu)\right] \qquad \text{for } n > 1, \\
\sin\theta P^1_1(\mu)d\mu &= d(\frac{1}{3}\mu^3 - \mu) \qquad \text{for } n = 1. \qquad (177)
\end{aligned}$$

These angular substitutions prevent, for example, the $n = 0$ component of S_ρ from numerically entering into the $n = 1$ term of Eq. (167): the product of two orthogonal functions can integrate to be slightly nonzero due to numerical error, unless the above substitutions are used. Therefore, any occurrence in Eqs. (167)–(169) of a term that appears on the left-hand side of one of Eqs. (177)–(177) was replaced by the equivalent expression on the right-hand side. The series in Eqs. (167)–(169) were terminated at $n = 10$.

For each computation, the value of $\tilde{s}$ was held fixed in successive iterations. Rather than holding $\tilde{\Omega}$ fixed (which, when tried, made the iterations diverge rapidly), the maximum value that $|\tilde{\Phi}|^2$ takes on the equatorial plane (by looking over all values of $\tilde{r}$ to find the greatest value of $|\tilde{\Phi}|^2$) was held fixed. Such fixing was accomplished by adjusting, at each iteration, the value of $\tilde{\Omega}$ via Eq. (166) so as to keep the maximum value of $|\tilde{\Phi}|^2$ at its target value. To hold the mass of the star fixed, we slowly adjusted the targeted maximum value of $|\tilde{\Phi}|^2$ (which in turn controls the adjusting of $\tilde{\Omega}$).

Just as was done in Sec. 3.4 of Ref. [9], the metric potentials ρ, γ, and $\tilde{\omega}$ were changed, from one iteration to the next, by only a fraction (typically 1/2, but this fraction was changed as deemed necessary) of the change computed—without such a damping factor, the solutions at each iteration tended to bounce around the final solution and converge more slowly. The partial derivatives in Eqs. (170)–(172) and (174) were evaluated by looking at the nearest neighbors of the point, as in

Sec. 3.5 of Ref. [9]. Typically, about 150 iterations were required for each computation.

When computing out the quadrupole moment M_2 (as defined in Sec. 5.4.3), we found that due to numerical error, M_2 would have a slightly nonzero value even when $\tilde{s}$ was set to zero (a nonspinning star should have no quadrupole moment). Similarly, S_3 would have a component in it which is proportional to S_1 (S_3 should vary as S_1^3 for slowly spinning stars). These effects are important when looking at slowly spinning stars, because a slight nonzero offset due to numerical error in, for example, M_2 makes a large difference in $M_2 M/S_1^2$ as S_1 goes to zero. Correcting for these effects required the subtraction of these numerical-error-induced components. For example, to get the corrected value of M_2 for a given mass and small spin, we subtracted the computed value of M_2 at the same mass but with no spin from the computed value of M_2 at the given mass and spin. Unfortunately, the large size of the offset made the S_3 computation for an $M = 0.06\lambda^{1/2}/m^2$ star too inaccurate, so we do not present this case in Fig. 5.4.4.

The code was checked against a one dimensional spherical boson star code (which in turn agrees with past work [6]): The relations between quantities, such as the mass of the star, the frequency $\tilde{\Omega}$, and the maximum value of the scalar field, agree with the spherical code typically to one percent or better. Changing the grid spacing, or changing the maximum value of n by factors on the order of two also produced changes typically less than one percent, even in the spinning case. We checked the code in the spinning case by directly computing the errors in the $\tilde{t}\phi$ and $\tilde{r}\tilde{r}$ components of the Einstein equations, for example computing

$$\frac{\langle | R_{\tilde{t}\phi} - (\tilde{T}_{\tilde{t}\phi} - \frac{1}{2} g_{\tilde{t}\phi} \tilde{T}) | \rangle}{\langle | \tilde{T}_{\tilde{t}\phi} - \frac{1}{2} g_{\tilde{t}\phi} \tilde{T} | \rangle}, \tag{178}$$

where $\langle\ \rangle$ denotes averaging over all grid points. This quantity (178) and the similar one for the $\tilde{r}\tilde{r}$ component, which should be zero ideally, were typically between one and six percent for different masses and spins. Thus, it appears that Einstein's equations are fairly well satisfied locally, and there are probably no serious errors in the code.

Copies of the numerical code are available from the author.

References

[1] F. D. Ryan, L. S. Finn, and K. S. Thorne, in preparation.

[2] F. D. Ryan, Phys. Rev. D **52**, 5707 (1995).

[3] R. Ruffini and S. Bonazolla, Phys. Rev. **187**, 1767 (1969). Discussions of later work concerning spherical boson stars can be found in the following review articles: A. R. Liddle and M. S. Madsen, Int. J. Mod. Phys. D **1**, 101 (1992). P. Jetzer, Phys. Rep. 220, 163 (1992). T. D. Lee and Y. Pang, Phys. Rep. 221, 251 (1992).

[4] Y. Kobayashi, M. Kasai, and T. Futamase, Phys. Rev. D **50**, 7721 (1994).

[5] V. Silveira and C. M. G. de Sousa, Phys. Rev. D **52**, 5724 (1995).

[6] M. Colpi, S. L. Shapiro, and I. Wasserman, Phys. Rev. Lett. **57**, 2485 (1986).

[7] The proof in Ref. [4] that boson stars cannot spin perturbatively corresponds to the quantization of the spin: the $s = \pm 1$ states are not perturbations of the $s = 0$ (nonspinning) state.

[8] G. B. Cook, S. L. Shapiro, and S. A. Teukolsky, Astrophys. J., **398**, 203 (1992)

[9] H. Komatsu, Y. Eriguchi, and I. Hachisu, Mon. Not. R. astr. Soc., **237**, 335 (1989). Note that the "Ω" of Ref. [9] (the angular velocity as measured at infinity), is not the same as our Ω or $\tilde{\Omega}$ (the frequency of the boson field). We avoided using the angular velocity Ω [which would equal Eq. (151) above], eliminating it by virtue of Ref. [9], Eq. (13).

[10] R. O. Hansen, J. Math. Phys. **15**, 46 (1974).

6 Accuracy of estimating the multipole moments of a massive body from the gravitational waves of a binary inspiral

Abstract

If the gravitational field of a massive, compact body is stationary, axially symmetric, and reflection symmetric across the equatorial plane, and if a much less massive compact object (such as a neutron star or a small black hole) were to orbit in a circle on the equatorial plane of the central, compact body, then the produced gravitational waves would carry the values of the central body's multipole moments. By detecting those waves and extracting from them the central body's lowest few moments, gravitational-wave detectors have the potential to test the black-hole no-hair theorem and search for exotic objects such as naked singularities and boson or soliton stars. This paper estimates how accurately we can expect to measure the central body's moments. The measurement errors are estimated using a combination of, first, the leading-order (of a post-Newtonian series) contribution of each moment to the gravitational-wave phase, second, an a priori probability distribution that constrains each moment's magnitude to a range appropriate for a compact body, and third, any relations that the multipole moments satisfy among themselves, which reduce the number of degrees of freedom for the waves (this is useful in cases when one is searching for a specific type of compact body). We find that the Earth-based LIGO detector cannot provide sufficiently precise measurements of enough multipole moments to search for exotic objects, but the space-based LISA detector can do so.

6.1 Introduction

Recently, construction has begun on several "high-frequency" Earth-based laser-interferometer gravitational-wave detectors, including the Laser Interferometer Gravitational-Wave Observatory (LIGO) [1]; and hopefully the European Space Agency's "low-frequency" Laser Interferometer Space Antenna (LISA) [2] will be flying by the year 2014. Among the promising observable events for Earth-based detectors are neutron stars or small black holes spiraling into massive black holes, $M_\odot \ll M \lesssim M_\odot$; and similarly promising for space-based detectors are white dwarfs, neutron stars, or small black holes spiraling into $\sim 10^5 M_\odot$ to $\sim 3 \times 10^7 M_\odot$ black holes [3, 4]. For LISA, binary inspirals where the smaller mass is a $\sim 10 M_\odot$ black hole would be of especial interest: at $\sim 10 M_\odot$, the orbiting object is less likely to be perturbed by other orbiting objects than would be a solar-mass compact object, and it would generate stronger gravitational waves than its solar-mass counterpart [2, 5, 6, 7]. Although the calculation of event rates depends on many assumptions, we might expect [2] to detect such events with a signal-to-noise ratio of ~ 40 for one year searches with LISA, for binaries at cosmological redshift $z = 1$.

The waves from such types of inspiral carry information of the central black hole's spacetime geometry, encoded in two sets of multipole moments [8]. If the central body is indeed a black hole, then the moments should satisfy a relation as dictated by the black-hole no-hair theorem [9]. Any discrepancies would signal either a violation of the no-hair theorem and general relativity, or that the central body is not a black hole but actually another type of compact object, such as a naked singularity or a boson or soliton star [10, 11]. In this paper, we will take the viewpoint of general relativity being correct, and that we are searching for non-black-hole, massive, compact bodies.

Of course, a discrepancy can either be actually physical or be merely a statistical error from the data analysis of the detected gravitational waves. The latter effect would be due to the matched filtering analysis measuring best-fit parameters for the waves' source which differ from the actual parameters by detector-noise-induced stochastic errors. In this paper, we will attempt to *estimate*

the errors [we use the word "error" to mean the standard error (the rms difference between the actual and measured values of a parameter)] that we can expect for measurements of the first few multipole moments of the central body.

Finn [12], Finn and Chernoff [13], Cutler and Flanagan [14], and Poisson and Will [15] have established the data analysis formalism (that we shall use and extend to measuring multipole moments) and have analyzed measurement accuracies for the mass and spin parameters of compact binaries for Earth-based detectors such as LIGO. Poisson [16] has used the same type of data analysis formalism for space-based detectors. His analysis shows how one can use measurements of binary inspirals to look for violations of general relativity or indications that the central body is not a black hole. In that analysis, the gravitational-wave phase is expanded in a power series around the frequency of gravitational waves at the last stable circular orbit (the orbit at which a test particle can no longer move on a circular geodesic and must plunge into the central body). The measured parameters in that power series become the parameters that describe the central body (or the theory of gravity, if one chooses the viewpoint that general relativity may not be correct). This type of parameterization would be suitable when assuming that the central body is a black hole or some type of similar object; however, it would be less useful when searching for objects vastly different from a black hole. For example, a spinning boson star [11] may have a radius larger than the last stable circular orbit for a black hole of the same mass. Such a case would not be well suited for the power series expansion around the frequency of gravitational waves at the last stable circular orbit.

Our analysis differs from Ref. [16] in that our classification of the central body is in terms of the multipole moment expansion of its external gravitational field around radial infinity. Correspondingly, our analytical expansion of the produced gravitational-wave phase is performed around the gravitational-wave frequency of zero. The multipole moment parameterization covers a much broader range of possible central bodies.

We have mentioned that we only provide estimates of the measurement errors in this paper.

An exact calculation would be very difficult. By confining our analysis to a simple case and using a simplified model gravitational waveform, we can calculate errors which should give some indication of what the errors would be in the exact calculation.

Here is a summary of our idealizing assumptions:

1. For simplicity, we will deal only with central bodies whose external gravitational field is stationary, axisymmetric, reflection symmetric across the equatorial plane, and asymptotically flat. With this assumption, the multipole moments can be described by two sets of scalars [8, 17, 18]: There are the mass multipole moments consisting of the mass M and higher-order multipole moments M_l (the mass quadrupole moment M_2, M_4, M_6, ...). In our units which we use here and throughout, we set $G = c = 1$, so that M_l has units of $(\text{mass})^{l+1}$. Since it will be more useful to deal with dimensionless quantities, we define the dimensionless moments $m_l \equiv M_l/M^{l+1}$. There are also the mass-current multipole moments S_l (the spin angular momentum S_1, the current octopole moment S_3, S_5, S_7, ...), for which we can define dimensionless counterparts $s_l \equiv S_l/M^{l+1}$.

2. The sizes of the errors that we will compute for the moments m_l and s_l, as well as for the other binary parameters such as the masses, will be functions of the values of those moments. However, for simplicity and for the sake of being able to present the results in a concise form, we will only compute the errors for the case in which the moments m_l and s_l are either zero or small enough that terms appearing in the gravitational-wave phase which are quadratic in these moments can be ignored in our analysis. Making this approximation miscalculates the errors for the moments by amounts which scale linearly with the moments, while it miscalculates the errors for all other parameters by amounts which scale quadratically with the moments [see Eq. (3.26) of Ref. [14] and surrounding discussion]. The errors as computed for this spherical or almost spherical case should be reasonable estimates for the errors in the general case. As we will see below in Sec. 6.4, there will be some cases when the errors on

the moments become $\gtrsim 1$, so that even if the best-fit measurement for a moment has it equal to zero, the actual value of the moment may not be small at all and our approximation of dropping quadratic terms becomes poor. Even in such cases, the errors should still be good as order of magnitude approximations. This is because terms quadratic in the multipole moments occur at a higher order in a post-Newtonian series and typically affect the waveform by a smaller amount.

3. Besides its mass and multipole moments, the central body has other parameters that can affect the waveforms. In this paper, we will not consider how such effects enter into the analysis. For example, the waveforms will depend on whether or not the central body has a horizon, but we will assume that the waves generated if the central body does not have a horizon are the same as those if the body does have one. Similarly, the waveforms will depend on whether or not the central body absorbs energy through tidal heating; we will assume it does not absorb energy.

4. We will assume that the inspiraling compact object has a sufficiently small mass μ ($\mu \ll M$) that its orbital path is close to being a geodesic of the central body's unperturbed spacetime geometry, and that this is true throughout the inspiral, up to a point just before the last stable circular orbit when the object plunges into the central body.

5. In general, the orbit will be both elliptical and out of the equatorial plane. The eccentricity e is probably small for the smaller mass binaries that Earth-based interferometers can detect, because gravitational radiation reaction tends to circularize orbits [19]. However, for $\sim 10^6 M_\odot$ central bodies studied by space-based detectors, the orbit may be highly eccentric due to recent perturbations by other orbiting objects [5, 7]. Unlike the case with eccentricity, the inclination angle ι between the orbital axis and the central body's symmetry axis is not driven to be small by radiation reaction [20]. Therefore, in general, the orbital motion will be very complicated, consisting of the orbiting object traveling (approximately) in an

ellipse, while that ellipse precesses in its plane, and while that plane itself precesses around the central body's symmetry axis. For this paper, to avoid these complications, we will only solve the problem in the ideal situation of the compact object traveling in the equatorial plane in a slowly shrinking, circular orbit.

6. We will assume that the inspiraling object travels through vacuum. This may not be a good assumption if an accretion disk surrounds the central body. We will also assume that any other orbiting objects do not significantly perturb the orbit of the object whose waves we are measuring. We will only consider the case when the equatorial size of the central body is smaller than the radius of the last stable circular orbit, although it is easy to modify our analysis below to account for the waves cutting off at a larger radius than where such a last stable circular orbit would be.

7. The predicted templates for the gravitational waveforms are not yet known. This is because the computation of the waves from the inspiral of a compact object around a body with arbitrary multipole moments is complicated by two-dimensional differential equations which are not separable and have not yet been solved. However, we do know how each multipole moment affects the phase of the gravitational waves to leading order in a post-Newtonian expansion [8]. With this information we should be able to get at least a good order of magnitude estimate for the errors.

8. We will assume a large signal-to-noise ratio S/N (as defined below). The limit of large S/N is necessary to simplify the analysis and so that we can be certain of detection in the first place.

9. We will use the noise curves for LIGO and LISA to compute the measurement accuracies. We will assume the noise is stationary and Gaussian. The noise curves for these detectors are only the expected ones; the actual curves might turn out to be different when the detectors are fully operational. Furthermore, space-based detectors will revolve around the sun [21],

thereby having changing angular sensitivity patterns. We will not incorporate this revolution effect in our analysis. However, it is partially taken into account through the fact that the signal-to-noise ratio will be reduced through the angular averaging that the revolution creates (see Ref. [2], Figure 1.3, and associated discussion).

10. The errors depend on how we model the possible values that the multipole moments can take. Below, we will give a model for the *a priori* probability distribution that is appropriate for a compact body of characteristic size (radius) r. Although this value of r is arbitrary, we will select a particular value ($r = 3M$) in our calculations.

This is certainly a long list of approximations and restrictions; however, it is reasonable to expect that they will not seriously compromise the primary intent of this paper: to find out the prospects for measuring multipole moments so as to determine whether or not it is worthwhile for theorists to pursue this calculation in greater depth. We will see that for LISA it is worthwhile.

Hopefully, many of the above restrictions will be removed in future, more sophisticated analyses, so that experimenters will have a complete set of numerically generated templates with which to work. These numerically generated templates will be accurate not only where the gravitational-wave frequency is near zero (where our analysis is valid) or near the frequency at the last stable circular orbit (where the analysis of Ref. [16] is valid), but also at all frequencies in between.

We will use the convention that the orbital angular momentum vector of the orbiting object points in the direction relative to which the mass-current moments are defined. For example, if the central body were a Kerr black hole and spinning in the same direction as the object revolves, then s_1 would be positive; if spinning in the opposite direction, then s_1 would be negative.

The binary will generally be at distances where the cosmological redshift z cannot be neglected. Therefore, the frequencies of the gravitational waves as measured are a factor of $(1+z)^{-1}$ of those that would be measured at the source. Similarly, it is $(1+z)\mu$ and $(1+z)M$ that are measured, as opposed to μ and M. The dimensionless multipole moments m_l and s_l are not affected by

the redshift factor. To make our equations easier to read, we will not write down these factors of $(1+z)$, although the conversion should be remembered that where below we write μ or M, we imply $(1+z)\mu$ or $(1+z)M$, respectively.

In Sec. 6.2, we will briefly review the method for computing the errors. In Sec. 6.3, we will construct a model of the gravitational waves in the time and frequency domains. We will also try to quantitatively understand the validity of using only the leading-order contribution of each moment (assumption 7 above). In Sec. 6.4, we will compute the errors for several different situations, and will deduce their implications for LIGO and for LISA.

6.2 Data analysis

The data analysis formalism used in this section is described in much greater detail in Refs. [12, 13, 14, 15]. In this section, we will summarize that formalism as needed for our purpose, and show how the multipole moments can be given an *a priori* probability distribution.

In the presence of a time-dependent gravitational-wave strain $h(t)$, the gravitational-wave detectors measure a signal $s(t) = h(t) + n(t)$, where $n(t)$ is noise which we assume to be Gaussian. We assume that the waveform $h(t)$ is one of many possible waveforms $h(t, \theta^i)$ for which we have theoretically-predicted templates, with θ^i being the parameters that describe the waves, including the multipole moment parameters. We do not know, from the gravitational-wave measurements, exactly what are the true values of θ^i. Rather, all we know is that if we have measured the signal $s(t)$, the probability distribution function for θ^i to be the correct values can be written in terms of the prior probability distribution and the inner product as (see Appendix 1 of Ref. [14])

$$p(\theta^i) \propto p^{(0)}(\theta^i) e^{-(n|n)/2} = p^{(0)}(\theta^i) e^{-(s-h|s-h)/2}. \tag{179}$$

Here, $p^{(0)}(\theta^i)$ is our *a priori* probability distribution of the parameters θ^i, and $(n|n)$ is the inner product (defined below) of $n(t)$ with itself. Although $p^{(0)}(\theta^i)$ can be modeled rather arbitrarily,

we choose a particular fairly unrestrictive model. We assume that the prior probability satisfies

$$p^{(0)}(\theta^i) = \prod_{\text{even } l} p^{(0)}(m_l) \prod_{\text{odd } l} p^{(0)}(s_l); \tag{180}$$

that is, we assume that there is a uniform prior probability distribution function for all parameters except the multipole moments, and that each moment is *a priori* independent of the other moments. Our assumption that the central body is compact (at least it has a small equatorial plane circumference since the inspiraling object is able to make tightly bound orbits) suggests that the magnitude of each moment m_l or s_l cannot be much greater than $(r/M)^l$, where r is some parameter that can be thought of as the characteristic size or radius of the compact body. This parameter is not necessarily associated with some physical radius of the central body; rather, it is just some parameter that we have to choose which restricts the multipole moments. More specifically, we assume prior probability distributions of the form

$$p^{(0)}(m_l) \propto \exp\left[-\frac{1}{2}\left(m_l \frac{M^l}{r^l}\right)^2\right], \tag{181}$$

$$p^{(0)}(s_l) \propto \exp\left[-\frac{1}{2}\left(s_l \frac{M^l}{r^l}\right)^2\right]. \tag{182}$$

We should not choose $r \gtrsim 6M$, since then the central body would not be compact and in such case we would not be able to measure the moments accurately anyway. On the other hand, we should not choose $r \lesssim M$, because we wish to consider a class of possible compact bodies broader than just black holes, and black holes themselves have moments satisfying $|m_l| \leq 1$ and $|s_l| \leq 1$, as a result of the no-hair theorem [8, 9, 18],

$$m_l + i s_l = (i s_1)^l, \tag{183}$$

and the restriction $|s_1| \leq 1$. Below, when we calculate values for the errors, we will mainly use the choice $r = 3M$, but also we we will show how the errors change when we change r.

Equations (181) and (182) state that the *a priori* probability distribution for each moment is centered around zero and has a width of $(r/M)^l$. One might raise the objection that centering the

distribution around zero is not the best choice. For example, most spinning objects have a negative mass quadrupole moment m_2 due to the equator's centrifugal bulge. However, our assumption is easy to work with, and involves a minimum of theoretical prejudices. One might also decide to model the central body as a spinning object which cannot rotate faster than the point at which it would centrifugally breakup and therefore might restrict s_l to be constrained like $(r/M)^{l-(1/2)}$ instead of $(r/M)^l$. We will not use this alternative model.

The inner product $(\cdot|\cdot)$ between two signals (or a signal and a template) is defined by [Ref. [14], Eq. (2.3)]

$$(h_1|h_2) = 2\int_0^\infty \frac{\tilde{h}_1^*(f)\tilde{h}_2(f) + \tilde{h}_1(f)\tilde{h}_2^*(f)}{S_n(f)}df, \tag{184}$$

where a tilde represents the Fourier transform, and $S_n(f)$ is the detector's noise spectral density: For Earth-based detectors, we follow Cutler and Flanagan [Ref. [14], Eq. (2.1)] and use the following approximate analytic fit to the expected LIGO noise curve for advanced interferometers [1]

$$\begin{aligned} S_n(f > 10\text{ Hz}) &= \frac{3\times 10^{-48}}{\text{Hertz}}\left[\left(\frac{f}{f_0}\right)^{-4} + 2 + 2\left(\frac{f}{f_0}\right)^2\right], \\ S_n(f < 10\text{ Hz}) &= \infty. \end{aligned} \tag{185}$$

where $f_0 = 70$ Hertz. For space-based detectors, we use the following fit to the LISA noise curve

$$S_n(f) = \frac{8\times 10^{-42}}{\text{Hertz}}\left[\left(\frac{f}{f_a}\right)^{-14/3} + 2 + 2\left(\frac{f}{f_\lambda}\right)^2\right], \tag{186}$$

where $f_a = 0.0015$ Hertz and $f_\lambda = 0.03$ Hertz. This fit is only valid for 10^{-4} Hertz $< f <$ 10^{-1} Hertz, to which we restrict our analysis. We choose this fit as it agrees with the noise curve in Fig. 1.3 of Ref. [2]. The term scaling like $f^{-14/3}$ is due to acceleration noise (see Table 3.3 of Ref. [2]), the term constant in f is due to optical-path noise (such as shot noise; see Table 3.2 of Ref. [2]), and the term scaling like f^2 is due to the gravitational waves having shorter wavelengths than LISA's round-trip arm-lengths.

The overall prefactors in these two noise curves do not affect our analysis. Rather, those

prefactors affect the signal-to-noise ratio, as computed by [Ref. [14], Eq. (2.5)]

$$S/N = (h|h)^{1/2}. \tag{187}$$

We assume the S/N to be a given number, and the overall amplitude of the signal h is normalized to give that number. This normalization can be done because the amplitude of h is inversely proportional to the distance to the binary [as we will see below in Eq. (195)]. Therefore, we assume that the binary is at the distance required to get the assumed S/N.

Denoting by $\bar{\theta}^i$ the best-fit values for the parameters θ^i, the probability that the true set of parameters is $\bar{\theta}^i + \Delta\theta^i$ is [Ref. [15], Eqs. (2.8) and (2.9)]

$$p(\bar{\theta}^i + \Delta\theta^i) \propto p^{(0)}(\bar{\theta}^i + \Delta\theta^i) e^{-\frac{1}{2}\Gamma_{ij}\Delta\theta^i\Delta\theta^j}, \tag{188}$$

where

$$\Gamma_{ij} = \left(\frac{\partial h}{\partial \theta^i} \middle| \frac{\partial h}{\partial \theta^j} \right). \tag{189}$$

The partial derivatives are evaluated at $\theta^i = \bar{\theta}^i$.

With our assumption that the best-fit parameters $\bar{\theta}^i$ have $m_l = 0$ and $s_l = 0$, then our prior probabilities are

$$p^{(0)}(\bar{\theta}^i + \Delta\theta^i) \propto e^{-\frac{1}{2}\Gamma^{(0)}_{ij}\Delta\theta^i\Delta\theta^j}, \tag{190}$$

where

$$\Gamma^{(0)}_{m_l m_l} = (M/r)^{2l} \text{ for even } l > 2, \tag{191}$$

$$\Gamma^{(0)}_{s_l s_l} = (M/r)^{2l} \text{ for odd } l > 1, \tag{192}$$

and all other components of the $\Gamma^{(0)}$ matrix are zero.

The error matrix can be computed by taking the inverse of the Fisher information matrix $\Gamma + \Gamma^{(0)}$ (see Appendix 6 of Ref. [14]):

$$\Sigma = (\Gamma + \Gamma^{(0)})^{-1}. \tag{193}$$

The error $\delta\theta^i$ (that is, the standard error, or the root-mean-square error) for each parameter θ^i is [Ref. [14], Eq. (2.8)]

$$\delta\theta^i = (\Sigma^{ii})^{1/2}. \tag{194}$$

We have to know the template forms $h(t, \theta^i)$; that is, how the waveform depends on all the parameters for which we are fitting. As we will see in the next section, these parameters consist of the overall signal amplitude, two integration constants (the time and phase of signal arrival), the masses μ and M, and the multipole moments m_l and s_l. Since we only need $\partial h/\partial m_l$ and $\partial h/\partial s_l$ (both evaluated around the spherical case) for Eq. (189), then we only need to know the waveform accurate to linear order in each of the moments with m_l and s_l. That is, we need to know the waveform assuming the central body is spherical, and how the waveform varies when each moment is varied.

6.3 The gravitational waveforms

In this section, we will first construct a model waveform as a function of the just mentioned parameters. We will then compute its Fourier transform. Finally, we will examine the validity of our assumption of only including the leading-order (in a post-Newtonian series) contribution of each moment.

The gravitational-wave strain $h(t)$ that a detector measures is very complicated: $h(t)$ is a linear combination of the waveforms $h_+(t)$ and $h_\times(t)$ that come from the source, with the coefficients in that combination being functions of the orientations of the detector's axes and the direction to the binary. Although these orientations change during the duration of the signal for space-based detectors which revolve around the sun, we ignore this slow modulation [21]. The waveforms $h_+(t)$ and $h_\times(t)$ themselves are complicated functions of the angles between the binary's axes and the line from the binary to the detector. All of the angular factors which go into determining the amplitude for the waves are combined into some function Q of the angles. For the purpose of trying to estimate the errors, the fact that Q is really a slowly changing function of time is not

important. Nor are we too concerned with the form of Q as a function of the angles for the same reason that we were not too concerned with the prefactors in the noise curves (185) and (186): the distance to the binary is adjusted as appropriate to give us the assumed S/N.

Not only is the overall amplitude of the signal not too important for our analysis, but also the exact form of the amplitude as a function of time is not nearly as important as the phase of the oscillating waveform. This is because there is a large number of cycles in the signal, so that the effect of a slight change in the parameters on the phase is on the order of that large number times greater than the effect of that slight change in parameters on the amplitude. Because of this, we can approximate [13, 14, 15] the waveform as having an amplitude as computed in the Newtonian limit for a spherical body. In addition, it is a sufficiently good approximation to examine only the dominant frequency F of the gravitational waves, which is twice the orbital frequency.

As the orbit shrinks, F is a slowly varying function of time t. The model waveform $h(t)$ can then be written as a function of F as [see Ref. [14], Eq. (2.12)]:

$$h(t) = \left(\frac{384}{5}\right)^{1/2} \pi^{4/3} Q \frac{\mu}{D} (MF)^{2/3} \cos\left(\int 2\pi F dt\right), \tag{195}$$

where D is distance to the source, chosen to give the assumed S/N.

The $F(t)$ appearing in Eq. (195) should be computed carefully, for if $F(t)$ were off by a small fraction, then after a number of cycles equal to half the reciprocal of that fraction, the template would go from in-phase to out-of-phase with the gravitational wave. Instead of dealing with $F(t)$, we use the dimensionless quantity $\Delta N(F)$, the number of cycles that the dominant gravitational-wave frequency spends in a logarithmic interval of frequency:

$$\Delta N \equiv \frac{F^2}{dF/dt} = F^2 \frac{dE/dF}{dE/dt}, \tag{196}$$

where E is the orbital energy of the binary.

For dE/dt, we add the exact post^4-Newtonian series expansion for a spherical black hole [Ref. [23], Eq. (43)], rounded off to six digit accuracy, and the leading-order (in a post-Newtonian

series) contribution of each moment [Ref. [8], Eq. (55)], resulting in

$$\begin{aligned}\frac{dE}{dt} &= -\frac{32}{5}\left(\frac{\mu}{M}\right)^2(\pi MF)^{10/3}\Bigg[1-3.71131(\pi MF)^{2/3}+12.5664(\pi MF)-4.92846(\pi MF)^{4/3}\\
&-38.2928(\pi MF)^{5/3}+[115.732-5.43492\ln(\pi MF)](\pi MF)^2\\
&-101.510(\pi MF)^{7/3}+[-117.504+17.5810\ln(\pi MF)](\pi MF)^{8/3}\\
&+\sum_{\text{even } l\geq 2}\frac{4(-1)^{l/2}\ (l+1)!!m_l(\pi MF)^{2l/3}}{3\ l!!}-\sum_{\text{odd } l\geq 3}\frac{8(-1)^{(l-1)/2}\ l!!s_l(\pi MF)^{(2l+1)/3}}{3\ (l-1)!!}\\
&-\frac{11}{4}s_1(\pi MF)\Bigg].\end{aligned} \tag{197}$$

For dE/dF, we add the exact expression for the spherical case [Ref. [22], Eq. (4)] to the leading-order and linear contribution of each moment [Ref. [8], Eq. (56)], resulting in

$$\begin{aligned}\frac{dE}{dF} &= -\frac{\pi M\mu}{3(\pi MF)^{1/3}}\Bigg[\frac{1-6(\pi MF)^{2/3}}{[1-3(\pi MF)^{2/3}]^{3/2}}\\
&-\sum_{\text{even } l\geq 2}\frac{(-1)^{l/2}(4l-2)(l+1)!!m_l(\pi MF)^{2l/3}}{3\ l!!}\\
&+\sum_{\text{odd } l\geq 1}\frac{(-1)^{(l-1)/2}(8l+12)l!!s_l(\pi MF)^{(2l+1)/3}}{3\ (l-1)!!}\Bigg].\end{aligned} \tag{198}$$

Combining Eqs. (196)–(198), we calculate ΔN as a post-Newtonian series, which, like $F(t)$, has to be calculated accurately. However, we do not expand out the $[1-6(\pi MF)^{2/3}]$ factor that came from dE/dF for the spherical case. This non-expansion was shown to greatly improve the accuracy of the template [see Ref. [22], Eq. (18)]. The result is [see Ref. [8], Eqs. (57)]

$$\begin{aligned}\Delta N &= \frac{5}{96\pi}\left(\frac{M}{\mu}\right)(\pi MF)^{-5/3}\Bigg[\sum_{n=0,2,3,4,5,6,7,8}a_n(\pi MF)^{n/3}[1-6(\pi MF)^{2/3}]\\
&+\sum_{n=6,8}b_n(\pi MF)^{n/3}\ln(\pi MF)[1-6(\pi MF)^{2/3}]\\
&-\sum_{\text{even } l\geq 2}\frac{(-1)^{l/2}(4l+2)(l+1)!!m_l(\pi MF)^{2l/3}}{3\ l!!}\\
&+\sum_{\text{odd } l\geq 3}\frac{(-1)^{(l-1)/2}(8l+20)l!!s_l(\pi MF)^{(2l+1)/3}}{3\ (l-1)!!}+\frac{113}{12}s_1(\pi MF)\Bigg].\end{aligned} \tag{199}$$

Above, the a and b coefficients are those that describe the post-Newtonian expansion around a spherical black hole: $a_0 = 1$, $a_2 = 8.21131$, $a_3 = -12.5664$, $a_4 = 52.2782$, $a_5 = -111.531$,

$a_6 = 335.734$, $a_7 = -716.863$, $a_8 = 1790.54$, $b_6 = 5.43492$ and $b_8 = 47.2175$. Even though Eq. (199) is really just part of a post-Newtonian series, we treat it as exact for our model of the waveform.

We need, for Eq. (184), the Fourier transform of $h(t)$. Following Refs. [13, 14, 15], we compute $\tilde{h}(f)$ from Eq. (195) using the stationary phase approximation:

$$\tilde{h}(f) = \mathcal{A} f^{-7/6} \exp[i\psi(f)], \tag{200}$$

where $\mathcal{A} = (Q/D)\mu^{1/2}M^{1/3}$ and

$$\psi(f) \;=\; 2\pi f\, t(f) - \phi(f) - \frac{\pi}{4}, \tag{201}$$

with

$$t(f) = \int \frac{dt}{dF} dF = \int \frac{\Delta N}{F^2} dF, \tag{202}$$

and

$$\phi(f) = \int 2\pi F \frac{dt}{dF} dF = \int 2\pi \frac{\Delta N}{F} dF. \tag{203}$$

Equation (200) has to modified to account for the waves' shutting off at the last stable circular orbit. We have to set $\tilde{h}(f)$ to zero for $f > 6^{-3/2}(\pi M)^{-1}$, the gravitational-wave frequency when the orbiting object plunges into the central body [14]. [Technically, this frequency changes with the mass M and with the multipole moments, and such variations enter into the $\partial h/\partial\theta^i$ terms in Eq. (189), but these variations can be ignored because they affect the amplitude of the signal, which is measured to far less accuracy than the phase.] Substituting our expression (199) for ΔN in Eqs. (201)–(203) and keeping the expression only to linear order in m_l and s_l yields

$$\begin{aligned}
\psi(f) \;=\; & 2\pi f t_* - \phi_* - \frac{\pi}{4} + \frac{3}{128}\left(\frac{M}{\mu}\right)(\pi M f)^{-5/3}\Bigg\{ \sum_{n=0,2,3,4,6,7} \frac{40 a_n}{(n-8)(n-5)} (\pi M f)^{n/3} \\
& - \sum_{n=0,2,4,5,7,8} \frac{240 a_n}{(n-6)(n-3)} (\pi M f)^{(n+2)/3} \\
& - \frac{40}{9}(a_5 - 6a_3)(\pi M f)^{5/3} \ln(\pi M f) + \frac{40}{9}(a_8 - 6a_6)(\pi M f)^{8/3} \ln(\pi M f)
\end{aligned}$$

$$
\begin{aligned}
&-20b_6(\pi Mf)^2[\ln(\pi Mf) - \frac{3}{2}] + \frac{40}{9}(b_8 - 6b_6)(\pi Mf)^{8/3}\left[\frac{1}{2}\ln^2(\pi Mf) - \ln(\pi Mf)\right] \\
&-24b_8(\pi Mf)^{10/3}[\ln(\pi Mf) - \frac{21}{10}] \\
&- \sum_{\text{even } l\neq 4} \frac{(-1)^{l/2}40(2l+1)(l+1)!!m_l(\pi Mf)^{2l/3}}{3(2l-5)(l-4)l!!} \\
&+ \sum_{\text{odd } l\geq 3} \frac{(-1)^{(l-1)/2}80(2l+5)l!!s_l(\pi Mf)^{(2l+1)/3}}{3(l-2)(2l-7)(l-1)!!} \\
&+\frac{113}{3}s_1(\pi Mf) - 50m_4(\pi Mf)^{8/3}\ln(\pi Mf)\Big\}, \qquad (204)
\end{aligned}
$$

where t_* and ϕ_* are integration constants from the integrals in Eqs. (202) and (203). These two parameters must be included in the list of parameters θ^i for which errors are computed. They can be *called* the time and phase of the signal, although such names are rather arbitrary since we only defined t_* and ϕ_* up to the addition of constants. One could easily redefine, by adding constants, t_* and ϕ_* to be the time and phase when F reaches some fiducial frequency F_*. Since we are interested more in the multipole moment parameters than in t_* and ϕ_*, we do not bother to do such redefinitions.

For the remainder of this section, we will try to understand how good or poor is our approximation of using only the leading-order contribution (of a post-Newtonian series) of each multipole moment. The relevance of this discussion depends mainly on the frequency range through which we measure the inspiral. For example, if the frequency at the beginning of the measured inspiral were a factor of ten less than at the end of the inspiral at the last stable circular orbit, then most of the cycles would be at frequencies where the post-Newtonian expansion would be good even to leading order. Consequently, our estimates of the errors on the lowest few moments would be good. Another case in which our approximation would be valid is if the gravitational-wave frequency at the last stable circular orbit were high and in a region of poor detector sensitivity, so that most of our information would come from the lower frequency portion of the waves. If, however, a significant portion of our information were to come from near the last stable circular orbit, then we would have to examine how well our approximation serves.

Our main concern is that our form for including the multipole moments in ΔN might for some reason be extremely poor near the last stable circular orbit, for example, due to poor convergence of some series. It is not so much our concern that higher-order post-Newtonian terms which are comparable to the leading-order terms might make a difference. In fact, we have experimented by "making up" higher-order post-Newtonian terms (with coefficients on the order of the leading-order term) for each moment, and found little differences in the errors as computed in the next section.

If there were some strong effect on ΔN and consequently $\psi(f)$ [note that $\psi(f)$ is derived exactly from ΔN; if the latter were exactly correct, then so would be the former], it would likely show up in the location of the last stable circular orbit where, by virtue of dE/dF going to zero, ΔN goes to zero. We can test the validity of the leading-order approximation by assuming small values of all moments m_l and s_l and computing the gravitational-wave frequency at the last stable circular orbit as computed by two ways, listed in the next two paragraphs. This test should be a sensitive indicator as to the accuracy of our approximation, because of the strong dependence of the gravitational-wave phase on the last stable circular orbit [22]; if we have calculated the last stable circular orbit's dependence on the moments to some accuracy then we are likely to have calculated the high-frequency gravitational-wave phase's dependence on the moments to a similar accuracy.

The first way of computing the last stable circular orbit is by looking at where the ΔN in Eq. (199) "thinks" it is; that is, where that ΔN goes to zero. Solving $\Delta N = 0$ gives the last stable circular orbit at frequency

$$F = \frac{1}{6^{3/2}\pi M}\left(1 + \sum_{\text{even } l\geq 2} g_l m_l + \sum_{\text{odd } l\geq 1} g_l s_l\right), \tag{205}$$

where the values of the g_l coefficients are listed in Table 1.

The second way is by computing where ΔN of the actual gravitational waves [as opposed to our model gravitational waves and the ΔN in Eq. (199)] would go to zero. This can be computed

because we can compute where the actual dE/dF goes to zero. We did this by writing a computer program to calculate out the metric with all the m_l and s_l up to $l = 32$ set to zero except one slightly nonzero moment. This program uses a method that we will not discuss in this paper because, first, the discussion would be lengthy, second, a future paper [24] will give details of the method, and third, the method is simply the inverse process of Fodor, Hoenselaers, and Perjés' method of computing the multipole moments given the metric [25]: we guess a metric, compute its moments using Ref. [25], and then modify the metric order-by-order in a power series in $M/(\text{radius})$. After we computed the metric, we calculated the frequency where a circular orbit's energy is minimal. The result is that this method predicts a last stable circular orbit of

$$F = \frac{1}{6^{3/2}\pi M}\left(1 + \sum_{\text{even } l\geq 2} h_l m_l + \sum_{\text{odd } l\geq 1} h_l s_l\right), \tag{206}$$

where the values of these h_l are also given in Table 1. It is easy to verify the first coefficient analytically ($h_1 = 11/6^{3/2}$), since the last stable circular orbit of a slowly rotating Kerr black hole can be computed (see Section 61 of Ref. [27]).

Examining Table 1, we see that for low values of l, the g_l and h_l are of the same order of magnitude, but at higher values they begin to differ greatly. For low values of l, then, our approximation of using only the leading order contribution of each moment m_l or s_l in ΔN should be adequate, for two reasons: First, with a low value of l, the moment has a large fraction of its effect on ΔN at frequencies much less than the frequency at the last stable circular orbit where the post-Newtonian expansion is good and the leading order term should be sufficient. Second, even at higher frequencies close to the frequency at the last stable circular orbit, the approximation should be at the correct order of magnitude. On the other hand, for higher values of l, neither of these two reasons is applicable. As it will turn out, however, the errors for the higher order moments will be primarily determined by the *a priori* information $\Gamma^{(0)}$, so that the severe disagreement between the g_l and the h_l for large l is unimportant.

6.4 Results

In this section, we will discuss the errors $\delta\theta^i$ for a variety of situations. All numbers were computed using Mathematica to numerically evaluate the $\delta\theta^i$ in Eq. (194) from Eq. (193), which uses the *a priori* information matrix in Eqs. (191) and (192) and the inspiral information matrix in Eq. (189), which in turn relies upon Eq. (184), either noise curve (185) or (186), and Eqs. (200) and (204).

While the diagonal terms in the error matrix give the errors, the off-diagonal terms contain information of the correlation coefficients [see Ref. [15], Eq. (2.12)]. We will not list these terms for lack of space. Usually, there is a strong correlation (correlation coefficient close to $+1$ or -1) between the time and phase parameters, the two mass parameters, and the first few (lowest order) multipole moment parameters. On the other hand, there is usually a weaker correlation between higher order moments, because the errors for higher order moments are primarily dependent upon the (uncorrelated) *a priori* probability distribution, as we will soon see. We will now focus only on the diagonal terms.

In computing the errors, the amplitude parameter $\mathcal{A}$ can be computed easily and separately from the others, because a glance at Eqs. (184), (189), and (200) shows that $\Gamma_{\mathcal{A}j} = 0$, where j is any other parameter besides $\mathcal{A}$. Thus $\mathcal{A}$ is uncorrelated with any other parameter. Its error is given by

$$\delta\mathcal{A} = \frac{\mathcal{A}}{S/N}. \tag{207}$$

We now consider the errors for the other parameters only.

The errors depend on how many multipole moment parameters $l_{\max}$ are included in the fit. For example, the error on s_1 would be greater if fitting for moments up to m_4 ($l_{\max} = 4$) than if fitting up to s_3 ($l_{\max} = 3$). As $l_{\max}$ increases, the dependence is at first very strong, but eventually the errors begin to approach certain values. If we are measuring the moments of an unknown object, then $l_{\max}$ has to be chosen to be infinite or, in practice, large enough such that the errors stop growing. If, on the other hand, we are trying to determine whether an object is a black hole or

not then we only have to fit up to $l_{\max} = 2$. This is because we can perform the fit assuming all the moments with $l > l_{\max}$ (s_3, m_4, ...) are given by Eq. (183), and then the test of whether m_2 satisfies Eq. (183) or not serves to check whether the object is a black hole or not. As another example, searching for a spinning boson star would require fitting up to $l_{\max} = 3$ [11].

When one knows any such relation that gives the higher-order moments (with $l > l_{\max}$) as functions of the lower-order moments (with $1 \leq l \leq l_{\max}$), all occurrences of the higher-order moments in Eq. (199) should be replaced with the functions of the lower-order moments. For the present though, we want to perform an analysis without specifying the relation. We can do this by replacing all the higher-order moments with zero, instead of with the (presently unspecified) functions of the lower-order moments. This is a good approximation, because a lower-order moment has a much stronger effect on ΔN (and consequently on the waveform and on the errors) through where it normally occurs at a low order in the post-Newtonian expansion than where it occurs in the replacement of a higher-order moment.

In Tables 2–7 (described in more detail in the following paragraphs), each column shows the error of the parameter listed at the top of the column. We actually give the base-10 logarithm, so that large negative numbers correspond to precise measurements. Each row corresponds to a different value of $l_{\max}$, the number of moments being measured. As $l_{\max}$ increases, the error on the $l_{\max}$-th moment (ten to the power of the rightmost number in that row) approaches the *a priori* error for the $l_{\max}$-th moment, $(r/M)^{l_{\max}}$. We should expect this, since the gravitational-wave measurement does not have enough information to make the error significantly smaller. When we get to such a value of $l_{\max}$ that the error is close to $(r/M)^{l_{\max}}$, then adding another row to the table (fitting for an extra moment) ceases to increase the errors for all the parameters.

For LIGO, we find discouraging results. In Table 2, we show the results of a best-case, albeit unrealistic, scenario: We assume that the small mass is only $\mu = 0.2M_\odot$, the smallest mass a neutron star can theoretically have, so that by being small there are many cycles falling in the LIGO band. We assume that the large mass is $M = 30M_\odot$ so that the final plunge occurs at

147 Hz and the final inspiral waves are near the frequency of greatest detector sensitivity. (There are over 11,000 gravitational-wave cycles from when the gravitational-wave frequency enters the LIGO band at 10 Hz until the plunge.) With a signal-to-noise ratio $S/N = 10$, we still find only a marginal capability of searching for black holes, as can be seen by examining the results for $l_{\max} = 2$. Say we made measurements of an inspiral giving best-fit measurements of $\overline{s_1} = 0.8$ and $\overline{m_2} = -.64$. Keeping with our assumption (made above in the introduction) that the errors on the moments are approximately independent of the best-fit values of the moments, then from the $l_{\max} = 2$ row in Table 2, we see that the error on s_1 is 0.05, and the error on m_2 is 0.56. Hence, we would not be able to confidently say that the compact body is a black hole, despite the best-fit parameters satisfying Eq. (183). Other choices of masses besides $0.2M_\odot$ and $30M_\odot$ usually give slightly worse results. Our "best-case" choice of masses was made assuming that the S/N for all cases is ten. Of course, one can always get better results by assuming a larger S/N; that is, assuming the binary is closer. However, unless we observe a binary at a much larger S/N, it appears that LIGO will not allow us to search for exotic objects or test the black-hole no-hair theorem.

On the other hand, we find encouraging results for the space-based detector LISA. The LISA mission is designed to last for two years, although the spacecraft may be functional for over a decade [2]. We therefore chose two year observation times in computing results—that is, we assume that we measure the inspiral from two years before the last stable circular orbit until the last stable circular orbit.

In Table 3, we see the results of a binary with $\mu = 10M_\odot$, $M = 10^5 M_\odot$, and $S/N = 10$. In the two years of observation, the gravitational-wave frequency F sweeps from 4.3×10^{-3} Hertz to 4.4×10^{-2} Hertz. In that time period, there are about 4.2×10^5 gravitational-wave cycles. For the same situation (except with different values of μ and M) described above where with LIGO we could not determine whether the body was a black hole or not, we can with LISA measure s_1 to within 0.0013 instead of 0.05, and we can measure m_2 to within 0.015 instead of 0.56, and hence

enable a determination of whether the object is a black hole or not.

In Table 4, we see the results for the same situation as in Table 3, but now with $S/N = 100$. Note that for small values of $l_{\max}$ where all errors in Table 3 are much less than the *a priori* errors, then increasing the signal-to-noise by a factor of ten as in Table 4 simply decreases the size of each error by a factor of ten. In Table 5, we see the same situation as in Table 3, but now with r set to $2M$ instead of its value in all the other tables, $3M$. Note that this makes little difference in rows in which $l_{\max}$ is small enough that all the errors are much less than the *a priori* errors anyway. In Table 6, we see the same situation as in Table 3, except now with the large mass $M = 10^6 M_\odot$. In this case, the gravitational-wave frequency F sweeps from 2.2×10^{-3} Hertz to 4.4×10^{-3} Hertz, in about 1.8×10^5 cycles. In Table 7, we see the same situation as in Table 3, except now with the small mass $\mu = 100 M_\odot$. In this case, the gravitational-wave frequency F sweeps from 1.8×10^{-3} Hertz to 4.4×10^{-2} Hertz, in about 1.8×10^5 cycles. Although these two larger mass cases have greater errors as shown in Tables 6 and 7 than those in Table 3, the larger mass cases will have a larger S/N than the smaller mass case, assuming the distance and angles between the binary and the detector are the same in all cases.

We should remember that the above results are only valid in the case when all our assumptions made in the introduction hold. In removing these assumptions, perhaps the most difficult step will be generalizing the results to eccentric and non-equatorial orbits. An orbit with high eccentricity e radiates very strongly and is very strongly affected by the spin of the central body [7], and by all of the multipole moments [8]. Similarly, a non-equatorial (with a large inclination angle ι) orbit around a spinning central body precesses [26], and the precession depends on the multipole moments [8]. If we knew the values of e and ι, and we knew that $e^2 \ll 1$ and $\iota^2 \ll 1$, then our analysis would still be valid, because the gravitational-wave phase evolution depends on small eccentricity or small inclination angle like e^2 or ι^2, respectively. [The gravitational-wave amplitude *does* have modulations of order e or ι at the precession frequencies associated with an elliptical orbit or a non-equatorial orbit [8]. However, because this precession frequency is different than

the gravitational-wave frequency, then a cross-correlation of two signals with precession using Eqs. (184) and (189) has the terms linear in e or ι mostly canceling out due to the integration of a highly oscillatory term.] In reality, we do not know *a priori* the values of e and ι or whether or not they are small, thus necessitating an analysis with general orbits rather than our circular orbits.

Despite the great number of assumptions we have made, we believe our results will still be accurate enough to convey the main message: that the prospect of using space-based detectors to search for non-black-hole, massive, stellar objects is promising and deserving of future efforts to remove our simplifying assumptions and enable a more careful analysis.

Acknowledgments

The author would like to thank Kip Thorne for valuable discussions. This work was supported by NSF grants AST-9417371 and PHY-9424337, and by NASA grant NAGW-4268.

References

[1] A. Abramovici, W. E. Althouse, R. W. P. Drever, Y. Gürsel, S. Kawamura, F. J. Raab, D. Shoemaker, L. Sievers, R. E. Spero, K. S. Thorne, R. E. Vogt, R. Weiss, S. E. Whitcomb, and M. E. Zucker, *Science* **256**, 325 (1992).

[2] P. Bender, I. Ciufolini, K. Danzmann, W. M. Folkner, J. Hough, D. Robertson, A. Rüdiger, M. C. W. Sandford, R. Schilling, B. Schutz, R. Stebbins, T. Sumner, P. Touboul, S. Vitale, H. Ward, and W. Winkler, *LISA: Laser Interferometer Space Antenna for the detection and observation of gravitational waves*, Pre-Phase A Report (1995).

[3] K. S. Thorne, in *Particle and Nuclear Astrophysics and Cosmology in the Next Millennium: Proceedings of the 1994 Snowmass Summer Study, Snowmass, Colorado, June 29–July 14, 1994*, eds. E. W. Kolb and R. Peccei (World Scientific, Singapore, 1995).

[4] B. F. Schutz, Class. & Quant. Grav. **13**, A219 (1996).

[5] D. Hils and P. L. Bender, Astrophys. J. **445**, L7 (1995).

[6] D. Hils and P. L. Bender, unpublished.

[7] M. Shibata, Phys. Rev. D **50**, 6297 (1994).

[8] F. D. Ryan, Phys. Rev. D **52**, 5707 (1995).

[9] B. Carter, chapter 6 of *General Relativity: an Einstein Centenary Survey*, eds. S. W. Hawking and W. Israel (Cambridge University Press, Cambridge, 1979).

[10] F. D. Ryan, L. S. Finn, and K. S. Thorne, in preparation.

[11] F. D. Ryan, in preparation.

[12] L. S. Finn, Phys. Rev. D **46**, 5236 (1992).

[13] L. S. Finn and D. F. Chernoff, Phys. Rev. D **47**, 2198 (1993).

[14] C. Cutler and É. E. Flanagan, Phys. Rev. D **49**, 2658 (1994).

[15] E. Poisson and C. M. Will, Phys. Rev. D **52**, 848 (1995).

[16] E. Poisson, Phys. Rev. D **54**, 5939 (1996).

[17] R. Geroch, J. Math. Phys. **11**, 2580 (1970).

[18] R. O. Hansen, J. Math. Phys. **15**, 46 (1974). In Hansen's paper, S_l is called J_l, and "mass-current" is called "angular momentum."

[19] P. C. Peters, Phys. Rev. **136**, B1224 (1964).

[20] F. D. Ryan, Phys. Rev. D **53**, 3064 (1996).

[21] M. Peterseim, O. Jennrich, K. Danzmann, Class. & Quant. Grav. **13**, A279 (1996).

[22] E. Poisson, Phys. Rev. D **52**, 5719 (1995).

[23] H. Tagoshi and M. Sasaki, Prog. Theor. Phys. **92**, 745 (1994).

[24] F. D. Ryan, in preparation.

[25] G. Fodor, C. Hoenselaers, and Z. Perjés, J. Math. Phys. **30**, 2252 (1989).

[26] T. A. Apostolatos, C. Cutler, G. J. Sussman, and K. S. Thorne, Phys. Rev. D **49**, 6274 (1994).

[27] S. Chandrasekhar, *The Mathematical Theory of Black Holes* (Oxford University Press, New York, 1983).

Table 1: The values of g_l and h_l, used in the formulas for the last stable circular orbit as calculated to leading order and to higher order, respectively.

l	g_l	h_l
1	3.08×10^{-1}	7.48×10^{-1}
2	6.69×10^{-2}	2.34×10^{-1}
3	-2.00×10^{-2}	-7.44×10^{-2}
4	-4.18×10^{-3}	-2.13×10^{-2}
5	9.48×10^{-4}	5.32×10^{-3}
6	1.96×10^{-4}	1.47×10^{-3}
7	-3.89×10^{-5}	-3.26×10^{-4}
8	-7.99×10^{-6}	-8.81×10^{-5}
9	1.47×10^{-6}	1.83×10^{-5}
10	3.02×10^{-7}	4.89×10^{-6}
11	-5.28×10^{-8}	-9.73×10^{-7}
12	-1.08×10^{-8}	-2.58×10^{-7}
13	1.82×10^{-9}	4.97×10^{-8}
14	3.73×10^{-10}	1.31×10^{-8}
15	-6.13×10^{-11}	-2.47×10^{-9}
16	-1.25×10^{-11}	-6.45×10^{-10}
17	2.02×10^{-12}	1.20×10^{-10}
18	4.12×10^{-13}	3.12×10^{-11}
19	-6.52×10^{-14}	-5.70×10^{-12}
20	-1.33×10^{-14}	-1.48×10^{-12}
21	2.08×10^{-15}	2.68×10^{-13}
22	4.24×10^{-16}	6.94×10^{-12}
23	-6.55×10^{-17}	-1.24×10^{-14}
24	-1.34×10^{-17}	-3.21×10^{-15}

Table 2: The error $\delta\theta^i$ for each parameter θ^i, when fitting up to the $l_{\max}$-th moment, using LIGO. We use the abbreviation $[\cdots] \equiv \log_{10}(\cdots)$. We assume $\mu = 0.2M_\odot$, $M = 30M_\odot$, $r = 3M$, and $S/N = 10$.

$l_{\max}$	$[\delta t_*/\mathrm{sec}]$	$[\delta\phi_*]$	$[\delta\mu/\mu]$	$[\delta M/M]$	$[\delta s_1]$	$[\delta m_2]$	$[\delta s_3]$	$[\delta m_4]$	$[\delta s_5]$	$[\delta m_6]$	$[\delta s_7]$	$[\delta m_8]$	$[\delta s_9]$	$[\delta m_{10}]$
0	-1.96	0.57	-3.22	-3.14	—	—	—	—	—	—	—	—	—	—
1	-1.07	1.04	-2.35	-2.12	-1.94	—	—	—	—	—	—	—	—	—
2	-0.45	2.16	-1.63	-1.47	-1.30	-0.25	—	—	—	—	—	—	—	—
3	-0.14	3.19	-1.00	-0.80	-0.45	0.24	0.83	—	—	—	—	—	—	—
4	0.34	3.25	-0.92	-0.72	-0.44	0.38	1.18	1.83	—	—	—	—	—	—
5	0.70	3.28	-0.64	-0.45	-0.44	0.56	1.19	1.83	2.36	—	—	—	—	—
6	0.75	3.28	-0.57	-0.39	-0.44	0.60	1.19	1.83	2.36	2.85	—	—	—	—
7	0.77	3.28	-0.53	-0.34	-0.43	0.61	1.19	1.83	2.36	2.85	3.33	—	—	—
8	0.78	3.29	-0.51	-0.33	-0.42	0.61	1.19	1.83	2.36	2.85	3.33	3.81	—	—
9	0.78	3.29	-0.51	-0.33	-0.42	0.61	1.19	1.83	2.36	2.85	3.33	3.81	4.29	—
10	0.78	3.29	-0.51	-0.32	-0.42	0.61	1.19	1.83	2.36	2.85	3.33	3.81	4.29	4.77

Table 3: The error $\delta\theta^i$ for each parameter θ^i, when fitting up to the $l_{\rm max}$-th moment, using LISA. We use the abbreviation $[\cdots] \equiv \log_{10}(\cdots)$. We assume $\mu = 10M_\odot$, $M = 10^5 M_\odot$, $r = 3M$, and $S/N = 10$.

$l_{\rm max}$	$[\delta t_*/\text{sec}]$	$[\delta\phi_*]$	$[\delta\mu/\mu]$	$[\delta M/M]$	$[\delta s_1]$	$[\delta m_2]$	$[\delta s_3]$	$[\delta m_4]$	$[\delta s_5]$	$[\delta m_6]$	$[\delta s_7]$	$[\delta m_8]$	$[\delta s_9]$	$[\delta m_{10}]$
0	1.74	0.75	-4.90	-4.80	—	—	—	—	—	—	—	—	—	—
1	2.71	1.33	-3.92	-3.70	-3.53	—	—	—	—	—	—	—	—	—
2	3.37	2.41	-3.17	-3.01	-2.89	-1.82	—	—	—	—	—	—	—	—
3	3.73	3.52	-2.49	-2.28	-1.94	-1.27	-0.66	—	—	—	—	—	—	—
4	5.43	4.69	-1.51	-1.34	-1.07	0.09	0.96	1.61	—	—	—	—	—	—
5	6.01	4.86	-0.72	-0.54	-0.95	0.50	0.99	1.62	2.35	—	—	—	—	—
6	6.08	4.94	-0.64	-0.46	-0.90	0.58	1.08	1.71	2.36	2.75	—	—	—	—
7	6.08	4.95	-0.64	-0.46	-0.89	0.58	1.14	1.80	2.36	2.84	2.98	—	—	—
8	6.08	4.95	-0.64	-0.46	-0.89	0.58	1.14	1.81	2.36	2.84	3.18	3.72	—	—
9	6.08	4.95	-0.64	-0.46	-0.89	0.58	1.14	1.81	2.36	2.84	3.22	3.75	4.23	—
10	6.08	4.95	-0.64	-0.46	-0.89	0.58	1.14	1.81	2.36	2.84	3.23	3.76	4.24	4.75

Table 4: The error $\delta\theta^i$ for each parameter θ^i, when fitting up to the $l_{\max}$-th moment, using LISA. We use the abbreviation $[\cdots] \equiv \log_{10}(\cdots)$. We assume $\mu = 10M_\odot$, $M = 10^5 M_\odot$, $r = 3M$, and $S/N = 100$.

$l_{\max}$	$[\delta t_*/\text{sec}]$	$[\delta\phi_*]$	$[\delta\mu/\mu]$	$[\delta M/M]$	$[\delta s_1]$	$[\delta m_2]$	$[\delta s_3]$	$[\delta m_4]$	$[\delta s_5]$	$[\delta m_6]$	$[\delta s_7]$	$[\delta m_8]$	$[\delta s_9]$	$[\delta m_{10}]$
0	0.74	-0.25	-5.90	-5.80	—	—	—	—	—	—	—	—	—	—
1	1.71	0.33	-4.92	-4.70	-4.53	—	—	—	—	—	—	—	—	—
2	2.37	1.41	-4.17	-4.01	-3.89	-2.82	—	—	—	—	—	—	—	—
3	2.73	2.52	-3.49	-3.28	-2.94	-2.27	-1.66	—	—	—	—	—	—	—
4	4.54	3.80	-2.40	-2.23	-1.97	-0.81	0.07	0.72	—	—	—	—	—	—
5	5.99	4.74	-0.73	-0.55	-1.12	0.47	0.59	0.95	2.35	—	—	—	—	—
6	6.05	4.87	-0.68	-0.50	-1.00	0.54	0.94	1.53	2.35	2.58	—	—	—	—
7	6.07	4.88	-0.66	-0.48	-0.99	0.56	0.94	1.53	2.35	2.81	2.68	—	—	—
8	6.07	4.88	-0.65	-0.47	-0.98	0.57	0.96	1.56	2.35	2.81	3.16	3.68	—	—
9	6.08	4.91	-0.65	-0.47	-0.96	0.58	1.04	1.67	2.35	2.82	3.20	3.74	4.10	—
10	6.08	4.92	-0.64	-0.46	-0.95	0.58	1.05	1.69	2.35	2.82	3.20	3.75	4.17	4.70

Table 5: The error $\delta\theta^i$ for each parameter θ^i, when fitting up to the $l_{\max}$-th moment, using LISA. We use the abbreviation $[\cdots] \equiv \log_{10}(\cdots)$. We assume $\mu = 10M_\odot$, $M = 10^5 M_\odot$, $r = 2M$, and $S/N = 10$.

$l_{\max}$	$[\delta t_*/\text{sec}]$	$[\delta\phi_*]$	$[\delta\mu/\mu]$	$[\delta M/M]$	$[\delta s_1]$	$[\delta m_2]$	$[\delta s_3]$	$[\delta m_4]$	$[\delta s_5]$	$[\delta m_6]$	$[\delta s_7]$	$[\delta m_8]$	$[\delta s_9]$	$[\delta m_{10}]$
0	1.74	0.75	-4.90	-4.80	—	—	—	—	—	—	—	—	—	—
1	2.71	1.33	-3.92	-3.70	-3.53	—	—	—	—	—	—	—	—	—
2	3.37	2.41	-3.17	-3.01	-2.89	-1.82	—	—	—	—	—	—	—	—
3	3.73	3.52	-2.49	-2.28	-1.94	-1.27	-0.66	—	—	—	—	—	—	—
4	4.96	4.23	-1.95	-1.78	-1.51	-0.38	0.49	1.15	—	—	—	—	—	—
5	5.23	4.28	-1.54	-1.36	-1.48	-0.22	0.50	1.15	1.50	—	—	—	—	—
6	5.26	4.28	-1.49	-1.31	-1.48	-0.20	0.50	1.15	1.50	1.80	—	—	—	—
7	5.26	4.28	-1.48	-1.30	-1.48	-0.20	0.50	1.15	1.50	1.80	2.10	—	—	—
8	5.26	4.28	-1.48	-1.30	-1.48	-0.20	0.50	1.15	1.50	1.80	2.10	2.41	—	—
9	5.26	4.28	-1.48	-1.30	-1.48	-0.20	0.50	1.15	1.50	1.80	2.10	2.41	2.71	—
10	5.26	4.28	-1.48	-1.30	-1.48	-0.20	0.50	1.15	1.50	1.80	2.10	2.41	2.71	3.01

Table 6: The error $\delta\theta^i$ for each parameter θ^i, when fitting up to the $l_{\max}$-th moment, using LISA. We use the abbreviation $[\cdots] \equiv \log_{10}(\cdots)$. We assume $\mu = 10M_\odot$, $M = 10^6 M_\odot$, $r = 3M$, and $S/N = 10$.

$l_{\max}$	$[\delta t_*/\mathrm{sec}]$	$[\delta\phi_*]$	$[\delta\mu/\mu]$	$[\delta M/M]$	$[\delta s_1]$	$[\delta m_2]$	$[\delta s_3]$	$[\delta m_4]$	$[\delta s_5]$	$[\delta m_6]$	$[\delta s_7]$	$[\delta m_8]$	$[\delta s_9]$	$[\delta m_{10}]$
0	3.92	1.92	-4.35	-4.74	—	—	—	—	—	—	—	—	—	—
1	4.92	2.84	-4.24	-3.28	-2.83	—	—	—	—	—	—	—	—	—
2	6.05	4.93	-2.00	-2.53	-1.01	-0.31	—	—	—	—	—	—	—	—
3	7.07	6.32	-1.79	-1.19	0.08	0.84	0.89	—	—	—	—	—	—	—
4	7.60	6.32	-1.51	-1.02	0.09	0.84	1.19	1.82	—	—	—	—	—	—
5	8.04	6.32	-0.70	-0.47	0.11	0.84	1.20	1.83	2.38	—	—	—	—	—
6	8.12	6.34	-0.57	-0.35	0.12	0.84	1.20	1.83	2.38	2.85	—	—	—	—
7	8.14	6.39	-0.50	-0.29	0.15	0.86	1.21	1.85	2.38	2.86	3.16	—	—	—
8	8.14	6.40	-0.50	-0.29	0.15	0.86	1.21	1.85	2.38	2.86	3.23	3.73	—	—
9	8.14	6.40	-0.50	-0.29	0.16	0.87	1.21	1.85	2.38	2.86	3.28	3.77	4.20	—
10	8.15	6.40	-0.50	-0.28	0.16	0.87	1.21	1.85	2.38	2.86	3.29	3.78	4.22	4.73

Table 7: The error $\delta\theta^i$ for each parameter θ^i, when fitting up to the $l_{\rm max}$-th moment, using LISA. We use the abbreviation $[\cdots] \equiv \log_{10}(\cdots)$. We assume $\mu = 100M_\odot$, $M = 10^5 M_\odot$, $r = 3M$, and $S/N = 10$.

$l_{\rm max}$	$[\delta t_*/\text{sec}]$	$[\delta\phi_*]$	$[\delta\mu/\mu]$	$[\delta M/M]$	$[\delta s_1]$	$[\delta m_2]$	$[\delta s_3]$	$[\delta m_4]$	$[\delta s_5]$	$[\delta m_6]$	$[\delta s_7)$	$[\delta m_8]$	$[\delta s_9]$	$[\delta m_{10}]$
0	1.46	0.48	-4.30	-4.15	—	—	—	—	—	—	—	—	—	—
1	2.39	1.16	-3.24	-3.05	-2.98	—	—	—	—	—	—	—	—	—
2	3.28	1.99	-2.29	-2.11	-2.60	-1.12	—	—	—	—	—	—	—	—
3	3.58	2.56	-1.87	-1.68	-1.98	-1.03	-0.41	—	—	—	—	—	—	—
4	4.63	3.77	-1.19	-1.01	-1.11	0.21	1.09	1.78	—	—	—	—	—	—
5	5.02	3.92	-0.72	-0.55	-0.93	0.53	1.12	1.78	2.33	—	—	—	—	—
6	5.06	3.95	-0.68	-0.50	-0.90	0.57	1.13	1.78	2.34	2.81	—	—	—	—
7	5.06	3.95	-0.67	-0.49	-0.90	0.57	1.14	1.80	2.35	2.83	3.23	—	—	—
8	5.06	3.95	-0.67	-0.49	-0.90	0.57	1.14	1.81	2.35	2.83	3.25	3.78	—	—
9	5.06	3.95	-0.67	-0.49	-0.90	0.57	1.14	1.81	2.35	2.83	3.26	3.78	4.28	—
10	5.06	3.95	-0.67	-0.49	-0.90	0.57	1.14	1.81	2.35	2.83	3.26	3.78	4.28	4.76

7 Scalar waves produced by a scalar charge orbiting a massive body with arbitrary multipole moments

Abstract

We present and implement a method for computing the scalar waves produced by a scalar charge orbiting on a circular, equatorial geodesic around a massive, compact body whose vacuum exterior spacetime is stationary, axially symmetric, and reflection symmetric across the equatorial plane. We use our method to compute numerically how the waves' luminosity depends on the multipole moments of the central body and on a scattering cutoff that we impose to model the body's non-vacuum interior.

7.1 Introduction

The European Space Agency's proposed Laser Interferometer Space Antenna (LISA) [1], which might be flying by the year 2014, will have the capability of making a variety of interesting gravitational-wave measurements [2, 3]. Among these is the detection of gravitational waves from the inspiral of a small compact object, such as a white dwarf, neutron star, or small black hole, into a $\sim 10^5 M_\odot$ to $\sim 3 \times 10^7 M_\odot$ central, compact body. These gravitational waves carry information about the external gravitational field of the central body, in particular, its multipole moments [4]. Measurements of the waves with LISA will allow for precise [5, 6] tests of the black-hole no-hair theorem and of general relativity, as well as for searches for exotic stellar objects [7] such as boson stars [8], soliton stars [9], and naked singularities.

To allow for this application, we must be able to solve for the gravitational waveforms produced when a small-mass object spirals into a much more massive central body with arbitrary multipole

moments. Unfortunately, solving the necessary gravitational-wave generation equations is difficult for many reasons, two in particular: First, even when assuming (plausibly) that wave emission has driven the central body's gravitational field into a stationary and axisymmetric state, thereby effectively reducing the dimensionality of the problem by two, the differential equations to be solved are still two-dimensional and nonseparable (in the spherical-polar-coordinate variables r and θ). (This is in contrast to the black-hole case, in which there is a separation of the r and θ variables via the Teukolsky formalism [10]). Second, the gravitational field has many tensor components and their differential equations presumably are coupled (by contrast with the black-hole case where Teukolsky identified a single decoupled tensor component from which all other aspects of the waves can be computed).

It would be useful to understand how to tackle the first problem without having the complication of the second problem. For this reason, we here will solve a simpler problem, but one which is still in many respects similar to the important gravitational-wave problem: that of computing the *scalar* waves produced by a scalar charge orbiting on a circular, equatorial geodesic in the vacuum, gravitational-field spacetime surrounding an uncharged body, but subject to the restrictions that the spacetime is stationary, axially symmetric, reflection symmetric across the equatorial plane, and asymptotically flat.

While the gravitational field in the vacuum surrounding the central, compact body is completely determined by its multipole moments, the gravitational field at small radii (call this the "interior" region) depends on the matter distribution of the central body (if matter is present). Because of this, the scalar waves or gravitational waves produced during an inspiral depend on whether the central body is a black hole or a naked singularity or a boson star, etc. For example, the gravitational field outside a spherical matter star is the same Schwarzschild metric as that outside a spherical black hole, but the waves around a matter star satisfy the boundary condition of regularity at the origin $r = 0$, while the waves around a black hole satisfy the condition of ingoing waves at the horizon.

In this paper, we do not wish to consider any specific type of central body. Instead, we will impose a type of cutoff (described below) which removes contributions to the scalar field due to scattering off of the interior region. This simple model would have to be replaced with the correct equations if one were studying a specific central body with a known interior metric.

Fortunately, our results will not differ too greatly from the results we would obtain with some specific model for the interior region: past work in gravitational-wave generation indicates that the effects of the interior region are small and, in some cases, not essential for computing the waves accurately enough for detection purposes. For example, the gravitational-wave energy that goes down the horizon of a static black hole of mass M when a particle orbits at radius r_0 is a small factor $\sim (M/r_0)^4$ of that which escapes to radial infinity; and for scalar radiation, the factor is $\sim (M/r_0)^3$ [11]. (Here and throughout, we use units where Newton's gravitational constant and the speed of light are set to unity.)

Our solution to the scalar-wave generation problem will be presented as follows: In Sec. 7.2, we will describe a division of the central body's gravitational field into the above-mentioned interior region which completely contains the central body and a vacuum exterior region to which we add the moving scalar charge. We will review how to compute the central body's vacuum metric in the exterior region, given its multipole moments. In Sec. 7.3, we will convert the scalar wave equation into flat-space language, which will lead to a convenient method of treating the interior region. In Sec. 7.4, we will outline an iterative method for solving the scalar wave equation. We will also show how to compute the luminosity of the scalar waves. In Sec. 7.5, we will give some details specific to our numerical implementation of our iterative method. In Sec. 7.6, we will give the results of our numerical calculations, showing in particular how the scalar-wave luminosity depends on the central body's multipole moments and on the size of the interior region. The methodology and understanding gained from our solution to this problem should assist in the solution to the more relevant gravitational-wave problem.

7.2 The exterior gravitational field of the central body

Before considering the scalar charge and scalar field, let us examine the gravitational field of the central body. Again, we assume that the central body has no scalar charge. Let us restrict the metric, with spherical polar coordinates r, θ, φ, and t, to be stationary (not a function of t), axisymmetric (not a function of φ), and reflection symmetric across the equatorial plane (the same at θ as at $\pi - \theta$). (It is very plausible that wave emission will have driven any central body into such an axisymmetric and stationary state—for example, this happens very quickly in the case of a black hole [12].) We use the $(-,+,+,+)$ sign convention for the metric.

We can divide the spacetime into two regions, the interior ($r < r_{\rm min}$) and the exterior ($r \geq r_{\rm min}$), where the choice of $r_{\rm min}$ (which, for compact objects, is typically a few times the mass of the body) is subject to the requirement that the metric in the exterior region satisfies Einstein's equations for vacuum. Later, when we consider the scalar field due to a *small* charge, we will assume that the stress-energy tensor due to the scalar field is small enough that the exterior metric can be considered to satisfy the vacuum Einstein equations.

For the rest of this section, we will consider only the vacuum, exterior region. We will see how the metric coefficients can be computed as power series in $1/r$, given the multipole moments of the metric.

The metric for a stationary, axially symmetric, vacuum spacetime can always be written in the form [this is Ref. [13], Eq. (6), in spherical rather than cylindrical coordinates]

$$ds^2 = -F(dt - \omega d\varphi)^2 + \frac{1}{F}\left[e^{2\gamma}(dr^2 + r^2 d\theta^2) + r^2 \sin^2\theta d\varphi^2\right], \tag{208}$$

where F, ω, and γ are functions of r and θ. The simplest way to classify such a metric is in terms of its multipole moments [14]; that is, writing the metric coefficients in a power series in $1/r$, each term multiplied by an angular function. By virtue of the reflection symmetry across the equatorial plane, the exterior metric can be completely described by a set of mass moments M_l ($l = 0, 2, 4...$) and spin moments S_l ($l = 1, 3, 5...$) [14, 4]. The mass monopole moment is just the

mass: $M_0 = M$. The spin angular momentum is S_1, the mass quadrupole moment is M_2, the spin octopole moment is S_3, etc.

Given the multipole moments, the metric can be computed using the process described throughout the remainder of this section. This process is just the inverse of Fodor, Hoenselaers, and Perjés' method of computing the multipole moments given the metric [13]. We will be very terse in describing the following formulas, because they are given and described in much detail in Refs. [4] and [13].

The method consists of two parts: first, finding a function $\tilde{\xi}(r,\theta)$ order-by-order in a power series in $1/r$, and second, plugging $\tilde{\xi}$ into some formulas to get the F, ω, and γ that appear in Eq. (208).

This $\tilde{\xi}$ has the property that it can be expanded as [Ref. [13], Eq. (15)]

$$\tilde{\xi} = \sum_{j,k=0}^{\infty} a_{jk} \frac{\sin^j\theta \cos^k\theta}{r^{j+k}}. \tag{209}$$

The a_{jk} can be nonzero only for nonnegative, even j and nonnegative k. Because of the metric's reflection symmetry across the equatorial plane, a_{jk} is real for even k and imaginary for odd k. All the coefficients a_{jk} with $j+k<l$ can be computed if all the a_{0j} with $j<l$ are known, by using the formula [Ref. [13], Eq. (16)]

$$\begin{aligned} a_{u+2,s} \;=\; & \frac{1}{(u+2)^2}\Big\{ -(s+2)(s+1)a_{u,s+2} + \\ & \sum_{v,w,p,q} a_{vw}a^*_{u-v-p,s-w-q}\big[a_{pq}(p^2+q^2 \\ & -4p-5q-2pv-2qw-2) \\ & +a_{p+2,q-2}(p+2)(p+2-2v) \\ & +a_{p-2,q+2}(q+2)(q+1-2w)\big]\Big\}. \end{aligned} \tag{210}$$

The sum is over all integer values of v, w, p, and q that give nonzero contributions, namely $0 \le v \le u$, $0 \le w \le s+1$, $0 \le p \le u-v$, $-1 \le q \le s-w$, and v and p even.

To compute $\tilde{\xi}$, we will compute order-by-order the coefficients a_{0l}. Suppose that we are at the

lth stage in this order-by-order iteration process, meaning that we know all the a_{0j} coefficients up to $a_{0,l-1}$ and we wish to determine a_{0l}. (At the first stage, only a_{00} is known, and its value is the mass $M = M_0$.) To determine a_{0l}, first we temporarily set a_{0l} to zero. It does not matter what values we temporarily give to the higher-order coefficients a_{0j} for $j > l$, since those values will not enter in at a low enough order to affect the lth stage.

Second, we compute all the a_{jk} with $j + k \leq l$ from Eq. (210) above. Third, we compute temporary values of the multipole moments (they are temporary, because we had temporarily set a_{0l} to zero) using the formula

$$M_l^{\rm temp} + iS_l^{\rm temp} = \left. \frac{S_0^{(l)}}{(2l-1)!!} \right|_{\bar{\rho}=0,\bar{z}=0}, \tag{211}$$

where these $S_a^{(n)}$ (not to be confused with the S_l) are functions of

$$\bar{\rho} \equiv \frac{\sin\theta}{r}, \ \bar{z} \equiv \frac{\cos\theta}{r}, \tag{212}$$

and are recursively computed by [Ref. [13], Eq. (23)]

$$S_0^{(0)} = \tilde{\xi}, \ S_0^{(1)} = \frac{\partial\tilde{\xi}}{\partial\bar{z}}, \ S_1^{(1)} = \frac{\partial\tilde{\xi}}{\partial\bar{\rho}}, \tag{213}$$

$$\begin{aligned} S_a^{(n)} \ = \ & \frac{1}{n}\Bigg[a\frac{\partial}{\partial\bar{\rho}}S_{a-1}^{(n-1)} + (n-a)\frac{\partial}{\partial\bar{z}}S_a^{(n-1)} \\ & + a\left([a+1-2n]\gamma_1 - \frac{a-1}{\bar{\rho}}\right)S_{a-1}^{(n-1)} \\ & + (a-n)(a+n-1)\gamma_2 S_a^{(n-1)} + a(a-1)\gamma_2 S_{a-2}^{(n-1)} \\ & + (n-a)(n-a-1)\left(\gamma_1 - \frac{1}{\bar{\rho}}\right)S_{a+1}^{(n-1)} \\ & - \Big[a(a-1)\tilde{R}_{11}S_{a-2}^{(n-2)} + 2a(n-a)\tilde{R}_{12}S_{a-1}^{(n-2)} \\ & + (n-a)(n-a-1)\tilde{R}_{22}S_a^{(n-2)}\Big]\left(n-\frac{3}{2}\right)\Bigg], \end{aligned} \tag{214}$$

in which $\tilde{R}_{11}$, $\tilde{R}_{12}$, and $\tilde{R}_{22}$ are given by

$$\tilde{R}_{ij} = \left[(\bar{\rho}^2 + \bar{z}^2)|\tilde{\xi}|^2 - 1\right]^{-2}\left(G_i G_j^* + G_i^* G_j\right), \tag{215}$$

with

$$G_1 = \bar{z}\frac{\partial\tilde{\xi}}{\partial\bar{\rho}} - \bar{\rho}\frac{\partial\tilde{\xi}}{\partial\bar{z}},\ G_2 = \bar{\rho}\frac{\partial\tilde{\xi}}{\partial\bar{\rho}} + \bar{z}\frac{\partial\tilde{\xi}}{\partial\bar{z}} + \tilde{\xi}, \tag{216}$$

and from these $\tilde{R}_{ij}$,

$$\gamma_1 = (\bar{\rho}/2)(\tilde{R}_{11} - \tilde{R}_{22}),\ \gamma_2 = \bar{\rho}\tilde{R}_{12}. \tag{217}$$

Then, fourth, we compute out the permanent value of a_{0l} by comparing the actual, given multipole moments with the temporarily computed moments [Ref. [4], Eq. (42)]:

$$a_{0l} = (M_l + iS_l) - (M_l^{\text{temp}} + iS_l^{\text{temp}}). \tag{218}$$

Fifth and finally, we repeat the process to find $a_{0,l+1}$. We continue the process until $\tilde{\xi}$ is determined to as high an order $l_{\max}$ as desired.

With $\tilde{\xi}$ determined as a power series in $1/r$, the metric functions F, ω, and γ can be computed as follows: The function $F(r,\theta)$ can be determined directly from $\tilde{\xi}$ by

$$F = \text{Re}\left[\frac{r-\tilde{\xi}}{r+\tilde{\xi}}\right]. \tag{219}$$

The function $\omega(r,\theta)$ is computed first by computing

$$\psi = \text{Im}\left[\frac{r-\tilde{\xi}}{r+\tilde{\xi}}\right], \tag{220}$$

and then integrating

$$\omega = -\int_r^\infty dr'\left[\frac{\sin\theta\cos\theta}{F^2}\frac{\partial\psi}{\partial\sin\theta}\right]\Bigg|_{\text{fixed }\theta}, \tag{221}$$

because the integrand in the above square brackets is $\partial\omega/\partial r$ [Ref. [15], Eq. (I.3b)], and $\omega = 0$ at $r = \infty$. Finally, $\gamma(r,\theta)$ can be computed from

$$\begin{aligned}\gamma \;=\; & -\int_r^\infty dr'\left[\frac{(F_{,r'})^2\sin^2\theta r'}{4F^2} - \frac{(\omega_{,r'})^2F^2}{4r'}\right.\\ & +\frac{F_{,r'}F_{,\theta}\sin\theta\cos\theta}{2F^2} - \frac{\omega_{,r}\omega_{,\theta}F^2\cos\theta}{2(r')^2\sin\theta}\\ & \left.-\frac{(F_{,\theta})^2\sin^2\theta}{4F^2r} + \frac{(\omega_{,\theta})^2F^2}{4(r')^3}\right]\Bigg|_{\text{fixed }\theta},\end{aligned} \tag{222}$$

because the integrand in the above square brackets is $\partial\gamma/\partial r$ [Ref. [15], Eqs. (I.4)] and $\gamma = 0$ at $r = \infty$ [16].

From the above Eqs. (208)–(222), we can compute each of the metric coefficients $g_{\alpha\beta}$ as power series in $1/r$, with each coefficient being a polynomial in $\sin\theta$. (There are no occurrences of $\cos\theta$, because of the reflection symmetry across the equatorial plane.) Even though each metric coefficient is only computed to a finite order (up to $1/r^{l_{\max}+1}$) of what is really an infinite series, we will consider these truncated series exact in the computations described below.

7.3 The scalar field equation

Next, we consider the effect of placing a scalar charge q into the spacetime, on a circular geodesic orbit with radius r_0 and angular frequency [Ref. [4], Eq. (9)]

$$\Omega = \frac{d\varphi}{dt} = \left.\frac{-g_{t\varphi,r} + \sqrt{(g_{t\varphi,r})^2 - g_{tt,r}g_{\varphi\varphi,r}}}{g_{\varphi\varphi,r}}\right|_{r=r_0,\theta=\pi/2}. \tag{223}$$

A real, scalar field ϕ is governed by the wave equation

$$g^{\sigma\nu}\phi_{;\sigma\nu} = 4\pi J, \tag{224}$$

(repeated Greek indices are summed) where the source J due to the scalar charge is given by

$$\begin{aligned} J(x) &= q\int d\tau\delta^{(4)}[x - z(\tau)] \\ &= \frac{q}{(-g)^{1/2}}\delta(r - r_0)\delta\left(\theta - \frac{\pi}{2}\right)\delta(\varphi - \Omega t)\int d\tau\delta\left(t - \frac{dt}{d\tau}\tau\right) \\ &= q\left[\frac{(-g_{tt} - 2g_{t\varphi}\Omega - g_{\varphi\varphi}\Omega^2)^{1/2}}{g_{\theta\theta}}\right]\delta(r - r_0)\delta\left(\theta - \frac{\pi}{2}\right)\delta(\varphi - \Omega t). \end{aligned} \tag{225}$$

On the first line of Eq. (225), x is the spacetime point and $z(\tau)$ is the world line of the charge. The $\delta^{(4)}[x - z(\tau)]$ is a proper-volume delta function, meaning that when integrated over proper volume, it gives a contribution of unity:

$$\int d(\text{proper volume})\delta^{(4)}[x - z] = \int drd\theta d\varphi dt(-g)^{1/2}\delta^{(4)}[x - z] = 1, \tag{226}$$

when the region of integration includes the event $x = z$. The delta functions on the remaining lines of Eq. (225) are ordinary, coordinate delta functions. The numerator in the large square brackets in Eq. (225) is $d\tau/dt$, which is the value of the τ integral on the previous line, while the denominator comes from $(-g)^{1/2}$, which happens to equal $g_{\theta\theta}$ on the equatorial plane.

In order to solve Eq. (224), we transform it to the language of flat-space by keeping on the left-hand side all terms for which we know the flat-space Green's function, and moving to the right-hand side all the other terms and treating them as source terms. Let η represent the flat-space spherical coordinate metric, with $\eta_{rr} = 1$, $\eta_{\theta\theta} = r^2$, $\eta_{\varphi\varphi} = r^2 \sin^2\theta$, $\eta_{tt} = -1$, and all other components equal to zero. Then, Eq. (224) can be rewritten in terms of the flat-space d'Alembertian operator as

$$\begin{aligned} \Box\phi &\equiv \eta^{\alpha\beta}\phi_{,\alpha\beta} - \eta^{\alpha\beta}\eta^{\mu\nu}\frac{1}{2}(\eta_{\nu\alpha,\beta} + \eta_{\nu\beta,\alpha} - \eta_{\alpha\beta,\nu})\phi_{,\mu} \\ &= 4\pi\hat{J}, \end{aligned} \tag{227}$$

where

$$\begin{aligned} 4\pi\hat{J} &= 4\pi J + (\eta^{\alpha\beta} - g^{\alpha\beta})\phi_{,\alpha\beta} \\ &\quad -[\eta^{\alpha\beta}\eta^{\mu\nu}\frac{1}{2}(\eta_{\nu\alpha,\beta} + \eta_{\nu\beta,\alpha} - \eta_{\alpha\beta,\nu}) - g^{\alpha\beta}g^{\mu\nu}\frac{1}{2}(g_{\nu\alpha,\beta} + g_{\nu\beta,\alpha} - g_{\alpha\beta,\nu})]\phi_{,\mu}. \end{aligned} \tag{228}$$

We can expand this out in terms of components as

$$\begin{aligned} 4\pi\hat{J} &= 4\pi J + (1 - g^{rr})\phi_{,rr} + \Big(\frac{1}{r^2} - g^{\theta\theta}\Big)\phi_{,\theta\theta} \\ &\quad +(-1 - g^{tt})\phi_{,tt} - 2g^{t\varphi}\phi_{,t\varphi} + \Big(\frac{1}{r^2\sin^2\theta} - g^{\varphi\varphi}\Big)\phi_{,\varphi\varphi} \\ &\quad +\frac{1}{2}g^{rr}g^{rr}g_{rr,r}\phi_{,r} - \frac{1}{2}g^{\theta\theta}g^{rr}g_{rr,\theta}\phi_{,\theta} \\ &\quad +\Big(\frac{1}{r} - \frac{1}{2}g^{rr}g^{\theta\theta}g_{\theta\theta,r}\Big)\phi_{,r} + \frac{1}{2}g^{\theta\theta}g^{\theta\theta}g_{\theta\theta,\theta}\phi_{,\theta} \\ &\quad -\frac{1}{2}g^{rr}g^{tt}g_{tt,r}\phi_{,r} - \frac{1}{2}g^{\theta\theta}g^{tt}g_{tt,\theta}\phi_{,\theta} \\ &\quad -g^{rr}g^{t\varphi}g_{t\varphi,r}\phi_{,r} - g^{\theta\theta}g^{t\varphi}g_{t\varphi,\theta}\phi_{,\theta} \\ &\quad +\Big(\frac{1}{r} - \frac{1}{2}g^{rr}g^{\varphi\varphi}g_{\varphi\varphi,r}\Big)\phi_{,r} + \Big(\frac{\cos\theta}{r^2\sin\theta} - \frac{1}{2}g^{\theta\theta}g^{\varphi\varphi}g_{\varphi\varphi,\theta}\Big)\phi_{,\theta}. \end{aligned} \tag{229}$$

We see that when ϕ is considered to satisfy the wave equation for flat-space, the source for ϕ is the contribution directly from the charge plus terms representing the scattering of the waves off the curvature. As we mentioned in the introduction, we wish to remove such scattering contributions due to the metric in the interior region. Thus, rather than solving Eq. (227), we will solve

$$\Box\phi = 4\pi\mathcal{J}, \tag{230}$$

where

$$4\pi\mathcal{J} = 0 \quad \text{if } r < r_{\min}, \qquad 4\pi\mathcal{J} = 4\pi\hat{J} \quad \text{if } r > r_{\min}. \tag{231}$$

By adjusting $r_{\min}$, we will learn the dependence of the scalar wave luminosity at radial infinity on $r_{\min}$, thereby giving us some idea as to the magnitude of the effect of the interior region, or equivalently, the magnitude of the error imposed when we remove the scattering contributions due to the interior region. We shall find that this error is quite small.

7.4 Solving the scalar wave equation

In this section, we will show how Eq. (230) can be solved iteratively, by setting ϕ to zero everywhere, then computing $4\pi\mathcal{J}$ (which at this first iteration is just equal to $4\pi J$) from Eqs. (229) and (231), then computing ϕ as the integral of the product of $4\pi\mathcal{J}$ and the Green's function for the flat-space d'Alembertian operator, then with this new value of ϕ, recomputing $4\pi\mathcal{J}$, then recomputing ϕ, etc., until convergence.

The scalar waves must be outgoing at radial infinity. Because $4\pi\mathcal{J}$ is zero around the origin (as opposed to being singular), ϕ has standing wave boundary conditions at the origin. With such boundary conditions, the solution to Eq. (230) is [Ref. [17], Eqs. (2.45a), (2.49), and (2.50a)]

$$\begin{aligned}\phi(r,\theta,\varphi,t) \;=\; & \sum_{l=0}^{\infty}\sum_{m=-l}^{l} -i\int_0^{\pi}\sin\theta'\,d\theta'\int_0^{2\pi}d\varphi' \\ & \int dt'\int d\omega'\,\frac{\omega'}{2\pi}e^{-i\omega'(t-t')}e^{im(\varphi-\varphi')}\mathcal{Y}_{lm}(\theta)\mathcal{Y}_{lm}(\theta') \\ & \times\left[\int_{r_{\min}}^{r} dr'(r')^2 h_l^{(1)}(\omega' r) j_l(\omega' r')\mathcal{J}(r',\theta',\varphi',t')\right.\end{aligned}$$

$$+\int_r^\infty dr'(r')^2 j_l(\omega' r) h_l^{(1)}(\omega' r') \mathcal{J}(r', \theta', \varphi', t')\Big], \tag{232}$$

where j_l is the spherical Bessel function, $h_l^{(1)}$ is the outgoing spherical Hankel function, and $\mathcal{Y}_{lm}(\theta)$ is the θ dependence of the spherical harmonic: $Y_{lm}(\theta, \varphi) = \mathcal{Y}_{lm}(\theta) e^{im\varphi}$.

Because we are dealing with a charge traveling in a circle at constant angular frequency through a stationary, axisymmetric metric, $\mathcal{J}$ can only depend on φ and t through the combination $\varphi - \Omega t$. Because of this, the source $\mathcal{J}$ can be decomposed into

$$\mathcal{J}(r', \theta', \varphi', t') = \sum_{l=0}^{\infty} \sum_{m=-l}^{l} \mathcal{T}_{lm}(r') \mathcal{Y}_{lm}(\theta') e^{im(\varphi' - \Omega t')}, \tag{233}$$

where

$$\begin{aligned} \mathcal{T}_{lm}(r') &= \int_0^\pi \sin\theta'' d\theta'' \int_0^{2\pi} d\varphi'' \mathcal{J}(r', \theta'', \varphi'', t'') \\ &\quad \times \mathcal{Y}_{lm}(\theta'') e^{-im(\varphi'' - \Omega t'')}. \end{aligned} \tag{234}$$

Despite its appearance, $\mathcal{T}_{lm}(r')$ does not depend on t'', because the integrand in Eq. (234) is a periodic function of $\varphi'' - \Omega t''$ and is integrated over a period of φ'', which is equivalent to integrating over a period of $\varphi'' - \Omega t''$ at any time t''.

Equation (234) can be used to simplify Eq. (232), yielding

$$\begin{aligned} \phi(r, \theta, \varphi, t) &= \sum_{l=0}^{\infty} \sum_{m=-l}^{l} -i \int dt' \int d\omega' \frac{\omega'}{2\pi} e^{-i\omega'(t-t')} e^{im\varphi} e^{-im\Omega t'} \mathcal{Y}_{lm}(\theta) \\ &\quad \times \Big[\int_{r_{\min}}^{r} dr'(r')^2 h_l^{(1)}(\omega' r) j_l(\omega' r') \mathcal{T}_{lm}(r') \\ &\quad + \int_r^\infty dr'(r')^2 j_l(\omega' r) h_l^{(1)}(\omega' r') \mathcal{T}_{lm}(r') \Big]. \end{aligned} \tag{235}$$

Integrating all the terms in Eq. (235) involving t' yields $2\pi\delta(\omega' - m\Omega)$, so that upon subsequent evaluation of the ω' integral, we get

$$\phi(r, \theta, \varphi, t) = \sum_{l=0}^{\infty} \sum_{m=-l}^{l} -im\Omega \mathcal{Y}_{lm}(\theta) e^{im(\varphi - \Omega t)} [A_{\text{out},lm}(r) h_l^{(1)}(m\Omega r) + A_{\text{in},lm}(r) j_l(m\Omega r)], \tag{236}$$

where

$$A_{\text{out},lm}(r) = \int_{r_{\min}}^{r} dr'(r')^2 j_l(m\Omega r') \mathcal{T}_{lm}(r'), \tag{237}$$

$$A_{\mathrm{in},lm}(r) = \int_r^\infty dr'(r')^2 h_l^{(1)}(m\Omega r')\mathcal{T}_{lm}(r'). \tag{238}$$

The iteration process to determine ϕ, which we mentioned at the beginning of this section, consists of taking the current value of ϕ, inserting it into Eqs. (229) and (231) to get $4\pi\mathcal{J}$, inserting that into Eq. (234) to get $\mathcal{T}_{lm}(r')$, inserting that into Eqs. (237) and (238) to get $A_{\mathrm{out},lm}(r)$ and $A_{\mathrm{in},lm}(r)$, and then inserting those into Eq. (236) to get the value of ϕ to use in the next iteration. However, in Sec. 7.5, we will point out a modification that must be imposed on $4\pi\mathcal{J}$ (at early iteration stages) to catalyze convergence of the iteration process.

From Eq. (236), we see that ϕ is the sum of modes labeled by l and m. Since the metric terms in Eq. (229) are functions of r and θ alone and not φ, the iteration process to find a mode of ϕ with one value of m is independent of the iteration process to find a mode of ϕ with another value of m. However, because the metric is a function of θ, two modes of ϕ with different values of l but the same value of m are coupled, so that the iterations for all the modes with that one value of m must be done simultaneously. Because the problem has reflection symmetry across the equatorial plane, and only Y_{lm}'s with even $l+m$ satisfy this property, then, for any m, we only have to consider modes with l equal to $|m|$, $|m|+2$, $|m|+4$, ..., etc. Moreover, we only have to consider positive values of m: Since ϕ is real, the mode with l, m must be the complex conjugate of the mode with l, $-m$. All modes with $m=0$ are time-independent and therefore do not contribute to scalar waves.

To compute the energy radiated to infinity, we take the stress-energy tensor for the scalar field,

$$T_{\sigma\nu} = \phi_{,\sigma}\phi_{,\nu} - \frac{1}{2}g_{\sigma\nu}(g^{\xi\zeta}\phi_{,\xi}\phi_{,\zeta}), \tag{239}$$

and sum the T_{rt} component over a sphere at radial infinity:

$$\frac{dE}{dt} = r^2 \int_0^\pi \sin\theta d\theta \int_0^{2\pi} d\varphi\ \phi_{,r}\phi_{,t}\Big|_{r=\infty}. \tag{240}$$

Since, as $r \to \infty$,

$$h_l^{(1)}(m\Omega r) \to e^{im\Omega r}\frac{(-i)^{l+1}}{m\Omega r} \quad \text{for } m \neq 0, \tag{241}$$

then, using Eq. (236), as $r \to \infty$,

$$\phi \rightarrow \sum_{m\neq 0}\sum_{l=|m|}^{\infty} A_{\mathrm{out},lm}(r=\infty)\frac{(-i)^{l+2}}{r}Y_{lm}(\theta,\varphi)e^{im\Omega(r-t)} + \text{time independent modes of } \phi \text{ with } m=0. \tag{242}$$

Substituting Eq. (242) into Eq. (240) gives

$$\frac{dE}{dt} = 2\sum_{m=1}^{\infty}\sum_{l=m}^{\infty} m^2\Omega^2 |A_{\mathrm{out},lm}(r=\infty)|^2. \tag{243}$$

Note the factor of 2: since ϕ is real, $A_{\mathrm{out},l,-m} = (-1)^l A^*_{\mathrm{out},lm}$, so that we only have to consider modes of ϕ with positive m and then multiply by two to count the contribution to the luminosity due to the modes with negative m.

The luminosity can be expressed as

$$\frac{dE}{dt} = \frac{4\pi}{3}\frac{q^2}{M^2}v^8\mathcal{L}, \tag{244}$$

where

$$v \equiv (M\Omega)^{1/3}. \tag{245}$$

The relativistic correction factor $\mathcal{L}$ (which is a function of v) for the luminosity is unity in the Newtonian limit of large orbital radii (the limit of $v \to 0$) [Ref. [18], Eq. (3.22)].

7.5 Some details of the implementation

In this section, we will discuss some of the details of our numerical evaluation. One can understand our numerical results (Sec. 7.6) without reading this section.

The iterations in solving for ϕ should be done carefully to prevent a possible pitfall: the phase of the waves as computed at the first iteration will differ from the phase of the final, desired solution by an amount which grows logarithmically with large radius. This is because the phase is the integral of $2\pi/(\text{wavelength})$, and at large r the wavelength in the curved space differs from that in flat-space by a term proportional to M/r. If ϕ at the first iteration is too different from its target, the iterations may not converge.

We have found two methods to remedy this problem. Our first method is by setting $4\pi\mathcal{J}$ to zero outside of some "outer radius" which is increased by a small amount at each iteration. This ensures that at each stage, the phase of the waves within this outer radius is close to the final, desired phase. Eventually, we have to stop increasing the outer radius at some large value $r_{\max}$, because of limits due to computational resources and due to the fact that increasing it further makes little difference to the results. In our calculations described in the next section, this large outer radius $r_{\max}$ is arbitrarily chosen to be $200\pi/\Omega$, which is 100 flat-space wavelengths of the longest length scalar waves. Our second method is by using in the iterations, for the initial form of ϕ, the final form of ϕ as computed with a slightly different set of parameters (rather than initially setting ϕ to zero every time). For example (this being the combination of methods that we use), we can use the first method to compute ϕ with, say, $v \equiv (M\Omega)^{1/3} = 0.3$, and then use the second method to compute ϕ with $v = 0.301$. Either method ends up giving the same results. The only difference is the computation time; the second method is quicker.

We compute the luminosity correction factor $\mathcal{L}$ using Eqs. (243) and (244). We approximate the $A_{\text{out},lm}(r = \infty)$ in Eq. (243) by averaging $A_{\text{out},lm}$ from $r = r_{\max} - 2\pi/\Omega$ to $r = r_{\max}$. This averaging partially suppresses a slight oscillatory behavior in $A_{\text{out},lm}$. We let ϕ iterate until the computed value of $\mathcal{L}$ at that iteration changes from its value at the previous iteration by less than 10^{-14}.

We partition the range of r from $r_{\min}$ to $r_{\max}$ into N zones, where N is a number typically chosen to be 2000. The boundaries between these zones can be denoted by ρ_1, ρ_2, ..., ρ_{N-1}. The first zone goes from $\rho_0 = r_{\min}$ to a slightly higher radius ρ_1, the second zone goes from ρ_1 to ρ_2, ..., and the Nth zone goes from ρ_{N-1} to $\rho_N = r_{\max}$. In the nth zone (for any $1 \leq n \leq N$), all quantities (the functions of the g-metric that appear in Eq. (229), the source terms $4\pi\mathcal{J}$ and $\mathcal{T}_{lm}$, and the scalar field terms ϕ, $A_{\text{out},lm}$, and $A_{\text{in},lm}$) are expanded as power series in $(r - \rho_{n-1})$. Each radial power series is truncated at ten terms [at $(r - \rho_{n-1})^{10}$].

The zones are spaced so that all the power series in each zone are valid and accurate throughout

that zone. This requires keeping $\rho_n - \rho_{n-1}$ significantly less than $1/\Omega$ (the order of a typical wavelength) and significantly less than ρ_n (so that the $1/r^l$ terms in the metric have well-converging expansions).

In each zone, the coefficients in the power series for the g-metric appearing in Eq. (229) are polynomials in $\sin\theta$ up to $(\sin\theta)^{l_{\max}}$. For ϕ, we look at modes with $1 \leq m \leq l \leq l_{\max}$, so that for all terms with one value of m, the radial power series coefficients of ϕ are polynomials in $\sin\theta$ up to $(\sin\theta)^{l_{\max}}$. [Since $l+m$ is always even, $\mathcal{Y}_{lm}(\theta)$ can be expressed as a finite power series in $\sin\theta$.] From Eq. (229), then, $4\pi\mathcal{J}$ will have radial power series coefficients that are polynomials in $\sin\theta$ up to $(\sin\theta)^{2l_{\max}}$. [Note that even though we impose the $l_{\max}$ restriction which limits the metric and ϕ to only go up to $(\sin\theta)^{l_{\max}}$, these truncated forms for the metric and ϕ must be considered exact—that is, $4\pi\mathcal{J}$ must be computed up to $(\sin\theta)^{2l_{\max}}$—for reasons dealing with the multiplication properties of the $\mathcal{Y}_{lm}(\theta)$ functions.] Through Eqs. (234), (237), and (238), the coefficients of $\mathcal{T}_{lm}$, $A_{\text{out},lm}$, and $A_{\text{in},lm}$ are not functions of $\sin\theta$. By using power series, we only have to consider the coefficients in these series at each iteration, which (in some ways) is an advantage over completely using a numerical-grid technique.

We arrange for one of the zone boundaries to fall at r_0. At this boundary, $A_{\text{out},lm}$ for $r > r_0$ and $A_{\text{in},lm}$ for $r < r_0$ pick up contributions due to the delta function in $4\pi\mathcal{J}$ at $r = r_0$. This delta function is due not only to $4\pi J$ [see Eqs. (225) and (229)] but also to $(1 - g^{rr})(\phi_{,r}|_{r_0^{(+)}} - \phi_{,r}|_{r_0^{(-)}})$, which is the contribution to $4\pi\mathcal{J}$ from the second term on the right-hand side of Eq. (229), because there is a discontinuity in the first derivative of ϕ at $r = r_0$.

When $v = (M\Omega)^{1/3} \simeq (M/r_0)^{1/2}$ is less than about 0.3, the convergence of the iterations is fast. Unfortunately, we find that for higher values of v, the iterations converge slowly; and this convergence rate is strongly, adversely affected by increasing the value of $l_{\max}$. Since the purpose of this paper is more for the development of an algorithm (for use in the more relevant gravitational-wave case) and for providing easily checkable results than for actually computing the scalar luminosity to high accuracy, we choose for $l_{\max}$ the low value of 4. If we were to choose

$l_{\max} = 6$ instead of $l_{\max} = 4$, the value of $\mathcal{L}$ would change by a fractional amount $\Delta\mathcal{L}/\mathcal{L} \sim 2 \times 10^{-6}$ at $v = 0.1$ and $\Delta\mathcal{L}/\mathcal{L} \sim 6 \times 10^{-3}$ at $v = 0.35$. (These differences are about 5 orders of magnitude larger than the differences that occur when the number of zones is changed from 2000 to 3000.) However, the computation would run much slower with $l_{\max} = 6$. Our numerical technique could use improvements in this high-v, high-$l_{\max}$ regime.

7.6 Results

As a first application of our method, we have computed $\mathcal{L}(v)$ for the spherically symmetric case when all moments besides the mass are set to zero. The cutoff $r_{\min}$ was set to $4M$. In Fig. 1, we show $\mathcal{L}(v)$ as a function of $v \equiv (M\Omega)^{1/3}$ from $v = 0$ to the last stable circular orbit at $v = 6^{-1/2}$. For comparison purposes, we label this particular $\mathcal{L}$ curve as $\mathcal{L}_0$.

Next, we consider how $\mathcal{L}$ depends on the inner cutoff $r_{\min}$, with the spacetime kept spherical. We have computed how $\mathcal{L}(v)$ changes when $r_{\min}$ is set to $2M$ instead of $4M$. It turns out that $(\mathcal{L} - \mathcal{L}_0)$ scales like v^6 for small values of v (where $\mathcal{L}_0$ is the luminosity described in the previous paragraph with $r_{\min}$ set to $4M$). The proportionality constant between $(\mathcal{L} - \mathcal{L}_0)$ and v^6 (for small v) is some number on the order of unity. Its actual value changes when we compute it with $l_{\max}$ set to 4, to 6, or to 8, and also changes depending on the values of the multipole moments. This changing constant is an artifact of the way we have written the curved-space metric and the scattering of waves off of it as power series in $1/r$, but truncated at $r_{\min}$: a change in $l_{\max}$ or a multipole moment results in a significant change in the metric and consequently $\mathcal{L}$ at small radii such as $r_{\min}$.

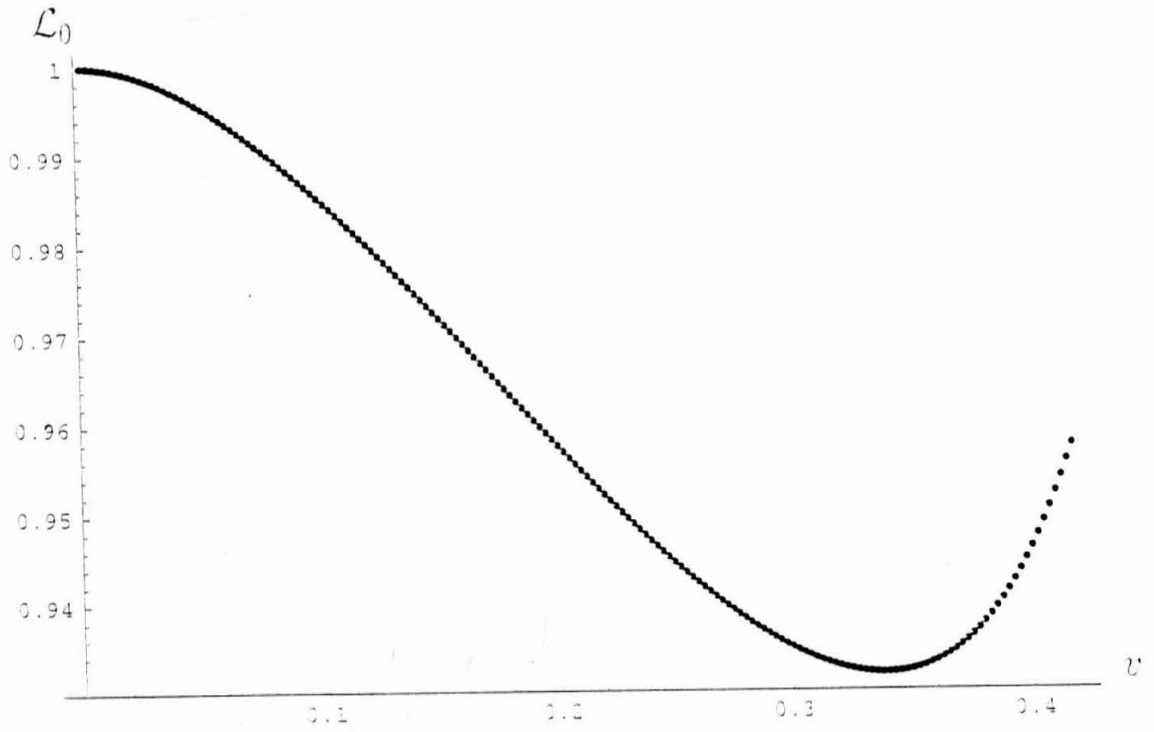

Figure 1: A graph of $\mathcal{L}_0$, the relativistic correction to the scalar-wave luminosity in the spherical case with $r_{\rm min} = 4M$, as a function of $v = (M\Omega)^{1/3}$. Here, Ω is the orbital angular velocity, and $r_{\rm min}$ is the radius inside which the spherical (Schwarzschild) metric, with mass M, is artificially replaced by the Minkowski metric of flat spacetime.

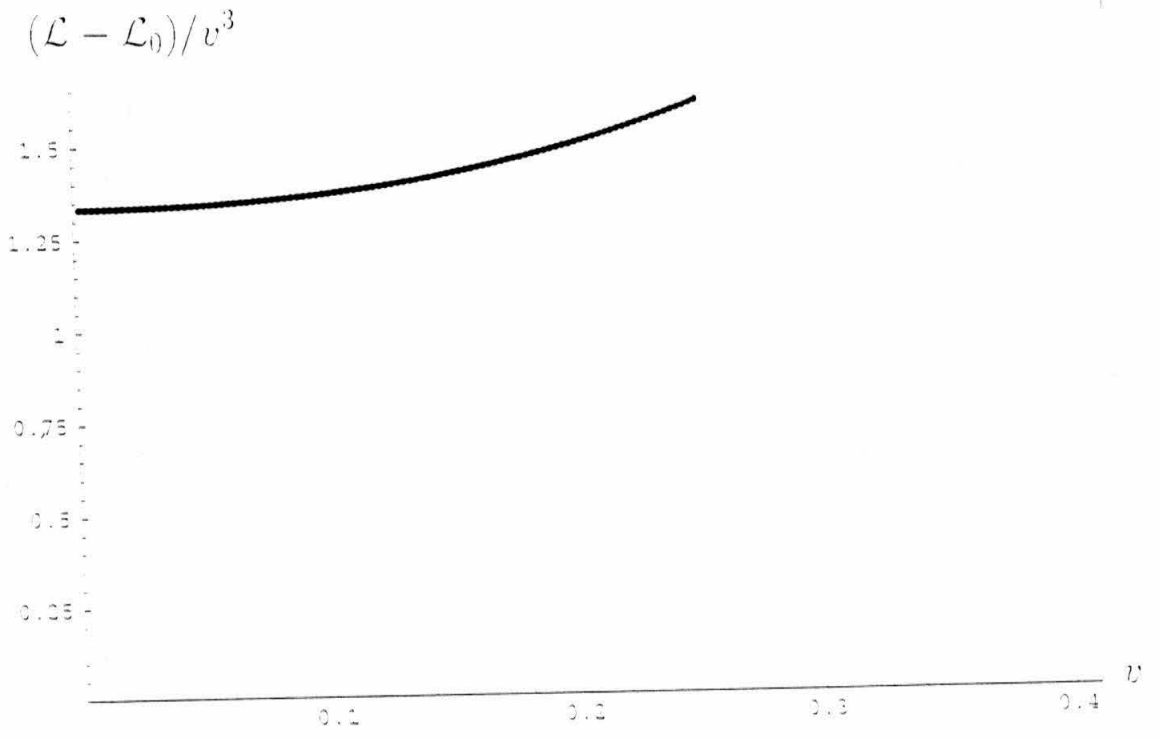

Figure 2: A graph of $(\mathcal{L} - \mathcal{L}_0)/v^3$ as a function of v, where the relativistic correction $\mathcal{L}$ to the scalar wave luminosity is computed for a spinning central body with $S_1 = -M^2$, and with all other moments zero, and with $r_{\min} = 4M$.

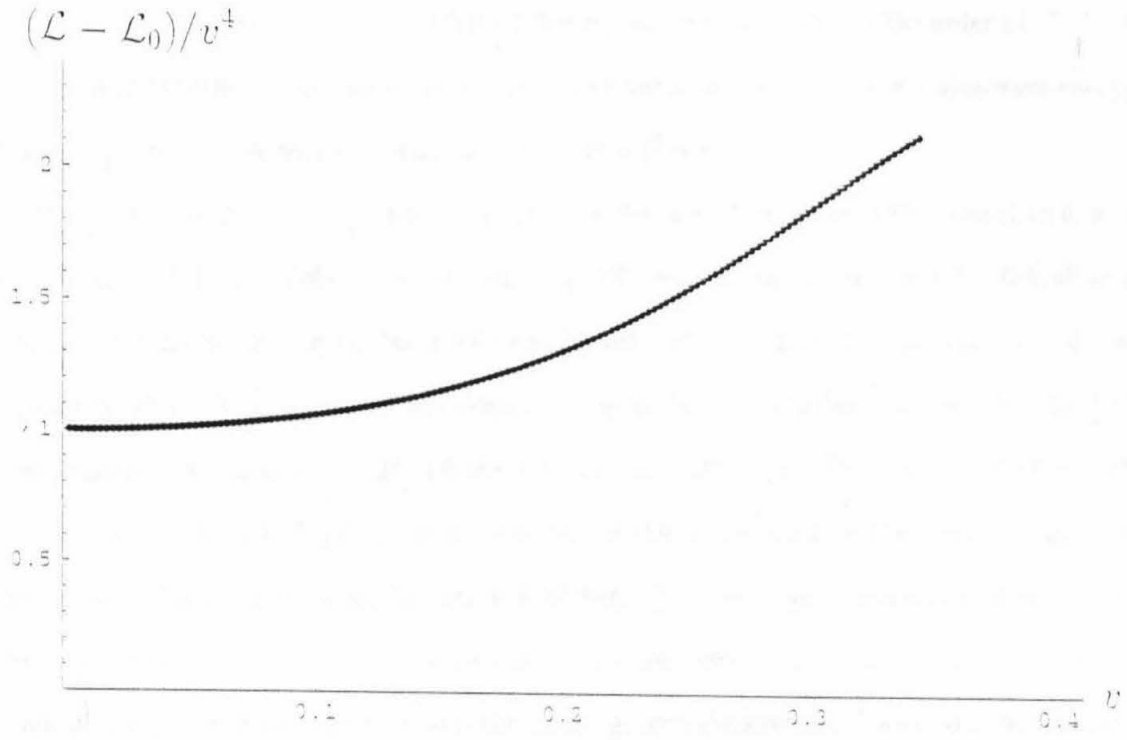

Figure 3: A graph of $(\mathcal{L} - \mathcal{L}_0)/v^4$ as a function of v, where $\mathcal{L}$ is computed for a quadrupole-flattened central body with $M_2 = -M^3$, and with all other moments zero, and with $r_{\text{min}} = 4M$.

What is important is that, for small v, $(\mathcal{L} - \mathcal{L}_0)$ always varies like v^6 with proportionality constant of order unity. If our simplified model for treating the interior region [by simply removing scattering from that region as in Eq. (231)] were replaced by the interior metric for, say, a boson star, then we would expect that the effect of this replacement would be on the order of v^6. This v^6 scaling is not unexpected, since, as we mentioned in the Introduction, the scalar-wave energy that goes down a black hole's horizon scales like $(M/r_0)^3 \sim v^6$ [11].

Next, we have computed the form of $\mathcal{L}(v)$ when the spin S_1 is set to $-M^2$ instead of 0, and $r_{\rm min}$ is left at $4M$. All higher-order moments are still zero. In Fig. 2, we plot $(\mathcal{L} - \mathcal{L}_0)/v^3$ as a function of v, from $v = 0$ to the last stable circular orbit at $v \approx 0.250$. The fact that $(\mathcal{L} - \mathcal{L}_0) \sim -(4/3)(S_1/M^2)v^3$ for small v is entirely explainable by the fact that the dominant (dipole radiation) contribution to $\mathcal{L}$ varies like $r_0^2\Omega^4$ and the fact that $r_0 \sim Mv^{-2}[1 - (2/3)(S_1/M^2)v^3]$ for small v. (See Sec. V.A of Ref. [4] for an explanation of this same effect in the gravitational-wave case. Interestingly, as discussed in Sec. V.B of Ref. [4], there is an additional contribution to the luminosity in the gravitational-wave case. This additional contribution arises because the inspiraling object perturbs the position of the spinning, central body; and this moving spin moment contributes to the radiation field and to the luminosity. But in our scalar-wave case, we assume that the central body is uncharged; and therefore we do not have any such additional contribution.)

We have also computed $\mathcal{L}(v)$ when all moments are zero except the mass and M_2, the latter of which is set to $-M^3$ instead of zero. In Fig. 3, we plot $(\mathcal{L} - \mathcal{L}_0)/v^4$ as a function of v up to the last stable circular orbit at $v \approx 0.344$. Similar to the case with $S_1 = -M^2$ mentioned above, the fact that $(\mathcal{L} - \mathcal{L}_0) \sim -(M_2/M^3)v^4$ for small v is due to the quadrupole moment's affect on $r_0(v)$.

Of course, these scalar-wave calculations are not of much physical interest in themselves. Only when generalized to the gravitational-wave case will such calculations be useful. However, our numerical scheme provides a framework for tackling the gravitational-wave case.

Copies of our numerical code are available from the author.

Acknowledgements

The author is grateful to Kip Thorne for his advice. This work was supported in part by NSF grant AST-9417371 and NASA grant NAGW-4268.

References

[1] P. Bender, I. Ciufolini, K. Danzmann, W. M. Folkner, J. Hough, D. Robertson, A. Rüdiger, M. C. W. Sandford, R. Schilling, B. Schutz, R. Stebbins, T. Sumner, P. Touboul, S. Vitale, H. Ward, and W. Winkler, *LISA: Laser Interferometer Space Antenna for the detection and observation of gravitational waves*, Pre-Phase A Report (1995).

[2] K. S. Thorne, in *Particle and Nuclear Astrophysics and Cosmology in the Next Millennium: Proceedings of the 1994 Snowmass Summer Study, Snowmass, Colorado, June 29–July 14, 1994*, eds. E. W. Kolb and R. Peccei (World Scientific, Singapore, 1995).

[3] B. F. Schutz, Class. & Quant. Grav. **13**, A219 (1996).

[4] F. D. Ryan, Phys. Rev. D **52**, 5707 (1995).

[5] E. Poisson, Phys. Rev. D **54**, 5939 (1996).

[6] F. D. Ryan, in preparation.

[7] F. D. Ryan, L. S. Finn, and K. S. Thorne (in preparation).

[8] R. Ruffini and S. Bonazolla, Phys. Rev. **187**, 1767 (1969). A. R. Liddle and M. S. Madsen, Int. J. Mod. Phys. D **1**, 101 (1992). P. Jetzer, Phys. Rep. 220, 163 (1992). M. Colpi, S. L. Shapiro, and I. Wasserman, Phys. Rev. Lett. **57**, 2485 (1986). F. D. Ryan, to appear in Phys. Rev. D.

[9] T. D. Lee and Y. Pang, Phys. Rep. 221, 251 (1992).

[10] S. A. Teukolsky, Phys. Rev. Lett. **29**, 1114 (1972). S. A. Teukolsky, Astrophys. J. **185**, 635 (1973).

[11] D. V. Gal'tsov, J. Phys. A: Math. Gen. **15**, 3737 (1982).

[12] W. H. Press and S. A. Teukolsky, Astrophys. J. **185**, 649 (1973).

[13] G. Fodor, C. Hoenselaers, and Z. Perjés, J. Math. Phys. **30**, 2252 (1989).

[14] R. O. Hansen, J. Math. Phys. **15**, 46 (1974).

[15] W. Dietz, in *Solutions of Einstein's Equations, Techniques and Results*, C. Hoenselaers and W. Dietz, eds. (Springer, Heidelberg, 1984).

[16] Equations (221) and (222), when evaluated on the equatorial plane, are Eqs. (22) and (28) of Ref. [4], except that those equations in that paper were incorrectly *written* (affecting no other equations), both being off by overall minus signs.

[17] K. S. Thorne, Rev. Mod. Phys. **52**, 299 (1980).

[18] D. E. Krause, H. T. Kloor, and E. Fischbach, Phys. Rev. D **49**, 6892 (1994). As they point out, their definition of the scalar field stress-energy tensor [their Eq. (3.3)] is a factor of $1/4\pi$ times the definition that we use [our Eq. (239)], so that their luminosity is likewise down by such a factor.